2015

STRIDE | Southeastern Transportation Research, Innovation, Development and Education Center

Final Report

Investigation of ATDM Strategies to Reduce the Probability of Breakdown

(2012-042S)

Mohammed Hadi, Ph.D., Florida International University
Lily Elefteriadou, Ph.D., University of Florida
Yan Xiao, Ph.D., Florida International University
Alexandra Kondyli, Ph.D., University of Florida
Ali Darroudi, Florida International University
Clark Letter, University of Florida

August 2015

U.S. DOT DISCLAIMER

Acknowledgment of Sponsorship

This work was sponsored by a grant from the Southeastern Transportation Research, Innovation, Development, and Education Center (STRIDE) at the University of Florida. The STRIDE center is funded through the U.S. Department of Transportation's University Transportation Centers Program. Additional financial support was provided by the Florida Department of Transportation. The authors would like to thank STRIDE and FDOT for their support of university-based research in transportation, and especially for the funding provided in support of this project.

STRIDE Project 2012-042S

Investigation of ATDM Strategies to Reduce the Probability of Breakdown

Mohammed Hadi, Ph.D., P.E.[1]
Lily Elefteriadou, Ph.D.[2]
Yan Xiao, Ph.D., P.E.[1]
Alexandra Kondyli, Ph.D.[2]
Ali Darroudi[1]
Clark Letter[2]

[1]Lehman Center for Transportation Research
Florida International University
Miami, FL

AND

[2]University of Florida Transportation Institute
University of Florida
Gainesville, FL

Southeastern Transportation Research, Innovation, Development, and Education Center
Gainesville, FL
2014
http://www.stride.ce.ufl.edu

TABLE OF CONTENT

LIST OF TABLES

TABLE PAGE

LIST OF FIGURES

FIGURE PAGE

ABSTRACT

Advanced Traffic and Demand Management (ATDM) strategies are increasingly being considered to reduce the probability and impacts of traffic flow breakdown. The goal of this project is to explore and assess methods to improve the operations at critical bottlenecks utilizing ramp metering and variable speed limit (VSL) algorithms that consider the probability of breakdown at recurrent bottleneck locations. The assessment of these ATDM strategies is based on microscopic simulation modeling. Existing simulation model calibration procedures and guidelines are first examined and enhancements are proposed in this study to account for the breakdown characteristics at bottleneck locations in the calibration process.

Various modifications are proposed to the existing fuzzy logic ramp metering system with the consideration of the probability of breakdown. The impacts of these modifications are evaluated using the calibrated simulation model. The results indicate that the probability of breakdown modifications may be able to provide some limited operational improvement at specific bottlenecks and/or along the entire network. However, there is no clear pattern regarding when these improvements can be observed and how different traffic demand levels may affect the impact of these modifications. Using an activation threshold to turn on ramp meters seems to be a viable alternative to time of day operation. This would allow less operator involvement and allow the activation process to become demand sensitive.

In addition, this study developed a shockwave-based VSL system which uses a heuristic switching logic based controller with specified thresholds of prevailing traffic flow condition locations. This VSL strategy aims to improve operations and mobility at critical bottlenecks. The performance of the proposed method was tested in simulation assuming that the data required by the method is collected first using traffic detectors and then using Connected Vehicles. The results

show that the considered VSL strategy can considerably decrease the maximum back of queue and the duration of breakdown.

EXECUTIVE SUMMARY

Advanced Traffic and Demand Management (ATDM) strategies are increasingly being considered to reduce the probability and impacts of traffic flow breakdown. Recent research has indicated that incorporating the probability of breakdown concept into strategies such as ramp metering seems to be promising in postponing the breakdown, reducing the average travel time, and reducing the time in congestion. Recent research also found that implementing Variable Speed Limits (VSL) strategies has the potential for reducing the impacts of breakdown. The USDOT Connected Vehicle program has just started investigating the utilization of connected vehicle technologies to support ATDM strategies of the types discussed above.

This project explored and assessed methods to improve the operations at critical bottlenecks utilizing ramp metering and VSL strategies with the consideration of the probability of traffic flow breakdown. The project also investigated methods for selecting optimal settings of the parameters of these algorithms to maximize traffic operational improvements. These strategies and their impacts were evaluated using the CORSIM mircosimulation tool. The effects of utilization of combinations of mobile and infrastructure devices to support these strategies were also explored in this study.

MICROSIMULATION CALIBRATION

The ATMS strategies considered in this study were assessed using CORSIM, a microscopic simulation tool. It is known that without calibration of simulation models, there is no assurance that the model's outputs are reliable and that the model will correctly predict the traffic performance for the projects as a result of improvements. The state of the practice in calibrating

simulation models is based on the capacity, volume and system performance values. Since the proposed ATMS strategies are mainly investigated as countermeasures to the impacts of breakdown conditions, the examination of the breakdown characteristics in the calibration procedure of traffic simulation models is important to ensure that simulation models can produce a reliable assessment. In this study, the wavelet transform was used to determine the start and end times of breakdown occurrence. Then, the breakdown characteristics as measured at the bottleneck locations were used as inputs to the calibration process. The calibrated simulation model was used in assessing the ramp metering and VSL strategies considered in this study.

INCORPORATING PROBABILITY OF BREAKDOWN IN RAMP METERING SYSTEM

This study investigated the probability of breakdown in ramp meter activation decision and also in metering rate determination, as explained next. The probability of breakdown was incorporated directly in the fuzzy logic ramp metering control algorithm to allow the algorithm to better react to potential traffic breakdown conditions. A series of simulation experiments were designed in this study to assess the modifications to the fuzzy logic ramp metering system on I-95 in Miami, FL. The northbound I-95 segment that is currently controlled by the fuzzy logic algorithm was first modeled in CORSIM and calibrated to replicate the existing operations. The modifications were tested at two ramp metering locations identified as recurring sources of congestion.

It was concluded that incorporating an activation threshold in the metering operation has the potential to improve or at least replace the current time of day activation. On average, the metering operations with the activation threshold outperformed the current time of day operations

by as much as 2.4% in terms of total network travel time. However, the results were inconsistent between individual runs, and the system was sometimes shown to experience increase in the total travel time. However, an advantage of linking ramp metering rate to breakdown probability is making metering more reactive to non-typical traffic congestion.

A number of different modifications were made to the fuzzy logic ramp metering algorithm to include the probability of breakdown. It was concluded that the effect of these changes on the ramp metering operations is to cause a slightly more strict metering strategy. The mainline showed some travel time improvement, but with more strict metering rates some delay was shifted toward the ramp vehicles. While the modifications showed some potential to improve traffic operations, the overall impact on the network performance was minimal. The total travel time showed improvement on the average, but was inconsistent when analyzing individual runs. It is possible that the inconsistencies are a function of the simulation experiment, and may not be observed in a field implementation.

Overall, it was concluded that the probability of breakdown inclusion in ramp metering may be able to provide some limited operational improvement at specific bottlenecks and/or along the entire network. However, there was no clear pattern regarding when these improvements are expected, and how different traffic demand levels can affect these impacts. Using an activation threshold to turn on ramp meters seems to be a viable alternative to time of day operation. This would allow less operator involvement and allow the activation process to become demand sensitive.

VARIABLE SPEED LIMIT

This study developed a shockwave-based VSL system which uses a heuristic switching logic based controller with specified thresholds of prevailing traffic flow condition locations. This VSL strategy aims to improve mobility at recurrent bottlenecks. Before breakdown occurrence, the proposed VSL tries to postpone breakdown by decreasing the inflow and achieving uniform distribution in speed and flow. After breakdown, the VSL system aims to dampen the congestion by reducing the traffic inflow to the congested area. The shockwave-based VSL system pushes the VSL influence area location upstream as the congested area propagates upstream. In addition, this study investigated the effect of using Connected Vehicle data instead of detector data on VSL system performance. Wavelet transform was used to analyze aggregated individual vehicles' speed data to determine the location of congestion.

The performance of shockwave-based VSL was compared to VSL systems with different fixed VSL message sign locations. The results show that shockwave-based systems outperform other VSL systems, and it can considerably decrease the maximum back of queue and duration of breakdown while increasing the average speed during breakdown. In addition, one of the important issues in implementing VSL systems is whether drivers will obey the speed limit signs. Sensitivity analysis was conducted on VSL system performance with different compliance rates. As expected, the results indicate that as the compliance rate increases, the VSL system is more successful. However, even with low compliance rates, the VSL system can improve traffic mobility at bottlenecks.

CHAPTER 1

INTRODUCTION

BACKGROUND

Traffic congestion is a critical issue that significantly impacts the economy (*1*). Recurrent congestion mainly occurs during peak periods when too many vehicles attempt to use a common roadway with limited capacity. Non-recurrent congestion also occurs due to incidents, special events, work zones, and weather events. Congestion is a source of productivity and efficiency loss, fuel wastage, and excessive air pollution. The areas that mostly suffer from these problems are large urban areas, but even smaller urban and rural areas are starting to suffer from this congestion.

Expanding road infrastructure is one of the solutions. Because of the cost of construction, funding availability, and right-of-way and environmental concerns, many of the congested corridors will not have additional infrastructure built for many years to come. Thus, it is important for transportation agencies and decision makers at the state, regional, and local levels to collectively invest in existing facilities and collaborate in better managing their multimodal transportation corridors with improved operational strategies and technology.

To address these challenges and ensure a safe and efficient transportation system, transportation practitioners are looking for a more efficient use of existing road networks. Therefore, there is a tremendous need to identify and implement effective operation strategies. Active Traffic and Demand Management (ATDM) strategies such as ramp metering and variable speed limit (VSL) are state-of-the-art methods that are increasingly being considered to improve the efficiency of the existing freeway system. In recent years, connected vehicle technologies have

been proposed to support more effective and efficient implementations of ATDM strategies, in addition to their use in other mobility, safety, and environmental impact application.

As the transportation community continues to develop advanced strategies to alleviate congestion, simulation models are expected to play a major role in assessing emerging ATDM strategies and Connected Vehicle applications. However, without effective calibration, there is no assurance that the model's outputs are reliable in replicating real-world performance. Several documents and results from research are available to provide guidelines for simulation model calibration and validation. However, these guidelines may need to be re-examined and possibly revised when considering the simulation of complex ATDM and Connected Vehicle strategies.

It is important to investigate the influence of the utilization of ramp metering and VSL on traffic operations, both with and without a Connected Vehicle component. Microscopic simulation modeling will play an important role in this investigation, taking into consideration the limited existing real-world applications of these strategies.

PROBLEM STATEMENT

Congestion can be categorized in two groups: recurrent congestion and non-recurrent congestion. Recurrent congestion starts at bottlenecks during peak hours when too many vehicles attempt to use a common roadway segment with limited capacity. Thus, the identification of strategy to improve traffic operation requires that bottlenecks are carefully analyzed, as they are a primary reason for traffic congestion.

When demand approaches or exceeds the bottleneck's capacity, breakdown will occur. The term "traffic breakdown" is used to describe the transition from under-saturated to over-saturated, or congested, conditions. After breakdown occurs, the maximum flow throughput at the bottleneck

is often lower than that of the maximum capacity observed before breakdown. Recurrent freeway bottlenecks may be caused by on-ramp traffic merges, lane drops, low posted speed limits, and/or spillbacks from off-ramps, among other reasons. Congestion is usually expressed as a stop-and-go operation, but more generally, it is observed as a slow-and-go operating condition. Ramp metering and VSL are among the strategies proposed to reduce the impacts of breakdown.

Agencies in the Southeast of the United States have started considering and implementing ramp metering. As examples, ramp metering utilizing a fuzzy logic algorithm has been implemented I-95 in Miami-Dade County, Florida. Ramp metering is also being assessed for other corridors in Florida. Ramp metering has also been deployed in Atlanta, GA. Previous ramp metering-related studies have indicated that incorporating the probability of the traffic breakdown concept in existing ramp metering algorithms seems to be promising in postponing the breakdown, reducing the average travel time, and reducing the time of congestion.

VSL strategies identify and disseminate the appropriate speed limits based on the prevailing conditions. In addition to the safety applications of these strategies, VSL strategies have been recommended upstream of bottlenecks with recurring congestion, to delay breakdown formation, as well as to dampen the shockwave produced once congestion starts. Several issues have been identified with VSL implementations, including the need to optimize the associate parameters and sign locations, and concerns about the levels of driver compliance.

The initial documentations from United State Intelligent Network Flow Optimization (INFLO) Program pointed out that the current speed harmonization implementations are fundamentally limited by their exclusive reliance on infrastructure based detection and information dissemination. The introduction of Connected Vehicles technology and associate Vehicle-to-Infrastructure communication will provide a basis to detect individual vehicle trajectories that can

be used as high-precision and detailed input data. Detailed traffic data can provide a better understanding of traffic conditions and thus better VSL implementations.

The above discussion indicates that ramp metering and VSL strategies have the potential to reduce the impacts of critical bottlenecks. However, there are still many questions to be answered before real-world implementations of this strategy. Simulation analysis can help answer these questions; however, there may be a need for additional calibration steps to improve its ability to model the proposed advanced strategies.

RESEARCH GOAL AND OJBECTIVES

The goal of this project is to explore and assess methods to improve the operations at traffic bottlenecks utilizing ramp metering and VSL algorithms, with the consideration of the probability of breakdown. Methods will also be developed for selecting optimal settings of the parameters of these algorithms to maximize traffic operational improvements. The specific objectives of this research are as follows:

1) Provide recommendations regarding calibration and validation procedure of traffic simulation models to improve the ability of the models to simulate the impacts of advanced strategies by considering traffic flow breakdown parameters, in addition to those currently used in calibrating traffic simulation models.
2) Develop and assess the effectiveness of modified ramp metering strategies that better address traffic breakdown.
3) Develop VSL strategies based on infrastructure data and assess their effectiveness in improving congestion and breakdown conditions at bottlenecks.
4) Develop VSL strategies based on Connected Vehicle data and assess their

effectiveness in improving congestion and breakdown conditions at bottlenecks.

5) Assess VSL strategies effectiveness under different compliance rates.

DOCUMENT ORGANIZATION

This document is organized into five chapters. Chapter 1 introduces the research background, describes the problems to be solved, and sets the goal and objectives to be achieved.

Chapter 2 presents an extensive literature review of breakdown characteristics, traffic micro-simulation calibration, VSL strategies implemented and previously researched and/or their outcomes, evaluation of VSL strategies, and related applications of Connected Vehicles.

Chapter 3 describes the framework of the proposed calibration approach for microscopic simulation that considers traffic flow breakdown parameters, in addition to the currently used parameters. Case studies are described in this section to examine the products of this research.

Chapter 4 presents the modifications to the existing fuzzy logic ramp metering algorithm with the consideration of the probability of breakdown and the evaluation results of these proposed algorithms.

Chapter 5 presents the proposed infrastructure-based and Connected Vehicle data-based VSL strategies. Application results of these VSL strategies are also discussed in this section.

Chapter 6 summarizes the main contributions, draws conclusions, and recommends issues for future research.

CHAPTER 2

LITERATURE REVIEW

This chapter first introduces freeway breakdown concepts and related literature on the subject. Then, it presents a detailed review of the current practices in micro-simulation calibration. Next, VSL algorithms, strategies, and their applications in the real-world are reviewed. Finally, the Connected Vehicle technology and applications are introduced.

BREAKDOWN

A freeway bottleneck location is identified by traffic congestion upstream and freely flowing traffic downstream. Bottleneck locations on freeways either have capacities less than or a demand greater than other locations. Bottlenecks may be caused by on-ramp demands, lane drops, low posted speed limits, and spillbacks from off-ramps. When demand approaches the bottleneck's capacity, breakdown will occur, which reduces the freeway's maximum throughputs. The term "breakdown" of flow on a freeway is used to describe the transition from speeds in the vicinity of the posted speed limit to congestion. Once a breakdown occurs, the maximum throughput can drop by 5-10%. Papageorgiou et al. (*2*) have shown that a capacity drop of 5% can increase the travel time by 20%. However, this could be higher or lower depending on the ratio of the demand to the capacity of the freeway.

Breakdown Definition

Various definitions for breakdown have been presented by a number of researchers. These definitions are based on the amount of speed reduction or based on the average speed during breakdown. Following are some of these definitions:

- Elefteriadou et al. (*3*) defined breakdown to have occurred, if at least one vehicle on the freeway is forced to reduce its speed by 10 mph or more.
- Graves et al. (*4*) defined breakdown to have occurred if the speed at a location is less than 30 mph during five consecutive one-minute intervals. Whenever the speed exceeds 30 mph for five consecutive one-minute intervals, the breakdown event is considered to have ended.
- Persaud et al. (*5*, *6*) defined breakdown as having occurred if the flow and speed drop suddenly at a location immediately downstream of a ramp for a duration of at least five minutes.
- Okamura et al. (*7*) defined breakdown to have occurred if the speeds are lower than 25 mph or the queue exceeds 0.62 miles for a duration of at least 15 minutes.
- Brilon (*8*, *9*) defined breakdown occurrence when a short time interval experiences a sharp speed reduction below the threshold of 43.5 mph. The amount of speed reduction should be more than 6.22 mph to be considered a sharp speed reduction. The short time interval was selected to be a one-minute interval; however, due to unavailability of data, a five-minute interval data was used.
- Kuhne et al. (*10*) defined breakdown to have occurred when traffic flow is greater than 1000 vehphpln with a sharp speed reduction below the threshold of 46.5 mph. The amount of speed reduction should be more than 10 mph to be considered a sharp speed reduction.

- The Manual on Uniform Traffic Control Devices (MUTCD) (*11*) defines breakdown occurrence as the condition that for 15-minute interval speeds are less than 40 mph.

Causes and Process of Breakdown

Finding the main cause of breakdown is the first step to control and mitigate breakdown. For this reason, the causes of breakdown have been a topic of increased interest among researchers.

Buckley and Yagar (*12*) discussed breakdown occurrence at an entrance ramp or lane drop, which they termed "capacity funnels". At a capacity funnel, drivers merge into minimal gaps in the adjacent lane. To reach a more acceptable distance headway in this adjacent lane, drivers attempt to increase the headway by slowing down. As a consequence, drivers upstream decelerate, causing a shockwave that moves upstream.

Banks (*13*) analyzed four bottlenecks using detector data and video surveillance. In three of these bottlenecks, the breakdown began with queue formation behind slower moving vehicles. As flows and densities increase, the lane change maneuver is prohibited. Eventually speeds of the platoons became unstable, resulting in sharp speed reduction. In the fourth case, breakdowns appeared both upstream and downstream of a divergence point. It was further noted that the merge and divergence rates during the breakdown were far greater than the typical capacity values.

Gazis and Herman (*14*) described the development of moving bottlenecks, which are caused by slow-moving vehicles. Their discussion of breakdown events on a two-lane freeway described how lane-changing vehicles that overtake slow vehicles in one lane interfere with traffic in the other lane, resulting in traffic creating a shockwave on this lane.

Elefteriadou et al. (*3*) analyzed two bottlenecks using video surveillance. Analyzed data showed that the presence of vehicle clusters indicates that a breakdown may occur.

Daganzo et al (*15*) presented a model that recognized that when one of the vehicles in the platoon wants to allow another vehicle to merge, it will slow down. Consequently, all of the cars in the platoon slow down, which causes instabilities that lead to congestion.

Daganzo (*16*) categorized drivers as two types: fast-moving and slow-moving. At freeway ramp merge locations, fast-moving vehicles stay in the passing lane with short headways, while on-ramp vehicles enter and stay in the shoulder lane. Eventually, fast-moving vehicles that entered from the on-ramp try to leave the shoulder lane and merge into the passing lane, which increases the passing lane's flow. When the mainline and/or the merging flows are high, the passing lane becomes saturated, and a congestion shockwave will move further upstream. Consequently, the fast-moving vehicles try to move into the shoulder lane before merging, since the passing lane speed is now lower. As a result, the queue on the passing lane eventually spills over onto the shoulder lane.

Identification of Bottleneck Location

Identifying the locations of traffic bottlenecks is an important part of highway management. There are several methods for identifying bottlenecks. Existing bottlenecks need to be identified from historical and current field measurements based on the breakdown definitions given above. A bottleneck location is likely to receive more demand than the available capacity for a period of time. The approximate location of a bottleneck is identified as the section between a detector location with the most congestion and its neighbor detector (with no congestion). For example, as mentioned earlier, previous studies considered merge points as possible bottleneck locations. Cassidy and Bertini (*17*) reported that examined bottlenecks occurred at fixed locations

approximately 0.62 miles downstream of on-ramps. They analyzed two bottleneck locations (metered and non-metered ramps) using detector data for this purpose.

Chen et al. (*18*) used an instrumented floating car method to find the locations of bottlenecks. It was mentioned that extensive data logging, as well as multiple days of data, are needed in order to remove non-recurrent bottlenecks. This approach is not sensitive to demand levels, and it may not be accurate enough due to limited runs and the stochastic nature of traffic that varies every day.

More commonly, bottleneck locations are identified using archived detector data. Cassidy and Bertini (*17*) used 30-second data to construct curves of cumulative vehicle counts and occupancy to observe the changes from free-flow conditions to queued conditions.

According to FHWA simulation guidelines, visual audit can be used as the primary method for finding bottleneck locations (*19*, *20*). Speed-distance contour plots that use detector data identify bottleneck locations. The use of multiple day data is to assure that a bottleneck is a recurring bottleneck.

Breakdown Characteristics

Aside from its primary causes, other characteristics define breakdown, such as duration of breakdown, average speed during breakdown, maximum pre-breakdown volume, and queue discharge. The queue discharge rate is defined as the long-run average of flow over the breakdown period. Maximum pre-breakdown flow is measured at different intervals, such as one-minute, five minutes, or fifteen minutes immediately before the breakdown occurs. These characteristics are important because this is how capacity is defined.

While the HCM calculates capacity based on the geometric conditions of the facility and treats it as a deterministic value, there is a significant amount of recent literature that suggests using other measures to estimate capacity, such as maximum flow before breakdown and queue discharge rate to measure capacity in the field to account for site specifications.

In addition to these characteristics, it was observed that at the same bottleneck location and for the same combinations of ramp and freeway flows, breakdown may or may not occur. And, if breakdown occurs, it occurs at different times. This phenomenon has gained a great amount of interest and attention among researchers in two aspects. First, researchers have come to recognize the stochastic nature of capacity and breakdown. There is still an ongoing question about which value of flow rate, either the maximum pre-breakdown flow rate or discharge flow rate, should be considered capacity for different applications. If capacity is a random variable, then what percentile of the distribution should be used as the descriptive statistic?

Eleftriadou et al. (*21*) studied two major bottlenecks over a 20-day period and concluded that pre-breakdown flow and queue discharge rate are distributed normally, and that the range can be several hundred veh/hr. Geistefeldt (*22*) suggested that the capacity design value should be defined as a specific percentile of the breakdown probability distribution. Another issue is identifying the breakdown probability model for use when considering breakdown. For instance, Elefteriadou et al. (*3*) developed a probabilistic model for a specific on-ramp merge bottleneck. The model estimates the breakdown probability based on the occurrence of ramp-vehicle clusters. Kondyli (*23*) suggested that lane change measures affect the breakdown probability, and driver lane-changing behaviors have a significant effect on breakdown. She developed a breakdown probability model based on this finding.

One of the concerns in studying and analyzing breakdown characteristics is the noise in traffic data. The most common way to overcome noise in the data is to aggregate traffic data over a certain time period (*18*, *24*). Another method is to use oblique cumulative curves. This method has been used specifically to study bottlenecks and find the start and end times of breakdown (*17*, *25*, *26*). Cumulative curves are effective in suppressing noise; however, changes in traffic patterns are not apparent. This is the reason in the aforementioned studies that these curves were plotted with an oblique time axis to magnify the changes in traffic conditions. In these curves, the identification of changes in traffic conditions, such as the starting time of breakdown, is based on the sudden decrease in the slope of the curve. Not compromising the original time resolution is one of the advantages of this method. However, this method requires adjusting the degree of the oblique axis for different situations, such as different locations and different demands, which makes this method difficult to apply. Muñoz and Daganzo (*25*) used an empirical fundamental diagram (FD) to identify the start and end times of breakdown. Zheng et al. (*27*) proposed a wavelet transform method for identifying the location of bottlenecks, starting time of congestion to upstream locations, and the start and end of breakdown.

Congestion Propagation

An important issue to investigate is that of congestion propagation once breakdown has occurred. Shockwave analysis is used for this purpose. A shockwave describes the boundary between two traffic states that are characterized by different densities, speeds and/or flows. Previous studies have based the calculation of shockwave speeds on the flow-density relationship. The shockwave speed is estimated as the difference of flow over the difference of density between the conditions upstream and downstream of the bottleneck.

Also, there is a great amount of empirical case studies on finding shockwave speed. With the availability of detector data, waves can be measured by comparing the speed or occupancy time series between adjacent detector stations. The detection of these waves, however, is not always accurate, considering the amount of noise in the detector data and the fact that point detectors are normally installed at 0.5-mile intervals. The literature is not consistent in terms of the range of values for shockwave speeds (*28*, *29*). Kerner (*30*) suggested that the shockwave speed differs for various roadway and weather conditions. Other literature reported that shockwave speeds at bottlenecks on Japanese urban expressways range from 11 to 12.5 mph (*31*), and from 10.5 to 15 mph (*32*). Lu and Skabardonis (*33*) examined the vehicle trajectory datasets collected as part of the FHWA NGSIM program at two freeways, and found an average congestion propagation speed of 11.4 mph. They also found that this speed is independent of the speed prior to congestion.

CALIBRATION

Traffic simulation is widely used and increasingly applied for the assessment of the performance of transportation systems, traffic operations, and management alternatives. Simulation is cost-effective, allows risk-free assessment, and provides an efficient assessment approach. However, without calibration, there is no assurance that the model's outputs are reliable and that the model will correctly predict traffic performance. Calibration is the adjustment of model parameters to improve the model's ability to reproduce local traffic conditions. To show the importance of calibration, Bloomberg et al. (*34*) showed that differences of 13% in the freeway speeds between real-world and simulation estimates for existing conditions that can produce differences of 69% in the forecasted freeway speeds for future conditions.

Trial-and-error Methods

Trial-and-error methods tend to be more frequently used in practice than other methods, as they are generally less complex and when performed by experienced modelers can produce good results. The trial-and-error methods involve an iterative adjustment process. This process continues until both precision requirements and performance target are met. This method is simple and easy to apply, but the choice of the feasible range often relies on the analyst's modeling experience and judgment to make a good choice. Chu and Liu (*35*) developed a four-step trial-and-error-based approach that includes the calibration of driver behavior models, route choice, origin-destination estimation and model fine tuning. Dowling et al. (*36*) developed another four-step trial-and-error method to calibrate a model. These four steps include error checking, calibration for capacity, calibration for demand, and overall analysis of performance.

Park and Schneeberger (*37*) proposed a nine-step calibration procedure. The three main components of the procedure are: 1) calibration component setup (data collection, selection of calibration parameters and MOEs); 2) calibration effort; and 3) evaluation and validation of the calibrated model. A case study corridor that was modeled in the VISSIM model was calibrated using this procedure. They used the results from the t-test to compare the simulation and field travel time means as the criterion to determine when a model is adequately calibrated. The case study only utilized a single day of data collection and generated the parameter sets based on a linear regression model, thus, it did not account for the day-to-day variability of traffic conditions.

Hourdakis et al. (*38*) proposed a four-step calibration and validation procedure that includes: 1) volume-based calibration; 2) speed-based calibration; 3) capacity-based calibration; and 4) validation. In each step, a quasi-Newton algorithm was used to find local optimum

parameters and, in all four steps, Theil's inequality was used as a goodness-of-fit measure. The proposed procedure was applied to a 12-mile long freeway network modeled using AIMSUN.

Dowling et al. (*19*, *20*) introduced a top-down calibration approach, which consists of a three-step calibration process: capacity as measured by queue discharge rate, and system performance calibration. Capacity calibration is very important, since it has a significant effect on the predicted system performance. The authors' recommendations include first focusing on changing network-wide parameters, and then changing link-specific parameters.

Gomes et al. (*39*) used three speed contours, corresponding to a heavy, a typical, and a light day of traffic to identify field bottlenecks. The calibration objective was to match the locations of the bottlenecks, bottleneck start times, queue lengths, and time durations. However, the study did not match flow data because of the large variations identified in traffic flow. In addition, no quantitative measures were developed.

Zhang and Owen (*40*) proposed a procedure that includes quantitative and statistical analyses at both the macroscopic and microscopic levels, as well as animation comparison. The performance measures used in this procedure were the average speed and traffic volume at the macroscopic level and the vehicle trajectory plot and headway distributions at the microscopic level. The animation comparison was conducted as a validation procedure. Based on their study, some of the advanced micro-simulation traffic models such as CORSIM and VISSIM are using multi-regime simulation logic. For example, car-following regimes in these models can be normal or uncomfortable. The uncomfortable regime is defined as the model allowing the distance between successive vehicles to be arbitrarily close when speeds are identical.

Zhang et al. (*41*) identified the parameters in the CORSIM simulation model that can affect the assessed capacity in the simulation. The analysis was based on investigating the impact of one

parameter at a time on the selected MOEs. The results showed that the car-following sensitivity multiplier and the mean free-flow speed greatly affect the MOEs. The Pitt car-following constant, lag acceleration/deceleration time, and time to complete lane change had medium effect. The rest of the car-following and lane-changing parameters did not have significant effects on the MOEs.

Ban et al. (*24*) introduced a three-step approach for bottleneck calibration. The first step is the visual assessment of the speed contour maps from simulation against real-world data. They also used binary speed counter maps, where each cell is 1 if it is congested, otherwise, it is 0. The second step consists of matching the binary speed contour maps from simulation against real-world data. The last step is a detailed speed calibration.

Halkias et al. (*42*) simulated a highway in Athens, Greece in order to assess bottleneck mitigation strategies. The queue lengths and speed values were the parameters considered for comparison between field measurements and simulation results. For further alternative analysis, the volume was increased by 20% to make sure that hidden demands had been considered and more severe downstream bottlenecks would not occur. They recommended that a wider perspective of freeway analysis is required, in addition to focusing on the bottleneck area to make sure that the investigated scenario will not lead to new bottlenecks downstream.

Zhang et al. (*43*) categorized calibration approaches into two groups. The most popular is the flow profile approach, which compares the simulation results against the field observations for every interval. The other approach is the fundamental diagram approach, which is based on capacity and the shape of the flow-occupancy diagram. This approach focuses on replicating field-observed capacities.

Most often, micro-simulation models are calibrated using data from a single time period and may fail to sufficiently represent traffic conditions outside of that specific time period. Rakha

(*44*) conducted a two-factor analysis of variance (ANOVA) to get a better understanding of the stochastic nature of traffic conditions. This approach requires comparing the results from a set of simulation runs with field data observed across different days. Least-squares error (LSE), least Poisson error (LPE), and visual inspection were used to measure the variability in link flows. Comparing the flow between days shows that LSE varies from 1.7 to 3.6 percent of the mean flow, and the LPE was found to vary from 3.2 to 5.2. A graph was used for visual inspection, in which the data points were scattered around the line of unbiased correlation (45° line). The authors recommended that all of these measures should be considered with each other, since in some cases, the error estimates do not coincide with the visual inspection.

Henclewood and Fujimoto (*45*) investigated the calibration of a model for two different periods, focusing on ten effective parameters. For this purpose, 1,000 different parameter sets produced by Monte Carlo simulation were used as inputs to VISSIM. Out of the 1,000 sets, there were 93 well-calibrated models for the first time period, and 34 well-calibrated models for the second time period. Only one parameter set was found to be sufficiently calibrated for both periods, based on travel time and saturation flow rates. They concluded that the calibration parameters should be allowed to change with respect to time to account for the changes in driving behavior and environment.

Heuristics-based Methods

One of the widely attempted approaches in micro-simulation model calibration is the use of the Genetic Algorithm (GA) in the calibration process. Three reasons that researchers frequently use to justify the choice of genetic algorithms are: 1) it does not need gradient information, which is usually not available due to the complex format of micro-simulation; 2) it avoids exhaustive

enumeration, which can save significant computational time; and 3) it always maintains a set of feasible solutions before reaching on optimum answer. In general, GA-based approaches consist of two primary components: 1) feasibility test, and 2) GA-based optimization. First, it is important to identify key parameters that have effects on the results. This could be done using different approaches such as the ANOVA or other statistical plots and visual observations. The feasibility test is used to determine whether or not the set of calibration parameter ranges are feasible. This step should be repeated until the feasibility test is satisfied by adjusting the range of parameters, which could be implemented using the Latin Hypercube Sampling (LHS). This algorithm is used to reduce the number of combinations to a reasonable level, while still covering the entire parameter surface. It is well known that conducting the GA optimization requires large running times compared to other optimization techniques, while often ensuring better solutions than other methods.

Schultz and Rilett (*46*) analyzed the effects of the car-following sensitivity factors distribution on CORSIM results. Two alternatives were first considered: random distribution, where each factor is an independent parameter, and one distribution, in which all factors are generated from a distribution of measures of central tendency and dispersion. Since the second alternative only requires two parameters (mean and variance), which make the process simpler, they chose to focus their study on the second alternative. Based on previous studies that indicated normal and log-normal distributions as two possible headway distributions, these two distributions were selected to generate the car-following sensitivity factors. Using the GA approach, they calibrated a simulation model for the IH-10 in Houston, Texas, for the AM and PM peak periods. Both proposed distributions produced better results compared to the default distributions for both

time periods. The results show that the optimal distribution for the AM peak is different from the one for PM peak. In addition, the log-normal distribution produced slightly better results.

Kim and Rilett (*47*) used a GA method to calibrate a CORSIM micro-simulation model for two corridor systems in Texas. Their study considered 19 parameters in CORSIM consisting of 11 car-following sensitivity parameters, 2 acceleration/deceleration parameters, and 6 lane-changing parameters. They implemented the binary coding method to code the 19-parameter set into a 121-bit binary string as an individual's chromosome in the GA. The large search space, described above, illustrates the importance of using an efficient optimization method.

Park and Qi (*48*) developed a GA-based procedure for calibrating the VISSIM micro-simulation model. They used the Latin Hypercube Design (LHD) to reduce the number of possible combinations of parameter values. Their calibration approach was tested using two case studies, including an isolated signal intersection and a highway segment with work zone. Travel time was considered the performance measure for both calibration and validation. Their approach reached the optimal solution after 10 generations in the GA optimization.

Lee et al. (*49*) introduced a simplified procedure for calibration. Since their previous study in utilizing a GA simulation calibration was not practical, it was not widely used by traffic engineers. Once all samples are evaluated using the LHS approach, the solution with the most promising fitness values are chosen. Case studies on urban signalized corridor and freeway section show that this procedure outperforms the previously used GA-based procedure.

Ma et al. (*50*) proposed a simultaneous perturbation stochastic approximation (SPSA) method-based calibration approach and used it to calibrate a system in Paramics. They compared the performance of their approach against other heuristic methods, such as the GA and the trial-

and-error iterative adjustment algorithm. This comparison was done by measuring the computation time, which showed that their method outperforms the other two methods.

Lee and Ozbay (*51*) proposed a Bayesian sampling approach in conjunction with the application of the SPSA optimization method. The Bayesian sampling technique was used to create unbiased initial input data covering the entire search space. They compared their approach to the standard SPSA-based approach, and the results showed that their approach requires less computation time. It is interesting to point out that based on their literature review, most of the previous studies failed to note that having the same mean between the observed data and simulation output does not imply that these distributions are identical. In validating the model, they compared its outputs with the distribution of the observed values using the Kolmogorov–Smirnov test to handle day-to-day traffic variations.

Paz et al. (*52*) introduced a calibration procedure based on the SPSA algorithm in order to calibrate all of the parameters simultaneously. This method is an iterative approach that uses gradient estimations of the objective function to determine an optimal solution.

Fellendorf (*53*) used the simulated annealing optimization method to calibrate a roundabout modeled in VISSIM micro-simulation. Queue positions were considered measurements of effectiveness. They reported that calibration results were promising.

Menneni et al. (*54*) introduced a calibration methodology based on an evolutionary optimization algorithm that uses the speed-flow relationship as a calibration objective to address the stochastic nature of capacity. They stated that instead of using a single numerical value, the distribution of capacity values should be used. Using a distribution allows the use of queue discharge flow and pre-queue flows that can be derived from the speed-flow graphs. They claimed that this approach can replicate the whole range of traffic behaviors since the speed-flow graphs

provide information on all three regions: free-flow, congestion, and discharge. They concluded that the results from this approach outperform the results from the calibration based on the objective functions that include the maximum 5-minute flow and maximum 5-minute flow sustained for 15 minutes.

Hollander and Liu (*55*) presented a rather comprehensive review of many of the current calibration methods, while attempting to highlight the fundamental requirements for calibrating microscopic simulation models. They provided a tabulated summary on the methods researchers used to calibrate different micro-simulation models and their stopping criteria to indicate that the calibration results are suitable. In examining these criteria, one may notice that many tend to be subjective due to their dependence on what is being modeled and the goals of the modeling effort.

In summary, traffic simulation models have been widely and increasingly applied for the assessment of transportation systems, traffic operations, and management alternatives because simulation is cost cost-effective, allows for a risk-free assessment, and provides an efficient assessment approach. However, without calibration, there is no assurance that the model's outputs are reliable or that the model will correctly predict the traffic performance expected in the real-world. Calibration is the adjustment of model parameters to improve the model's ability to reproduce local traffic conditions.

VARIABLE SPEED LIMIT

Traffic congestion is a critical social issue that is encountered on a daily basis. It appears in the peak hour when too many vehicles attempt to use a common roadway with limited capacity. It is a source of productivity and efficiency loss, fuel wastage, and excessive air pollution. The

areas that mostly suffer from these problems are large cities and freeways. Expanding road infrastructure is one of the solutions, but often is constrained by the limited availability of right-of-way and capital investments. More efficient use of existing road networks is a promising solution that transportation practitioners are examining. Therefore, there is a tremendous need to understand the effects of different dynamic control methods on freeway operations, as well as to identify cost-effective control strategies to address identified issues with operations. Advanced Traffic and Demand Management (ATDM) strategies, such as ramp metering, variable speed limits, and Connected Vehicles, are among the methods that are increasingly being considered to improve the efficiency of the existing freeway systems.

Static speed limits are designed to provide motorists with a safe driving speeds. While these safe speeds are effective during ideal conditions, they fail to provide recommended safe speeds during adverse weather or congested driving conditions (*56*). Variable Speed Limit (VSL) systems dynamically adjust the speed limit based on the prevailing traffic condition, road surface condition, and weather condition information. Such strategies are used to deal with congestion, incidents, weather and/or special events by reducing congestion impacts and crash risk. Infrastructure based dynamic message signs are used to disseminate the VSL to drivers, although in-vehicle information devices can also be used.

Over time, two general applications have evolved for the use of speed limits. The first emphasizes the safety benefits of VSL, such as reducing the number of rear–end collisions and traffic homogenization (*57*); whereas the second is more focused on avoiding or mitigating traffic flow breakdown by reducing the input flow at bottlenecks using VSL (*58*). For this second type of application, the VSL signs are installed upstream of the bottlenecks, with recurring congestion as a way to reduce the speed of the congestion build-up shockwave produced once congestion starts.

A theoretical study by Kohler (*59*) showed that when the headways in a chain of vehicles are below a certain bound, the traffic becomes unstable. The inhomogeneities in the traffic stream readily lead to the small disturbances needed for congestion to set in. Inhomogeneities can be raised from speed differences between consecutive vehicles in one lane, speed differences among lanes, or flow differences among lanes. Through the use of VSL control, traffic planners hope to achieve a more uniform distribution of traffic density over freeway links, thereby preventing the high traffic density that leads to traffic breakdown.

This section first summarizes the known the effects of implementation of VSLs in the real-world. Then, it provides an overview of the evaluation of VSL algorithms conducted in past research using simulation. Finally, it summarizes driver behaviors around VSLs, as reported in previous studies.

Implementation of VSLs

VSL systems have been implemented in some locations in the UK, Netherlands, USA, Germany, Australia, and New Zealand to control speed. Currently, there is a very limited amount of documentation describing the quantitative safety and operational impacts. Mobility-related benefits have been derived mostly from the use of simulation. However, safety benefits were documented for several of the systems based on real-world data.

Most of the VSL systems were implemented as safety countermeasures to address adverse weather conditions. In Tennessee, a VSL system was implemented in 1993 along a 19-mile freeway segment on I-75 utilizing 10 signs. This system's goal was to reduce the occurrence of crashes due to visibility reduction during adverse weather conditions, especially fog. The posted speed limits and messages were automatically selected based on data collected using

environmental sensor and vehicle detectors. The system had the ability to close down the entire stretch of roadway during severe fog conditions and divert traffic. There were no crashes due to fog after the system was implemented (*60*).

In Arizona, a VSL system based on a fuzzy control algorithm was implemented in 1998 along I-40 in order to find appropriate speeds for different weather conditions and road surface conditions (*61*).

In Washington, a VSL system was implemented in 1997 (and is still active) on I-90 across the Snoqualmie Pass. The system's goal was to improve safety and inform motorists of road conditions and weather information. It was found that VSLs may lose their effectiveness without enforcement by the State Patrol and that VSLs reduce the mean speed and increase the speed standard deviation (*61*, *62*).

In the Netherlands, a VSL system was installed in 1991 along the A16 motorway on a 7.4-mile segment utilizing 16 signs. The system's goal was to improve safety during fog conditions. The posted speed limit was automatically switched and selected based on the visibility and crash occurrence. The normal posted speed limit was 62 mph, and if the visibility dropped below 460 feet, the posted speed limit would be reduced to 50 mph; and for visibility below 230 feet, the posted speed limit would be 37 mph. Furthermore, when an incident was detected, a speed limit of 31 mph was posted on the first sign upstream of the incident, and 43 mph on the second sign upstream of the incident (*60*). Zarean et. al (*63*) evaluated this system and showed that drivers reduced their mean speeds by about 5-6 mph during fog conditions.

Rämä (*64*) conducted a more detailed study on weather-controlled speed limits and signs. The study looked at two scenarios compared to a control case: one in the summer where the maximum speed limit was 75 mph, and one in the winter where the maximum speed limit was 62

mph. The control cases were the normal operating procedures in the summer and winter months. In the winter, during adverse road conditions, the speed limit was lowered to 50 mph. A 2.1 mph decrease in speeds was observed. It was noted that during adverse conditions, when it is harder for drivers to observe VSL sign, that affect driver visibility, the VSL was very effective in reducing the speeds compared to the control case. The study showed that the VSLs decreased the mean speed and standard deviation of speeds.

Several VSL systems were implemented to smooth flow and reduce congestion-related crashes. A study of European VSL implementations shows that VSLs can stabilize traffic flow in congestion and thus decrease the probability of crashes. However, some of the cases in the United States show that the VSL system failed to improve mobility. The first variable speed limit system in the United States was implemented on a 3.2-mile freeway segment of M-10 in Detroit, Michigan in 1960, and it had 21 VSL sign locations. The system was designed to alert motorists to slow down when approaching congestion and accelerate when leaving a congested area. The posted speed limits were manually switched and selected by the operator based on CCTV and plots of freeway speeds. The posted speed limits were allowed to vary between 20 mph and 60 mph, with an increment of 5 mph. The evaluation results showed that the VSL system failed to improve the situation and had no effect on vehicle speeds. The system was terminated sometime after 1967 (*60*).

In New Jersey, a VSL system was implemented in the 1960s along the New Jersey Turnpike, on over a 148-mile freeway segment utilizing 120 signs. This system's goal was to reduce speed limits during congested conditions. Later, the system became part of ITS system that warns drivers of lane closures and crashes to improve safety and mobility. The posted speed limits were automatically switched and selected based on the average travel speeds. The posted speed

limits were allowed, varying between 30 mph and the normal posted speed limit (65 mph, 55 mph, or 50 mph, depending on the freeway segment) with an increment of 5 mph. The main six conditions that caused the switching of the posted speed limits were: vehicle collisions, traffic congestion, construction, icy road conditions, snowfall, and fog. Based on the Turnpike Authority observation, the system's performance was satisfactory. They noted, however, that the system needed enforcement by the police (*61*, *62*).

In Florida, a VSL system was implemented in 2008 along a 9-mile portion of I-4. The system's goal is to enhance safety during congestion. Traffic conditions are classified as either free-flow, light congestion, or heavy congestion, based on occupancy. The posted speed limits are supposed to be 30 mph for heavy congestion (occupancy greater than 28%), 40 mph for light congestion (occupancy between 16%-28%), and the normal speed limit, 50 mph for free-flow (occupancy less than 16%). The speed limits were selected automatically every 120 seconds. Each sign is linked to two or three downstream detectors, and the occupancy value is averaged between them. The system also ensures that the posted speed limit does not change by more than 10 mph between two adjacent sets of VSL signs (*65*). In an evaluation study, it was determined that since vehicles were not complying with the reduced speed limits, the VSL system was not effective (*66*).

In England, a VSL system was implemented in 1995 on the M25 motorway on a 14-mile segment with 23 VSL signs. The system's goal was to smooth traffic flow by reducing stop-start driving in order to respond to congestion. The posted speed limits were decreased from 70 mph to 60 mph when the volume exceeded 1,650 vehicles per hour per lane (vph/lane), and further lowered to 50 mph when volume exceeded 2,050 vph/lane. Each VSL sign is linked to a downstream detector location. Evaluation of results showed that the traffic accidents decreased by 10-15%, and the compliance rate with the VSL system was a very high (*60*).

Another example of using VSL to improve safety is the implementation in Seattle, Washington in 2010. The overhead signs display individual speeds for each lane and warn of approaching lane closures and traffic congestion. The posted speed limit varies from 40 mph to 60 mph, based on speed and volume data. The speed limit is enforced by the Washington State Patrol (*67*).

In Sweden, a VSL system was installed in 2004 along the E6 motorway in Mölndal. At first, the VSL was implemented as an advisory speed limit, but was later changed to an enforceable speed limit. Lind (*68*) tried to determine how the VSL was perceived by motorists in both the enforceable and advisory implementations. Before the VSL system was implemented, the posted speed limit was 43 mph. The speed limit for free-flow conditions was raised to 56 mph. In dense traffic, the posted speed limit was reduced in a stepwise manner. At a traffic flow rate of 950vph/lane, the speed was reduced to 43 mph. It can be further reduced to 31 and 17 mph, depending on the density. Two-thirds of interviewed drivers indicated that they supported the VSL and considered reductions of queue lengths and hectic driving scenarios as benefits of the system. When the advisory speed limit was displayed, the crashes were reduced by 20%, and when the enforceable speed limit was displayed, the crashes were reduced by 40%. The results showed an increase in the average speed for all driving conditions, and as much as a 25 mph increase in potential queue formation scenarios.

In some cases, the VSL system focuses on special types of vehicles. In Denver, Colorado, a VSL system was implemented in 1995 along the Eisenhower Tunnel on I- 70. This system's goal was to enhance truck safety by displaying vehicle-specific safe operating speeds for long downgrades. The posted speed limit for the trucks was computed automatically based on the truck weight, speed, and axle configuration. The speed limit was advisory, and evaluation results showed

that truck-related accidents declined on the steep downhill grade sections after the implementation of the VSL system, even though the truck volume increased (*60*).

Young (*69*) studied the effectiveness of VSL signs on a 100-mile stretch of I-80. The study showed that the average vehicle speeds were reduced by 0.47 – 0.75 mph for every 1 mph reduction in the posted speed limit. Lee et al. (*70*) found that for highly congested locations, the VSL provided a reduction in a crash potential of 25%, but it increased travel time.

Papageorgiou et al. (*71*) studied the impact of VSLs on the flow-density fundamental diagram through simulation of a motorway in Europe. The posted speed was selected based on a threshold control algorithm, with possible speed limits of 60 mph, 50 mph, and 40 mph. The study showed that the 50 mph setting resulted in the highest improvements in traffic flow. The 40 mph setting was useful at high occupancies for safety reasons, but it did not improve the mobility. They explained the impacts by utilizing the flow-density fundamental diagram and showing a decrease in the slope of the relationship under-critical conditions, shift of the critical density to higher values, and higher flows at the same occupancy values in overcritical conditions.

Several studies showed that the mean speeds decrease when a VSL is implemented, indicating that the VSLs do affect the speed at which motorists drive. Several studies that showed the speed standard deviation is also expected to decrease, which is associated with safety benefits. Although the safety benefits of implementing the VSL control have been well-established, most of the previously developed VSL control strategies' effects on improving traffic flow efficiency and the impacts on capacity is unclear (*59*). Based on this literature review, a very limited number of implemented VSL systems have documented improvement on traffic mobility. The VSL system called "SPECIALIST," presented by Hegyi et al. (*72*), showed improvement in traffic mobility. This VSL system is implemented in order to deal with moving congestion by reducing inflow

traffic to congested area. This strategy successfully resolved 77% of shockwaves, resulting in a travel-time saving of 35 vehicle-hour per shockwave.

Evaluation of VSL Algorithms

Simulation is a very valuable tool for assessing the impact of changes in the transportation system and selecting optimal alternatives without actually implementing and testing them in the field. Most of the studies on VSL, especially for evaluating its impact on mobility and congestion, were conducted using simulation. The previously developed VSL algorithms developed for traffic mobility applications can be categorized into two groups: 1) reactive algorithms, which set the speed limit based on the current traffic conditions; and 2) predictive algorithms, which set the speed limit based on predication modules using current traffic conditions.

Lee et al. (*70*) used a crash prediction model to assess the safety effects of VSL based on the simulation model PARAMICS. With this model, three detector locations relay information to a controller that averages their values into one crash potential value. When crash potential exceeded the threshold, the speed limits were selected and reduced based on the average speeds. The normal speed limit is 55 mph and will be reduced to 31 mph if the average speed is less than 37 mph; 37 mph if the average speed is between 37 and 44 mph; 44 mph if the average speed is between 44 and 50 mph; and 50 mph if average speed is higher than 50 mph. The results found that the reduction in speed limits can reduce the average total crash potential, and the greatest reduction in crash potential is expected to occur at the locations with high traffic turbulence, such as at a bottleneck. However, the VSL also resulted in an increase of travel time.

Abdel-Aty et al. (*73*, *74*) evaluated the safety benefits of VSL on I-4 in Orlando, Florida using PAPAMICS. The algorithm reduced speeds upstream of congestion, and raised the speed

limits after a congested area. This study considered low-speed and medium- to high-speed as two speed regimes. The results indicated that the VSL system has safety benefits in the medium to high-speed regions; however, for the low-speed region, which is the congested area, the system did not produce safety benefits. The results also show that changing the speed abruptly outperforms gradual speed changes. Aside from safety benefits, this algorithm also decreased the travel time, according to the simulation analysis results.

Piao et al. (*75*) assessed the safety benefits of in-vehicle VSL instead of roadside VSL using the microscopic simulation model AIMSUN. VSLs were applied when the speed difference between a queuing section and the upstream section was greater than 12.5 mph. It was assumed that all vehicles were equipped with in-vehicle devices to communicate their speeds and receive VSL. The posted speed limits ranged between 62 mph and 37 mph, with a 5 mph increment. The simulation results showed that the VSL reduced speed differences, small time headways, small time-to-collision events, and lane change frequency. This overall reduction creates homogenization and reduces crash potential. The authors also indicated that large speed variations could occur because some vehicles did not have the in-vehicle device.

Hegyi et al. (*76*) developed and assessed a predictive model for coordination of VSLs to eliminate shockwaves at bottlenecks using the METANET simulation tool. The objective of this model was to minimize the travel time with safety constraints to prevent large speed limit fluctuations. It uses rolling horizon values to continuously update the optimal solution. The results showed that the model is successful in surpassing the shockwave, and it created a scenario with less congestion and higher outflow.

Lin et al. (*77*) assessed two online algorithms for VSL controls at highway work zone operations. The first algorithm focused on minimizing the queue upstream of the work zone

location by reducing approaching traffic speed so as to increase the average headway for vehicles to merge onto adjacent lanes; while the second one aimed at maximizing the throughput under some predefined safety constraints. The simulation results by CORSIM showed that the second algorithm produced more promising results than the first one in terms of reducing the speed variance, although the average speed did not change significantly.

Allaby et al. (*78*) evaluated the impacts of a candidate VSL system on a 5-mile section of the Queen Elizabeth Way in Toronto, Canada using the microscopic simulator PARAMICS. A VSL control strategy was designed to reduce vehicle speeds upstream of the bottleneck, in order to provide safer deceleration for vehicles approaching the queue and to increase the mean bottleneck speed by reducing stop-start conditions. The VSL algorithm was based on a decision tree that uses threshold values for flow, occupancy, and average travel speed. The base speed used was 62 mph, and it could be reduced to 50 mph and 37 mph based on the threshold values. If the volume is less than or equal to 1600 vphpl, the next step is to consider occupancy. If occupancy is less than or equal to 15%, the maximum speed limit (62 mph) is posted. If the occupancy is greater than 15%, the average speed determines which speed is displayed. If the volume is greater than 1600 vphpl, the logic skips straight to the calculation based on the average speed. Each VSL sign was linked to an adjacent loop detector, and each sign operates individually. The results of the simulation showed that the implementation of the VSL signs could significantly improve safety in higher congestion levels; however, the use of the VSL signs had negative impacts on travel time. The most desirable results were observed under moderate congestion.

Hegyi et al. (*76*, *79*) expanded their original work described earlier to modeling predictive control through coordination of VSLs and ramp metering. It was suggested that the VSLs should be used if the speed limits can limit the flow sufficiently; however, if the flow becomes too large,

ramp metering should be implemented. The authors suggested that the integrated use of both technologies can produce more favorable results.

Another study on safety and mobility benefits of the integration of ramp metering and VSL was done by Abdel Aty and Dhindsa (*73*) using PARAMICS. The result indicated that the VSL and ramp metering are more effective when integrated together. The best implementation strategy included speeds that were incremented by 5 mph over a half mile. It was indicated that for safety improvements, the best scenario was to only increase the downstream speeds.

Ghods et al. (*80*) investigated the use of ramp metering and VSL using METANET. They used an adaptive genetic-fuzzy algorithm to provide a corresponding metering rate and variable speed limits based on local speed, density and queue length of the on-ramp. Using fuzzy logic allows for input data to have partial membership to a category, as opposed to the traditional "crisp" membership or non-membership options. The study indicated that the genetic fuzzy ramp metering and VSL control improved the total time spent in the system (TTS) by 15.3%.

Carlson et al. (*81*) expanded the work of Papageorgiou (*71*) to explore the integration of ramp metering and VSL to address potential bottleneck or high volume merging situations using the METANET simulation tool. Four scenarios were evaluated: no-control, VSL control, ramp metering, and integrated control. The study showed that when applied upstream, the VSL can act similarly to ramp metering, where the flow is held back on the mainstream rather than on the ramp. The traffic arriving at the bottleneck is temporarily reduced, and the system delays the propagation of the congestion. The VSL case decreased TTS by 15.3%, and when VSLs and ramp metering are used in conjunction with each other, the TTS was reduced by as much as 19.5%. They concluded that VSL can improve traffic flow and capacity by reducing the capacity drop at

bottlenecks. However, at uncongested conditions, the VSL has negative impacts on mean speed and flow efficiency.

Elefteriadou et al. (*82*) evaluated the use of three different VSL algorithms: the VSL algorithm presented by Allaby et al. (*78*, *82*, *83*), the VSL algorithm implemented on I-4 in Orlando, Florida, and the VSL algorithm implemented on the M25 in England. The evaluation assessed the impacts of these VSL systems on two bottlenecks on I-95 in Miami, Florida using CORSIM. Different threshold values, as well as several different VSL sign locations, were tested. They concluded that the algorithms tested improved the mobility at bottlenecks and areas upstream of the bottleneck, and increased the throughput by a maximum of 120 to 360 vph. They found that the best performing algorithm and scenario is not the same for both bottleneck locations, and that the best sign location is not the same for all algorithms and scenarios. The results showed that improper selection of thresholds or sign positioning can cause negative impacts on traffic conditions; hence, they recommended an optimization-based study to obtain optimal thresholds, sign locations, and detector locations.

Talebpour et al. (*84*) explored the impacts of early shockwave detection on breakdown formation and safety. They used the Allaby et al. (*77*) speed limit decision tree with different thresholds. They found a significant improvement in traffic flow characteristics under congested conditions. The results indicate that a 10% compliance with the VSL is sufficient enough to achieve the desired outcomes. The results also suggest that finding the optimal location of speed limit signs is important because it is most effective. However, the authors recommend future studies on these findings.

Many researchers used the macroscopic traffic flow model METANET for testing their VSL strategies (*81*). Wang (*85*) compared the results of macroscopic simulation and microscopic

simulation. Although macroscopic simulation showed improvement in traffic flow, microscopic simulation studies did not show the same results and demonstrated that their proposed VSL could not improve the traffic flow. They concluded that macroscopic simulation, because it aggregates traffic data using a generalized car-following model, failed to capture individual vehicle transitory responses and the secondary shockwaves generated by the VSL system.

Driver Behavior around VSLs

As mentioned in the previous sections, one of the most important issues in implementing VSLs is driver behavior, and whether or not drivers will obey speed limit signs. There were a few projects, such as the I-4 project in Orlando, Florida, in which the VSL was not successful or effective because drivers were not complying with reduced speed limits (*65*). The effectiveness of a VSL system is dependent on the driver's acceptance and compliance rate of the system. Increased compliance of variable speed limits can be accomplished through enforcement strategies, and by making drivers more aware of the current speed limit and the specific strategies of VSL implementation.

Tignor et al. (*86*) suggested that the key to increasing compliance with VSL is automated enforcement. In England, automated enforcement improved compliance with VSL, resulting in a 5-10% increase in capacity, and a 25-30% decrease in the number of rear-end collisions. After the initial installation of auto-enforcement cameras, it was discovered that the flash produced by the cameras was enough to make drivers obey the posted speed limit as long as there were active cameras in a few locations. For this reason, locations of actual cameras were rotated so that drivers would never know which cameras were actually taking pictures.

Rämä (*87*) studied the effect of warning messages on VSL compliance in Finland. The VSL posted two speed limits: 62 mph during good road conditions, and 50 mph during adverse weather conditions. It was shown that during poor weather conditions, providing a warning message with the speed limit reduced the mean speed by 1.55 mph, while the mean speed was higher if the speed limit was posted without a warning message. The author suggested that there would be more of an acceptance of VSLs if drivers knew why the speed limits were being reduced.

Brewer et al. (*88*) investigated the effectiveness of several speed control devices, such as a speed display trailers, DMS with radar, and orange border speed limit signs on the compliance with speed control in work zones. The results indicated that drivers will reduce their speed when their actual speed is displayed. However, adding an orange border to a speed sign does not greatly increase the compliance, even though it increases the visibility of the sign. Based on data from the study, the authors concluded that drivers will travel at the speed at which they feel the most comfortable with, unless they are aware of potential enforcement.

CONNECTED VEHICLE TECHNOLOGY

As stated before, road mobility significantly contributes to the society's economy and welfare. However, the increase in the number of vehicles is creating new problems, such as longer travel times and reduced travel time reliability. To address these challenges and ensure a safe and efficient transportation system, advanced vehicle technologies are being developed by automobile manufacturers and after-market companies. These technologies can be categorized into two major groups: Assisted Driving Systems/Autonomous vehicles and Connected Vehicle.

This section presents a review of previous research on assisted driving systems and Connected Vehicle technologies and their applications, as related to this effort.

Assisted Driving System

Driver assistance systems are based on the idea that an on-board computer can assist drivers with a more comfortable and safer drive by using sensors and cameras connected to a central vehicle information system that recognizes potentially dangerous situations. This system provides warnings to the driver or directly intervenes in the driving process by braking or accelerating. These types of systems can be classified as the following: side assist, front assist, brake assist, blind corner monitor and parking, and rear assist. This technology could affect the flow of traffic, particularly with respect to car-following, lane-changing and gap acceptance characteristics (*89*).

Elefteriadou et al. (*89*) evaluated assisted driving systems, focusing on two technologies: Adaptive Cruise Control (ACC) and Lane Change Assist (LCA) by using the micro-simulation software CORSIM. CORSIM was modified to model assisted driving technology. The evaluation considers different demand and market penetration scenarios.

The ACC technology allows the vehicle to decelerate when getting closer to the preceding vehicle and accelerate again to the preset speed when traffic allows, using either a radar or laser technology setup. The driver is able to choose the desired maximum speed and the time headway derived automatically by the vehicle's equipment. The LCA also provides warnings to drivers of traffic presence at a target lane while a driver is changing lanes, as indicated by the driver activating a turn signal (*89*).

The simulation results indicated that, for lower demands, the ACC results in slightly increased speeds, while in congestion, the ACC increases the speed significantly. Congestion is

eliminated even for the lowest market penetration scenario tested (20% ACC). One potential disadvantage of the ACC is that bottlenecks can be created at locations where a significant number of drivers are likely to turn their ACC off. The ACC is based on the concept of constant time headways, and it results in a decrease in throughput because the ACC produced, on the average, longer time headways. When LCA technology was present without ACC, the number of lane change maneuvers and throughput increased, but the travel time remained constant. When both LCA and ACC were present, conditions improved significantly (*89*).

Connected Vehicles

In the United States, the Connected Vehicle (CV) effort has been led, in a significant part, by the United States Department of Transportation (USDOT). It is envisioned that every car manufactured in the U.S. will be equipped with a communications device and a GPS unit. The goal is to provide a communications link between vehicles on the road (vehicle-to-vehicle communication – V2V)and an instrumented road system (vehicle-to-infrastructure communication – V2I) in order to increase the safety, efficiency, environmental sustainability, and convenience of the transportation system.

The Connected Vehicle concept is supported by the development and prototyping of a particular type of wireless communications technology, referred to as dedicated short-range communications (DSRC). DSRC is a main contender for a communications method due to its technological advantages, such as fast, secure, two-way and broadband connections in a mobile environment. It is the only technology that meets the requirements for the safety applications of CV (*90*). DSRC allows drivers within a certain distance of each other to be connected. That means

two vehicles or a vehicle and infrastructure can exchange information only when their distance is less than a certain distance.

Although DSRC communication is required for safety application, cellular communication technology satisfies many mobility applications of Connected Vehicle. In all likelihood, combinations of Connected Vehicle with DSRC and cellular communication technology will be used in the future, in combination with the autonomous vehicle technology described in the previous section.

V2V Applications

Using Vehicle-to-Vehicle (V2V) communication, each vehicle will know where other vehicles are located, whether in blind spots, stopped ahead on the highway but hidden from view, around a blind corner, or blocked by other vehicles. In fact, V2V has the ability to replace all of the sensors and cameras with one advisory sensor that provides all-around, instantaneous traffic intelligence. This promises a better and significantly less costly way of sensing other vehicles in the vicinity while driving. The information received from the devices can be transmitted to the driver through visual, audible and tangible warnings.

Park et al. (*91*) evaluated the deployment of freeway merge assistance to provide advisory messages at heavy weaving areas through V2V using VISSIM simulation. The evaluated algorithm calculates the acceleration rates and headway based on the collected gap information on freeway lanes. If the headway is greater than a minimum safety distance, the advisory is produced. The results indicated that in addition to safety benefits, this assistance can improve the mobility as well; however, it requires at least a 90% compliance rate to work properly.

Rim et al. (*92*) developed a travel time estimation model that uses V2V and V2I to estimate lane-level travel times. They modeled a 4.6-mile highway segment in the VISSIM simulation software. They found that with a 20% or higher market penetration, a mean absolute relative error in travel time estimation of 6% to 8% is achievable.

Ni et al. (*93*) considered a more general scenario, which incorporates three types of driving modes enabled by Connected Vehicle technology: non-CV, CV assisted, and CV automated. In the CV-assisted mode, drivers receive advisories and safety warnings, while in the CV-automated mode, a vehicle is operated by CV-enabled automatic driving features; however, the driver may take over at any time. The purpose of their study was to estimate the capacity benefits of CV technology using CORSIM simulation. The results indicated a 20% to 50% increase in capacity when CV is fully deployed.

V2I Applications

One type of application of Connected Vehicle is the safety application, which is designed to increase situational awareness and reduce or eliminate crashes. There are various types of safety applications; three main safety applications of Connected Vehicle are the suggestive messages advising drivers about potential dangers, urgent messages warning drivers for taking immediate actions, and secondary actions taken by vehicular control when drivers fail to comply with warnings or advisories. For example, the cooperative Intersection Collision Avoidance System (CICAS) is a major application that aims to improve intersection safety using these three applications (*89*). According to a study by Najm et al. (*94*), these applications could potentially address about 75% of all crashes involving all vehicle types.

The Connected Vehicle technology promises to provide a data-rich travel environment. One important application of the V2I is probe vehicle data collection. The transportation communications network captures real-time data from on-board units located inside vehicles such as automobiles, trucks, and buses. The three major elements in V2I communication for collecting probe data are: On-Board Unit (OBU), Roadside Equipment (RSE), and a mobile communication technology such as DSRC. OBUs are installed in vehicles to record vehicle activity data during certain time intervals. These recorded activities are called "snapshots," which include data such as speed, position, turn signal activation, brake status, airbag activation and so on. OBU memory size is limited, and the total number of snapshots that can be stored in these devices is called the "buffer size." When a vehicle enters a RSE coverage range, the information is transmitted to the infrastructure and the memory of the OBU is cleared.

Periodic snapshots are recorded at set time intervals. Based on current protocol (SAE J2735), the recording time interval is set based on the vehicle speed. If the speed is greater than 60 mph, the recording time of travel is 20-second intervals. For speeds less than 20 mph, the snapshots are recorded at 4-second intervals. For speeds between 20 mph and 60 mph, a linear interpolation is used to calculate the intervals. When a vehicle does not move for five seconds, periodic snapshots are no longer recorded. When the speed exceeds 10 mph, the snapshots are recorded again. Event-triggered snapshots are recorded when vehicle status elements change (such as airbag activation). However, Dion et al. (*95*) recommended fixed-interval snapshots, preferably at short intervals. Also, they recommended recording snapshots while the vehicles are stopped.

Shladover and Kuhn (*96*) investigated the quality of Connected Vehicle probe data for adaptive signal control, incident detection, and weather condition monitoring systems. Assuming 100% market penetration, they concluded that the data collected based on current probe data

protocol provides an acceptable representation of normal traffic conditions, assuming 1- to 2-minute data latency is acceptable.

Dion et al. (*95*) evaluated the probe data generated in the Connected Vehicle environment using the Paramics traffic simulation software. They performed sensitivity analysis on the effect of the number of RSEs, RSEs communication range, OBU buffer size and snapshot generation interval, and market penetration on the utility of probe data. They also investigated the quality of link travel time estimates from Connected Vehicle probe data.

Kianfar et al. (*98*) investigated a Genetic Algorithm-based optimization method to find optimal placements of RSEs in the urban network for the purpose of travel time estimation using the VISSIM traffic simulation software. The results suggested that in order to improve accuracy for limited number of RSEs, the travel time estimation interval should be increased.

Li et al. (*99*) developed an event-based method that uses probe data and signal timing to estimate the queue length. Different from data collected using loop detectors, probe data can provide a lower bound on the queue length even if the market penetration rate is low. The result showed when the penetration rate is 50%, the mean absolute percentage error (MAPE) is less than 18%; and, for low penetration such as 10%, MAPE is around 60%.

Because traffic flow information is not a reliable indicator of congestion, Kattan and Saidi (*100*) developed a probe-based adaptive ramp metering based on CV data and compared the results with a detector-based and pre-timed ramp metering approach using PARAMICS micro-simulation. The probe-based approach takes as its main input the space mean speed extracted from vehicle probes moving constantly on the entire freeway. The results indicated that the probe-based algorithm outperformed the two other algorithms. The sensitivity analysis showed that larger penetration rates would not significantly change the results. A 10% penetration rate is expected to

be enough for a reliable probe-based ramp metering. The results showed that the probe-based ramp metering still performs better than other algorithms at low penetration rates like 3%. However, for very low penetration, such as 1%, the detector-based algorithm produces better results.

Instead of relying on limited data from point detectors, Goodall et al. (*101*) developed a rolling horizon traffic signal control algorithm called the "predictive microscopic simulation algorithm (PMSA)" to minimize delay over a 15-second period using data from V2I connections. Simulation results showed that with greater than a 50% penetration rate at low- and mid-level volumes, the algorithm is able to significantly improve the performance. However, the performance worsens during saturated and oversaturated conditions.

Recently, CV data was used in queue length estimation. In the literature, researchers used this estimation to increase the effectiveness of adaptive traffic signal controllers and avoid queue spillback upstream intersections. Christofa et al. (*102*) developed two different queue spillback detection methods based on Connected Vehicle data. The first one, called "gap-based detection," is based on the stopping position of the last equipped vehicle that joins the queue. The second method, the shockwave-based detection, is based on Connected Vehicle data and signal timings of the upstream intersection. The results showed that for different penetration rates, both methods can detect the occurrence of spillbacks in more than 80% of the cycles. Venkatanarayana et al. (*103*) used the position of the last Connected Vehicle in the queue to find the queue length. Comert and Cetin (*104*) presented a method based on distribution of the number of queued vehicle and market penetration rate and the position of the last Connected Vehicle to find the number of vehicles in the queue. Even if one CV is queued, their methodology is able to estimate the queue length.

Connected Vehicle technology was also recommended for transit sign priority. With real-time data about passenger loadings and current schedule adherence, the priority can be set more

intelligently, which makes public transportation more efficient (*105*). Liao et al. (*106*) conducted a simulation study to take advantage of the already equipped GPS/automatic vehicle location system on the buses. The results indicated up to a 15% decrease in bus travel time during peak hours.

SUMMARY

In this chapter, a comprehensive review was prescribed first on topics related to traffic breakdown, and micro-simulation calibration. Since traffic simulation models are widely used and increasingly applied for the assessment of transportation systems, it is important to have a well-calibrated model in order to have a reliable assessment.

Later in this chapter, VSL systems implemented in the real-world are reviewed and their effects on traffic safety and mobility are discussed. Active Traffic and Demand Management (ATDM) strategies such as variable speed limit (VSL) are state-of-the-art methods that are increasingly being considered to improve the efficiency of the existing freeway system. VSL strategies identify and disseminate the appropriate speed limit based on the prevailing traffic conditions, road surface conditions, and weather conditions. Although the traffic safety benefits of implementing the VSL system in the real-world are well-established, very few of the previously developed VSL strategies have documented improvement on traffic mobility. Finally, a review of different applications of Connected Vehicle was conducted.

CHAPTER 3

SIMULATION CALIBRATION

INTRODUCTION

As stated earlier, microscopic simulation has been used to assess advanced strategies to reduce the probability of breakdown such as ramp metering and VSL strategies. Well-calibrated simulation models are critical to achieving the specific objectives of the calibration process; this process must consider the simulation project's objectives. As mentioned in the previous section, researchers developed methodologies and guidelines for traffic simulation model calibration and validation. One of the most important and widely used guidelines in this regard is the Federal Highway Administration's guideline presented in the Traffic Analysis Toolbox Volume III and IV (*19*, *107*). The calibration methodology according to the FHWA guidelines consists of three steps: 1) capacity calibration, 2) traffic volume calibration, and 3) system performance calibration. The calibration procedure developed in this study extends the FHWA procedure by including an additional step that involves the consideration of breakdown characteristics, which is critical for successful assessments of advanced traffic management strategies that address breakdown when using simulation models for this purpose.

CALIBRATION METHODOLOGY

Figure 3-1 shows an overview of the modified calibration procedure presented in this research. In this figure, the additional step, which shows the breakdown characteristics calibration process, is highlighted by the dotted line.

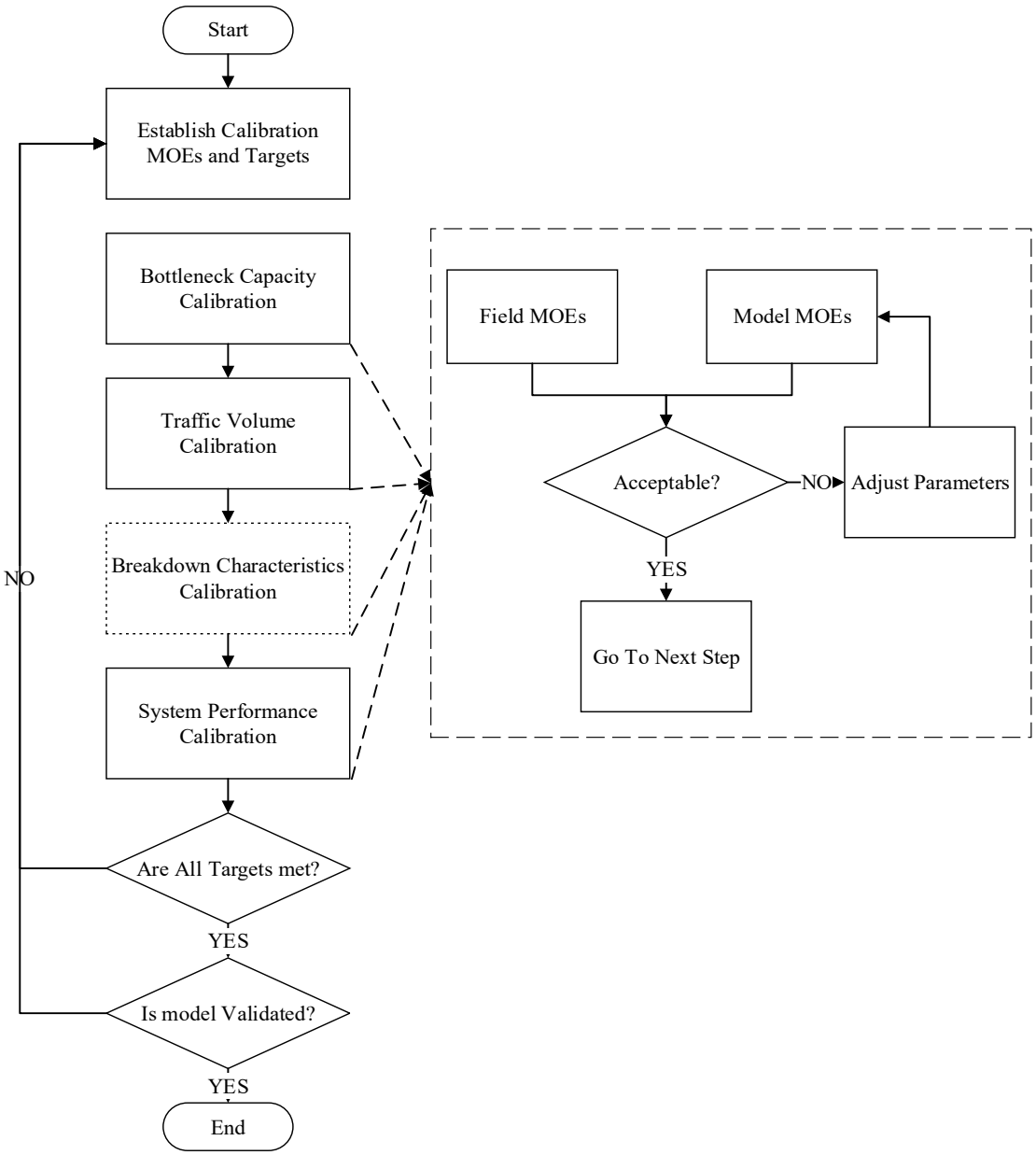

Figure 3-1. Flowchart calibration procedure.

In this research, the procedure is tested using the CORSIM micro-simulation tool (Version 6.2). CORSIM is a stochastic micro-simulation model that was developed based on the FHWA's developments of simulation models in the late 1970s, and consists of two traffic simulation models: (a) NETSIM for simulating arterials, and (b) FRESIM for simulating freeways. The CORSIM

micro-simulation model has three main sets of calibration parameters related to driver behavior on freeways: free-flow speed, car-following, and lane-changing parameters. The free-flow speed parameters in CORSIM consist of the mean free-flow speed and the free-flow speed multipliers. The mean free-flow speed is a link-specific parameter. Using the HCM procedure, the free-flow speed can be estimated as follows:

$$FFS = 75.4 - f_{LW} - f_{LC} - 3.22TRD^{0.84} \quad (3\text{-}1)$$

where FFS is the estimated free-flow speed (mph); f_{LW} is an adjustment factor for lane width (mph); f_{LC} is an adjustment factor for right shoulder lateral clearance (mph); and TRD is the total ramp density (ramp/mile). The free-flow speed can also be estimated based on field estimation. The free-flow speed multiplier is a global parameter, and it is a percentage multiplier for each driver type of the mean free-flow speed. A more aggressive driver receives a higher multiplier reflecting a higher free-flow speed. The multiplier specification provides a distribution of free-flow speed by driver type.

CORSIM uses the PITT car-following model, which incorporates the vehicle spacing and speed differential between the lead and following vehicle as two independent variables, as follows:

$$d_{FL} = L_L + PITT + ku_F + bk(u_F - u_F)^2 \quad (3\text{-}2)$$

where d_{FL} is the vehicle spacing between the front bumper of the lead vehicle and front bumper of following vehicle, L_L is the lead vehicle length, $PITT$ is the PITT car-following constant, k is the driver sensitivity factor, b is a calibration constant that equals 0.1 if the speed of the following vehicle exceeds the speed of the lead vehicle, otherwise it is set to zero, u_F is the speed of the following vehicle, and u_L is the speed of the lead vehicle. Basically, the rule is that the follower

vehicle maintains a safe distance gap from the leader vehicle, and in the case where the gap is not sufficient, the follower vehicle decreases the speed. The default car-following sensitivity factors for CORSIM, which reflects the aggressiveness of the drivers and governs how vehicles follow each other, are represented by a discrete distribution that starts with a value of 1.25, which decreases at an increment of 0.10 by driver type to a value of 0.35 for the most aggressive drivers. The calibration of the driver sensitivity factor can be achieved by changing the driver distribution, which is a global parameter and/or changing link-specific adjustment parameter.

Lane-changing can be categorized in three groups: 1) mandatory due to blocked lane, exiting freeway or lane drop; 2) discretionary is based on whether the driver is satisfied with driving conditions on his/her current lane, and 3) anticipatory because of warning signs. The lane-changing algorithm inputs are affected by the characteristics of drivers, vehicle performance, and prevailing traffic conditions. In CORSIM, the lane-changing algorithm can be calibrated using a number of parameters, including the time-to-complete-a-lane-change, the gap acceptance parameter, the percent driver yielding at merge point, the multiplier that simulates the desire for a discretionary lane change, and the advantage threshold for a discretionary lane change. As mentioned above, there are a large number of parameters to be considered when calibrating a microscopic model like CORSIM, which translates into a number of combinations of these parameter values. In addition, many of the parameters are continuous variables rather than discrete, increasing the number of possible solutions. The complexity of the calibration can be illustrated by considering the following example. If 10 parameters need to be modified in the calibration and each discrete parameter has 5 levels, then there are 5^{10} = 9,765,625 combinations that need to be tested. As reported in the reviewed literature, many of proposed heuristic optimization-based calibration approaches require long simulation running times and may produce parameters that are

not notably different from manually calibrated parameter sets. Furthermore, in some cases, these methods fail to consider important aspects of the modeling process that can be captured by experienced modelers using manual calibration. Optimization methods can still reduce the effort required for calibration and the dependency on the expertise and judgment of the users. A manual trial-and-error calibration approach is used in this study. However, the concepts discussed hereinafter can be extended to automated calibration methods in future works.

Capacity Calibration

Identifying the locations of bottlenecks is the first step in capacity calibration in simulation modeling. There are several methods for identifying bottlenecks. With the increased deployments of traffic detectors associated with traffic management systems, the simplest way to identify bottleneck location is by using traffic detector-measured speed. The approximate bottleneck location is between the most downstream detector with congestion and its downstream detector location at free-flow condition. According to the FHWA simulation guidelines (*19*), a visual audit can be used as the primary method for identifying bottleneck locations. Utilizing contour maps is a widely used method to visualize traffic conditions. Speed, volume, or occupancy can be visualized on a time-space diagram utilizing a color scheme representing the range of traffic conditions. These maps can be used as an effective tool for bottleneck analysis, since they provide a clear image of existing traffic conditions, including the locations of the congested areas and the extent of congestion. However, it is important to consider multiple days in the analysis to ensure that a bottleneck is a recurring bottleneck and that the model is not over-fitted to one day. If incident and weather data are available, then the days with incidents and bad weather conditions should be isolated in the analysis.

The HCM procedure allows for calculating capacity based on the geometric conditions of the facility and treats it as a deterministic value. However, it is preferable to measure capacity based on the maximum flow before breakdown and the queue discharge rate during congestion in the field to account for site specifications. The queue discharge rate is defined as the long-run average of flow during the breakdown period. The maximum pre-breakdown flow was measured at different aggregation intervals, such as one minute, five minutes or fifteen minutes immediately before the breakdown occurs. Figure 3-2 shows how the pre-breakdown flow and queue discharge rates are identified in this study, based on the above discussion. The FHWA guidelines recommend the use of the queue discharge rate as the capacity in simulation model calibration, since it is more stable and easier to measure. For modeling and assessing the benefits of advanced strategies that seek to prevent or delay breakdown, it is important to examine both the maximum pre-breakdown flow and queue discharge rate. Thus, in this research, both parameters are considered in the calibration. This is important since estimating accurate capacity drops, which is the difference between the maximum pre-breakdown flow and the queue discharge rate, which is necessary to evaluate the advanced alternative strategies that are proposed to reduce congestion. It is not clear whether the calibrated simulation models will be able to replicate the drop in throughput due to the difference between pre-breakdown capacity and queue discharge rate. This study, in addition to pre-breakdown flow and queue discharge, considers the fundamental diagram for further capacity analysis. Fundamental diagrams are constructed from both simulation runs and real-world data to present the flow-occupancy relationship at the bottlenecks. This fundamental diagram is important since it shows the variation of capacity between days; also it can show the critical density where flow reaches capacity, among other things, which are important to modeling breakdown.

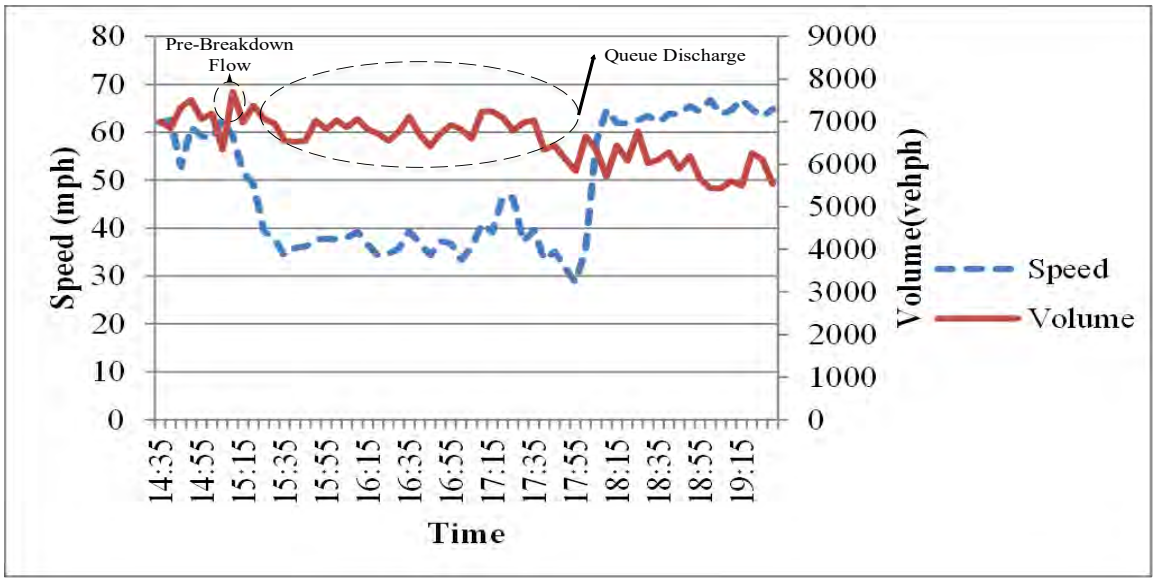

Figure 3-2. Pre-breakdown flow and queue discharge rate estimation.

It is important that the micro-simulation model replicates the bottleneck locations and the capacities at these locations. At this stage, network-wide parameters, such as the car-following sensitivity factors and lag acceleration and deceleration time are fine-tuned for the purpose of capacity calibration. Later, as there may be multiple bottlenecks on the facility with different characteristics, the car-following sensitivity multiplier, which is a link-specific parameter, may need to be fine-tuned for each bottleneck individually. The link-specific parameter calibration does not mean only adjusting the link parameter for the bottleneck link, as it may need to adjust the parameter of upstream links, as well as to represent local conditions properly. In addition, this adjustment should be made to obtain measured or estimated capacity and queue discharge rate and not merely to produce the observed queue lengths.

Traffic Volume Calibration

Volume-based calibration will result in a model with volumes that are close enough to observed traffic volumes. In this study, a node diagram is used as an important tool to have a better understanding of the volume variation in space for each time interval (15 minutes in our case) compared to field data. The goal of the calibration process is to reach a good fit to real-world volume. Given that all input volumes are correct and verified and the bottleneck capacities are calibrated, this step is necessary to ensure correct parameters to eliminate any artificial bottlenecks in the simulations. This is achieved by changing calibration parameters, especially link-specific parameters such as the reaction points for the cars exiting at the off-ramps, which was found to have significant influence in creating artificial bottlenecks if not well set. Since this data is not available from field measurements, the right values are found using the trial-and-error approach to prevent the generation of unrealistic bottlenecks. As defined by FHWA guidelines, the MOE criteria used in volume calibration is defined based on Geoffrey E. Havers (GEH) statistics, as follows:

$$GEH = \sqrt{\frac{2(E-V)^2}{E+V}} \tag{3-3}$$

where E is simulation estimated volume and V is a field volume. GEH is computed at each time interval (15 minutes) for each individual link. At each time interval, GEH should be less than 5 for at least 85% of freeway links. In addition, it is recommended to compute the GEH for the whole network by summation. The resulting network-wide GEH should be less than 4.

In order to come up with a well-calibrated model, the volume-related MOE statistics are estimated individually for each bottleneck location. For the most upstream bottleneck, the MOE statistics are calculated for the links upstream of that bottleneck and link-specific parameters are adjusted. Once the simulated output meets the criteria at this bottleneck location, the calibration

procedure moves to the next bottleneck. In other words, in each step, the focus is on calibrating the links related to one bottleneck, between the upstream bottleneck and this bottleneck to reach desirable results. This procedure continues until the entire network satisfies the calibration criteria. If all links have not been reached desirable and required accuracy, the procedure starts again.

Breakdown Characteristics Calibration

When modeling advanced strategies, the breakdown characteristics at the bottleneck, in addition to capacity and queue discharge rates, must be examined. Aside from the main causes of breakdown, traffic breakdown has other characteristics that need to be examined, as mentioned in the literature review, such as the average speed during breakdown, duration of breakdown and the beginning and end time of breakdown.

In addition to the abovementioned characteristics, the breakdown stochasticity is another important consideration. It was observed that, in the real-world, at the same bottleneck location and for the same combinations of ramp and freeway flows, breakdown may or may not occur. When it occurs, it can occur at different times. This stochastic nature of capacity has received a great amount of interest and attention among researchers in two areas: 1) its impacts on a freeway's capacity assumptions, and 2) finding the probability of breakdown occurrence based on upstream traffic conditions such as traffic flow, occupancy or combinations of the variables (*21*, *22*).

The goal of this research is to provide a procedure to extend the calibration of simulation models and also consider breakdown characteristics. This calibration, combined with the capacity and queue discharge calibration, is meant to consider the operations at the bottleneck location in a greater level of details, as needed when modeling strategies that prevent breakdown. As mentioned, there are different definitions of breakdown occurrence (section 3.1.1). Estimates of

the breakdown characteristics and bottleneck capacity depend on these definitions. In addition, traffic data contains noise, which reduces the accuracy of the estimated breakdown characteristics, such as the starting time of breakdown and its duration. Wavelet transform is an effective time–frequency decomposition tool that is widely used in analyzing and extracting information from non-stationary signal time-series. Wavelet transform is capable of identifying sharp changes in signals (*106*).

This research uses the definition presented by Elefteriadou et al. (*3*) and the wavelet transform method (section 3.1.5) to identify the start and end times of the breakdown, and the rest of estimates are based on this time window. After estimating the breakdown characteristics based on field measurements and simulation results, the link-specific parameters at the bottleneck locations are fine-tuned as necessary to simulate real-world conditions.

It is interesting to compare the real-world stochasticity mentioned above with the stochasticity of simulation models, described next. Stochastic simulation models output different results for simulation runs with the same inputs but different seed numbers. Thus, there is a need to run microscopic simulation models like CORSIM multiple times with different random seed numbers to account for the stochasticity of these models. The required minimum number of runs is determined based on the variance and the mean of the measures of effectiveness and acceptable confidence level, as follows:

$$n = \left(\frac{s.Z}{\varepsilon}\right)^2 \tag{3-4}$$

where n is the minimum required number of model runs; s is the standard deviation of the examined performance measures; ε is the required accuracy in the same units as performance measurement; and Z is the static value for a required confidence level.

Testing the adequacy of the sample size in volume-based calibration and system performance calibration based on Equation 3-4 is necessary. However, the stochastic nature of breakdown and capacity requires additional consideration of how bottleneck capacity and breakdown characteristics calibration vary in the simulation runs, compared to real-world variations. The FHWA guideline reported that the results from individual runs for the same demands but different seed numbers in CORSIM micro-simulation can vary by up to 25 percent. Higher standard deviations may be expected for facilities operating at or near capacity. The above discussion leads to two reasons that individual model runs, each with different seed numbers, should be considered individually when examining breakdown characteristics and capacity calibration rather than averaging the results from all runs, as is currently done:

1. If the real-world breakdown stochastic nature is to be replicated in simulation, in one model run the breakdown may occur at a specific time, and in another run it may occur in another time, or it may even not occur at all. As Figure 3-3 shows, using the average value of system performance results in smoothed values that dilute the high congestion levels in runs with longer traffic breakdown durations. In addition, when examining the changes in average performances such as speed from multiple runs with time, sharp changes in these measures indicating breakdown are also eliminated.
2. A question raised here: Can these variations between runs reflect real-world variations due to the stochastic variations in traffic stream characteristics? In other words, is a simulation model capable of assessing breakdown probability? This question has not been answered in the literature.

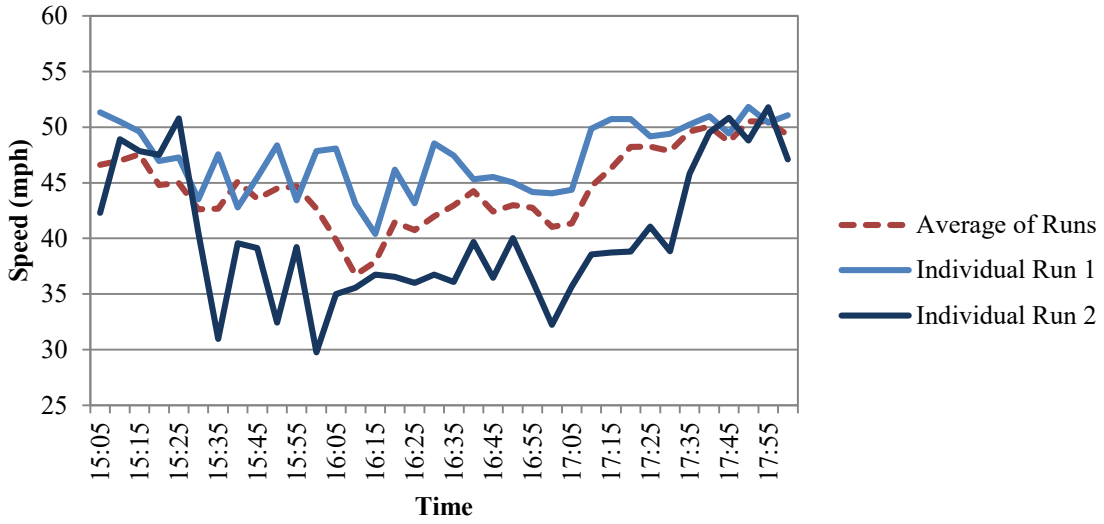

Figure 3-3. Speed data from CORSIM output for one individual run and average of runs.

This study considers the probability of breakdown as one of its main characteristics. As a result, in this step of calibration, the probability of breakdown based on the simulation model is compared with the probability of breakdown based on real-world data. For these reasons, individual runs will have to be considered when studying simulation abilities to assess breakdown characteristics and capacity.

The probability of breakdown is modeled using a large sample size of traffic data, such as volume or occupancy, at the bottleneck location and upstream location. The probability of breakdown can be developed using the Kaplan-Meier method, which is a product-limit method (*110*). This estimation is non-parametric. The distribution function of the breakdown occupancy, *F(o)*, is:

$$F(o) = 1 - \prod_{i:\, o_i \le o} \frac{n_i - 1}{n_i} \qquad (3\text{-}5)$$

where o is the freeway occupancy, o_i is the freeway occupancy during the breakdown interval i, and n_i is the number of intervals with a freeway occupancy of o. This probability is calculated in this study based on real-world multiple day detector data and simulation runs with different seed numbers, and the results are compared.

System Performance Calibration

This is the last step of the four-step calibration process. By now, the simulation model is calibrated based on bottleneck capacity, traffic volume, and breakdown characteristics. This step is to ensure that system performance measures such as speeds, queue lengths and congestion levels are similar to field data. Additional fine-tuning of simulation model parameters may be required at this stage. The FHWA guideline points out that the visual audit of speed profile should be used as an important tool for this purpose. Comparing speed counter maps of simulation results against field detector data will show the ability of the calibrated model to adequately replicate speed patterns at bottleneck locations, queue build-up and dissipation, and the extent of congestion.

In addition to the visual comparison, this study uses the correlation coefficient (r) as a goodness-of-fitness between simulation and real-world values, as indicated in the following equation:

$$r = \frac{1}{N-1}\sum_{i=1}^{N}\frac{(x_i-\bar{x})(y_i-\bar{y})}{\sigma_x\sigma_y} \quad (3\text{-}6)$$

where N is a number of volume estimates, x_i is the simulated volume estimate, y_i is the real-world volume estimate, $\bar{x}$ and $\bar{y}$ are sample average, and σ_x and σ_y are the sample standard deviation.

In addition, the simulation model is further calibrated using goodness-of-fit measures, including the mean absolute error (MAE), mean absolute normalized error (MANE), Theil's Inequality Coefficient, and root mean squared normalized percent error, (RMSNPE) as follows:

$$MAE = \frac{1}{N}\sum_{i=1}^{N}|x_i - y_i| \tag{3-7}$$

$$MANE = \frac{1}{N}\sum_{i=1}^{N}\frac{|x_i - y_i|}{y_i} \tag{3-8}$$

$$\text{Theil's inequality coefficient} = \frac{\sqrt{\frac{1}{N}\sum_{i=1}^{N}(y_i - x_i)^2}}{\sqrt{\frac{1}{N}\sum_{i=1}^{N}y_i^2} + \sqrt{\frac{1}{N}\sum_{i=1}^{N}x_i^2}} \tag{3-9}$$

$$\text{RMSNPE} = 100 \times \sqrt{\frac{1}{N}\sum_{i=1}^{N}\left(\frac{x_i - y_i}{y_i}\right)^2} \tag{3-10}$$

where N is a number of estimates, x_i is the simulated estimate, y_i is the real-world estimate. These measures are estimated for both speed and volume estimates.

MAE uses the absolute value of the difference between the observed and simulated measurements; thus, it gives equal weights to all errors, and consequently the measurements with larger errors will contribute more to the value of MAE. Some other measures (such as MANE, PRMSNE) depend on the normalized differences, which are percentage errors decided by actual value of measurements. Even for a small difference, a small value of a measurement generates a larger percentage error, which might lead to overemphasizing on a minor fluctuation that is common in the nature of traffic phenomena. Simultaneous consideration of these two types of measurements in the analysis will help avoid these common mistakes. Furthermore, Theil's Inequality Coefficient is used to analyze how well the simulation model is able to replicate the variability in the field data.

Wavelet Transform

A wavelet, $\psi(t)$, is a real or complex mathematical function. Wavelets can be categorized as discrete and continuous. Discrete wavelets are more efficient than continuous wavelets due to their ability to inverse the transform procedure to obtain data without noise (*111*). However, in this study we use continuous wavelets because we do not aim to analyze data with filtered noise, and furthermore, the continuous wavelet is more accurate. The general formulation of continuous wavelet transform (CWT), which is a wavelet transform coefficient (output) of a continuous signal $\chi(t)$, is:

$$T(\alpha,\beta) = w(\alpha)\int_{-\infty}^{\infty}\chi(t)\psi(\frac{t-\beta}{\alpha})dt \quad (3\text{-}11)$$

where α is the scale parameter, and β is the translation parameter. Scale parameter controls dilation and contraction of the wavelet, and translation parameter is about controlling the movement of the wavelet along the time dimension. The $w(\alpha)$ is a weighting function that normalizes the energy at all scales. This function is typically considered to be $\frac{1}{\sqrt{\alpha}}$. In this research, velocity, $v(t)$, is considered a continuous signal. Note that whenever $\alpha = 1$ and $\beta = 0$, wavelet function is called "mother wavelet." There are different popular wavelet families, such as Haar, Daubechies, Meyer, Gaussian, Mexican hat, Morlet, and Coifman. Finding the optimal mother wavelet is not important in practice since all of them provide similar results, which are almost optimal (*112*). Like Zheng et al. (*27*), Mexican hat wavelet, as defined in (3-11) and shown in Figure 3-4, was selected in this study to analyze traffic data. The Mexican hat mother wavelet is the second derivative of the Gaussian distribution function, $e^{-\frac{t^2}{2}}$.

$$\psi\left(\frac{t-\beta}{\alpha}\right) = \left(1 - \left(\frac{t-\beta}{\alpha}\right)^2\right) e^{-\left(\frac{t-\beta}{\alpha}\right)^2} \quad (3\text{-}12)$$

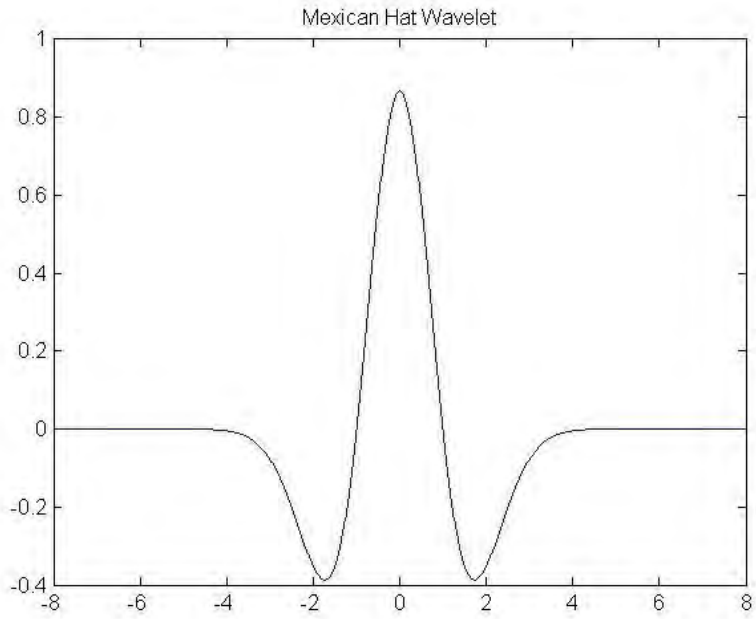

Figure 3-4. Pre-breakdown flow and queue discharge rate estimation.

By plugging (3-11) into (3-10), a wavelet transform of speed, $v(t)$, can be formulated, as follows:

$$T(\alpha,\beta) = \frac{1}{\sqrt{\alpha}} \int_{-\infty}^{\infty} v(t) \left(1 - \left(\frac{t-\beta}{\alpha}\right)^2\right) e^{-\left(\frac{t-\beta}{\alpha}\right)^2} dt \quad (3\text{-}13)$$

In specific α and β, signal energy is defined, as follows:

$$E_{\alpha,\beta} = |T(\alpha,\beta)|^2 \quad (3\text{-}14)$$

A plot of $E_{\alpha,\beta}$ is known as a scalogram. The scalogram can be integrated across α or β, or across both to produce total energy. The average wavelet energy at β can be computed by

averaging wavelet transform coefficients for different scales using the admissibility constant, as follows:

$$E_\beta = \frac{1}{\max(\alpha)} \int_0^\infty |T(\alpha, \beta)|^2 d\alpha \quad (3\text{-}15)$$

The fact that E_β is based on wavelet transform across different scales rather than the most dominant ones makes wavelet transform an effective tool for analyzing the speed data at a bottleneck. Wavelet energy increases when there is a sharp change in the speed data.

β is usually selected based on the time resolution of the original signal. The maximum value of α should be controlled by the boundary effect in order to capture details of the original signal. The boundary effect can be identified by large wavelet transform coefficients at end of the signal range. This effect exists because the signal range is infinite, and the external range is assumed to be zero. In other words, at the boundaries of a signal range, there is change from zero to an actual value, which leads to large wavelet coefficients. As the value of α increases, a longer duration of signal is being affected by the boundary effect, which means that the maximum value of α should be small enough such that a considerable portion of the signal is not affected by this effect. A common way to avoid this effect is to consider more data and extend a signal's range, and not consider the additional data in wavelet transform coefficients.

CASE STUDY

The modified calibration methodology proposed in this study was tested using the I-95 northbound freeway facility in Miami, Florida as one example. The calibration results are presented in this section.

Study Corridor

The case study network used in this research is a 12-mile segment of the I-95 northbound freeway facility in Miami, Florida, as shown in Figure 3-5 in the PM peak period. The locations of the bottlenecks in the PM peak are highlighted in this figure. In this segment, 38 true presence microwave detectors are installed, providing 20-second traffic data including speed, volume, and occupancy measurements. The starting point of the network is located on the I-95 mainline at NW 8 Street, and the ending point is located on I-95 at NE 187 Street. In this research, the simulation model for the PM peak period is from 3:00 PM to 6:00 PM.

Calibration Results

To identify the locations of the recurrent bottlenecks, 14 days were chosen as representatives of normal days on the corridor. In this research, a normal day is defined as a weekday, with a PM peak period that is free of incidents, special events, and weather events in the study area. To highlight the variation between the congestion levels for the selected normal days, a congestion index is calculated as the mean relative difference of field speed against free-flow speed at all freeway segment locations during the study period, as follows:

$$CI = \frac{1}{N}\sum_t \sum_i \frac{S_{FFS,i} - S_{i,t}}{S_{FFS,i}} \qquad \forall S_{FFS} > S_{i,t} \tag{3-16}$$

where CI is the congestion index, $S_{FFS,i}$ is the free-flow speed for segment i, and $S_{i,t}$ is the speed at segment i, at time interval t.

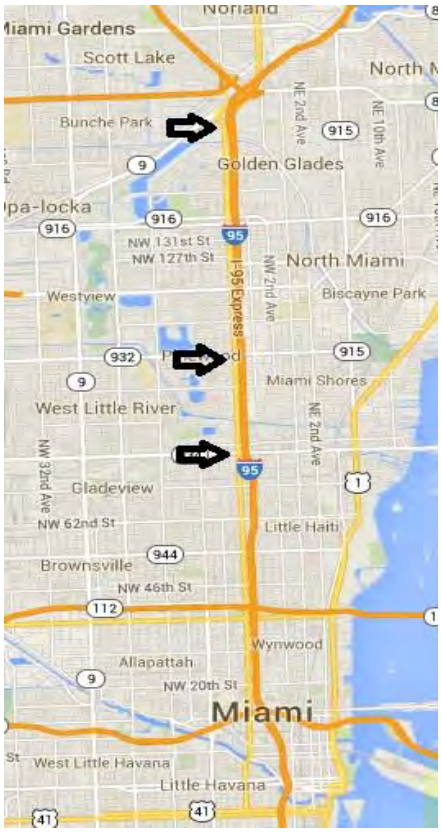

Figure 3-5. Study area.

In this study, a visualization technique was used to identify the congested areas and bottleneck locations. Utilizing speed-distance counter plots created based on detector data of normal days during the PM peak, it was possible to identify the three locations highlighted in Figure 3-5 as bottleneck locations. Based on the congestion index values and visual audit, three days were selected to represent heavy day, a medium day, and a light day. Figure 3-6 shows the speed-distance counter maps for these three days. These figures use detector data aggregated over a one-minute period. In the figures below, the red regions correspond to low speeds, according to the scale given in the legend. In this way, the speed contour plot clearly shows the locations of the bottlenecks and associated queue built-up and dissipation.

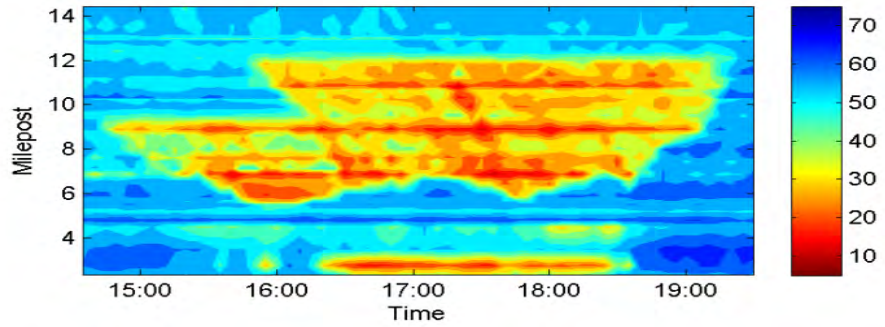

(a) Speed counter map- 04/01/11

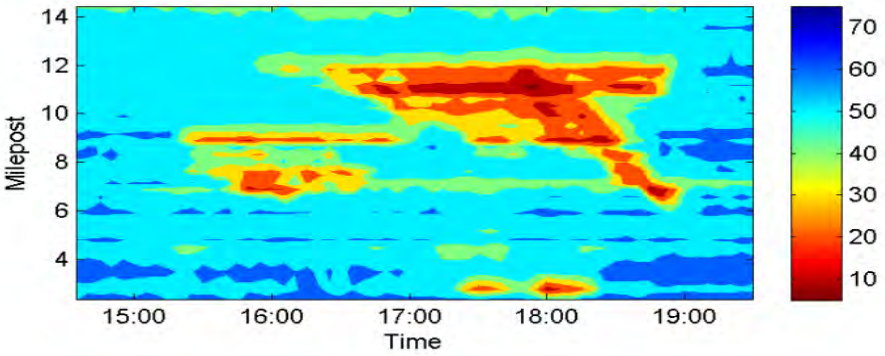

(b) Speed counter map- 05/20/10

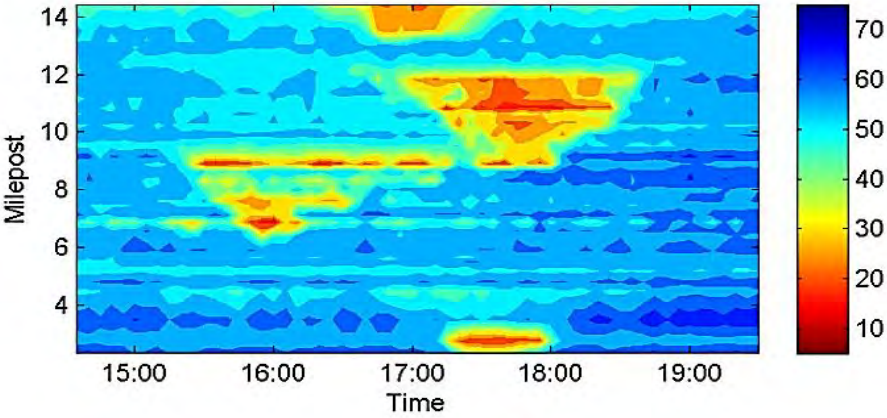

(c) Speed counter map- 05/12/10

Figure 3-6. Speed contour maps based on real-world data.

Two of the three bottlenecks are located immediately downstream of merging on-ramps. The third is caused by spillback from an off-ramp to Florida's Turnpike, a major limited access facility in the region. To reduce the congestion at the bottlenecks caused by merging on-ramps, as is the case with the first two bottlenecks, a fuzzy logic-based ramp metering strategy was

implemented, operating from 3:30 PM till 6:00 PM in the northbound direction. A run time extension (RTE) code was developed by Eleftriadou et al. (*82*) to simulate this ramp-metering strategy in CORSIM, and it was also used in this study to simulate ramp metering. The implemented ramp metering strategy is shown, based on before-after assessments, to improve system performance. However, as can be seen in Figure 3-6, the current implementation of the ramp metering is not able to eliminate the identified three bottlenecks.

In order to determine the various breakdown characteristics at each bottleneck, it was necessary to estimate the breakdown starting time and the duration of breakdown. This research uses the definition presented by Elefteriadou et al. (*3*) and the wavelet transform method to identify the start and end times of the breakdown, and the rest of the estimates are based on this time window. The results show that using each of these two methods leads to similar results. Figure 3-7 presents the calculation of the wavelet energy of speed data at the bottlenecks.

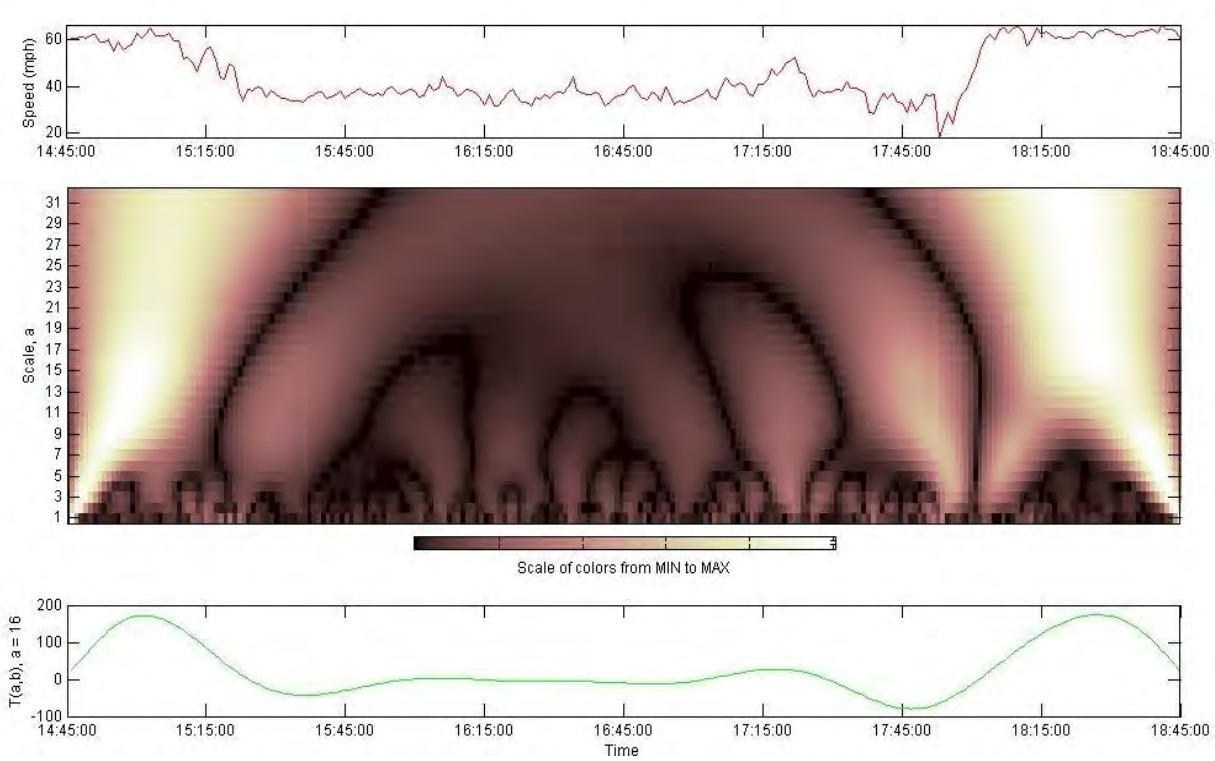

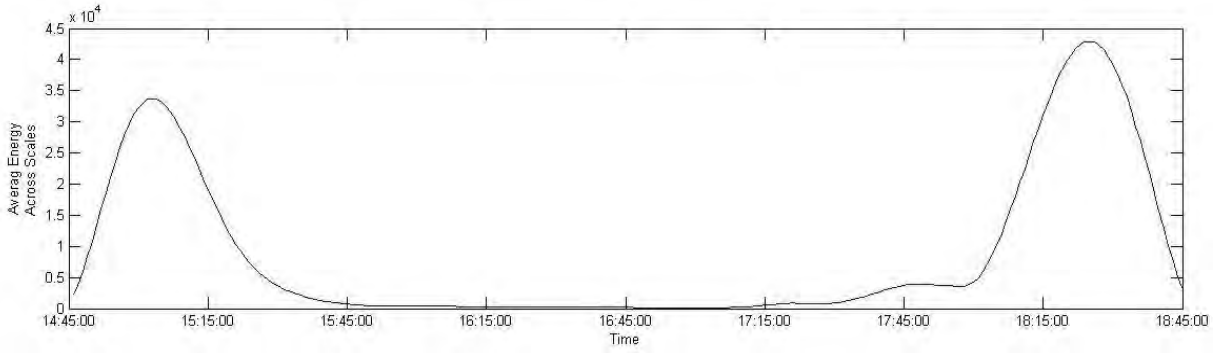

Figure 3-7. Illustration of wavelet transform and energy calculation. (a) Time series plot of speed at the second bottleneck at 05/12/10; (b) Contour map of the absolute values of wavelet transform coefficients, $|T(\alpha,\beta)|$, from scale $\alpha = 1-32$; (c) WT coefficients, $T(\alpha,\beta)$, at scale $\alpha = 16$; (d) The temporal distribution of average wavelet-based energy across scales.

Figure 3-7 (c) shows the temporal distribution of energy. The lighter regions of the contour represent larger values of the wavelet transform coefficients, which lead to higher wavelet energy. The peak of wavelet energy indicates the sharp change in the speed data. Figure 3-7 (d) shows wavelet energy for the computed speed time-series using Equation 3-15 and clearly indicates the start and the end of time breakdown.

When a breakdown occurs, congestion propagates and the shockwave starts to move to upstream locations. As a result, sometimes neighboring bottlenecks impact each other and merge together. For this reason, the duration of the breakdown at the upstream bottlenecks is calculated as much as possible for days with no or small impacts from downstream bottlenecks. Tables 3-1 to 3-3 present the various breakdown characteristics for the three bottlenecks based on real-world data for different days. These tables clearly show the difference between the pre-breakdown capacity and the queue discharge rate, and the significant variation in the breakdown occurrence and duration between days. It is also interesting to note that the queue discharge rate and the speeds prior to and after breakdown have similar values for different days.

Using speed contour maps and the breakdown information for different days, May 12, 2010 was used as the day for the calibration of the basic parameters. The selected day has a median congestion level and bottlenecks that do not have a considerable effect on each other compared to other days. The simulation model was calibrated based on the above-mentioned day, while considering two other selected days to make sure that the calibrated model was able to capture traffic variations and was not over-fitted to one special input data. In addition, sensitivity analyses on some global parameters were performed to ensure the accommodation of different traffic demands on different days. The stochasticity of breakdown was identified utilizing real-world data from different normal days in a one-year study period.

Table 3-1. Breakdown Characteristics at First Bottleneck Based on Real-world Data

Date	Starting time (hh:mm)	Duration (hh:mm)	Speed before breakdown (mph)	Pre-breakdown flow (vph)	breakdown speed (mph)	Queue Discharge (vph)	Speed after breakdown (mph)	Recovery flow after breakdown (vph)
5/12/10	15:35	1:00	55.43	8076	31.1	6814	56.95	6888
5/20/10	15:20	2:40	55.39	7188	28.4	6571	-***	-
6/17/10	17:20	0:40	53.75	7644	30.01	6261	-	-
10/6/10	15:05	2:55	55.8	6732	27.03	6375	-	-
10/7/10	15:30	2:30	50.81	7584	29	6475	-	-
11/4/10	15:45	2:15	55.47	7632	28.1	6427	-	-
11/16/10	15:40	2:20	58.11	7092	32.44	6356	-	-

11/18/10	15:05	2:25	58.62	7452	27.58	6813	50.14	6696
11/30/10	15:25	2:35	55.88	7620	28.08	6423	-	-
1/18/11	15:25	2:35	57.97	7668	28.32	6535	-	-
2/12/11	-*	3:00	54.13	7836	27.76	6501	-	-
3/15/11	15:45	2:15	57.19	8160	30.6	6594	-	-
3/20/11	-**	-	-	-	-	-	-	-
4/1/11	15:05	2:55	55.22	7536	28.36	6369	-	-
Average	15:35	2:18	55.67	7555	28.98	6501	53.55	6792
Standard Deviation	0:34	0:40	2.01	371	1.52	160	3.41	96

Table 3-2. Breakdown Characteristics at Second Bottleneck Based on Real-world Data

Date	Starting time (hh:mm)	Duration (hh:mm)	Speed before breakdown (mph)	Pre-breakdown flow (vph)	breakdown speed (mph)	Queue Discharge (vph)	Speed after breakdown (mph)	Recovery flow after breakdown (vph)
5/12/10	15:25	2:35	59.48	7380	36.69	6840	-***	-
5/20/10	-*	3:00	62.15	7200	36.25	6775	-	-
6/17/10	16:20	1:40	62.23	7044	38.42	6870	-	-
10/6/10	16:55	1:05	47.09	7128	33.82	6684	-	-
10/7/10	-**	-	-	-	-	-	-	-
11/4/10	15:25	2:35	54.10	7272	33.56	6689	-	-
11/16/10	15:30	2:10	56.02	7380	33.08	6808	50.29	6768

11/18/10	-	3:00	55.08	7296	33.68	6622	-	-
11/30/10	15:20	2:40	55.56	7152	34.33	6616	-	-
1/18/11	-	3:00	57.31	7338	34.89	6823	-	-
2/12/11	-	3:00	55.43	7548	35.13	6770	-	-
3/15/11	15:35	2:25	56.58	7568	33.75	6572	-	-
3/20/11	-	-	-	-	-	-	-	-
4/1/11	-	3:00	56.83	7287	33.75	6653	-	-
Average	15:47	2:30	56.49	7299	34.78	6727	50.29	6768
Standard Deviation	0:33	0:35	3.80	152	1.53	95	0.00	0

Table 3-3. Breakdown Characteristics at Third Bottleneck Based on Real-world Data

Date	Starting time (hh:mm)	Duration (hh:mm)	Speed before breakdown (mph)	Pre-breakdown flow (vph)	breakdown speed (mph)	Queue Discharge (vph)	Speed after breakdown (mph)	Recovery flow after breakdown (vph)
5/12/10	17:00	1:00	55.43	9192	23.03	7596	-***	-
5/20/10	16:20	1:40	55.39	9024	23.50	7686	-	-
6/17/10	16:55	1:05	53.75	8820	23.03	7778	-	-
10/6/10	16:15	1:45	55.8	8676	24.67	7910	56.39	7632
10/7/10	16:30	1:30	50.81	8796	25.65	8001	-	-
11/4/10	16:50	1:10	55.47	8532	26.58	7727	-	-
11/16/10	16:45	1:15	58.11	9024	23.26	7634	-	-

11/18/10	16:05	1:55	58.62	8832	25.58	7684	-	-
11/30/10	16:30	1:30	55.88	8382	26.08	7827	-	-
1/18/11	16:45	1:15	57.97	8856	23.28	7759	-	-
2/12/11	16:30	1:30	54.13	9228	23.42	7805	-	-
3/15/11	16:30	1:30	57.19	8832	26.26	7859	-	-
3/20/11	-**	-	-	-	-	-	-	-
4/1/11	16:05	1:55	55.22	9240	25.51	7782	-	-
Average	16:32	1:27	55.67	8880	24.60	7773	56.39	7632
Standard Deviation	0:17	0:17	2.01	251	1.32	108	0.00	0

*: The breakdown started prior to 3:00 PM, starting time of this study's analysis.

**: The breakdown did not occur.

***: The breakdown did not recover prior to 6:00 PM, ending time of this study's analysis.

The study area was modeled in the CORSIM micro-simulation model. The model was executed for 10 runs, each with different seed numbers. Table 3-4 presents the average network speed for each of the runs. Using Equation 3-4, based on an allowable error of 0.5% of the mean and a 95% confidence level, the required number of runs was estimated to be 9. Hence, executing the model for 10 runs is deemed to be adequate.

Table 3-4. Average Network Speed for Each Simulation Run

Run #	1	2	3	4	5	6	7	8	9	10
Average Network Speed (mph)	48.22	47.89	48.48	47.46	48.43	48.35	47.81	48.42	48.69	48.20

As mentioned earlier, the CORSIM micro-simulation model calibration normally addresses three sets of parameters for driver behaviors: free-flow speed, car-following, and lane-changing parameters. The free-flow speed parameters in CORSIM consist of the mean free-flow speed and the free-flow speed multipliers. The free-flow speed multiplier is a global parameter, and it is a percentage multiplier for each driver type of the mean free-flow speed. The multiplier provides a distribution of free-flow speed by driver type. The default values range from 88% to 112%. Inspired by the Kondyli et al. study (*110*), four different distributions were used as inputs to the model in this study, and the results were compared to have a better understanding of the effect of these distributions on system performance. Distribution 1 (from 92% to 108%) has less variability in the driver type, while distribution 3 (from 84% to 116%) and distribution 4 (from 75% to 125%) have greater variations than the default distribution (distribution 2). As Figure 3-8 (a) indicates, for the three modeled days, as the distribution becomes less variable, the congestion level in the network decreases. At the bottlenecks, as variability in the multiplier increases, the average speed during breakdown decreases, and the duration of breakdown becomes larger.

The calibration of the car-following sensitivity factor can be achieved by changing the driver distribution, which is a global parameter and/or changing the link-specific adjustment parameters. Similar to the sensitivity analysis conducted on the free-flow speed multipliers, three distributions were examined so as to understand the impacts of the driver sensitivity factor's distribution on the simulation results for the three modeled days. Distribution 1 (from 1.12 to 0.49) has less variability of the multiplier by driver type, while distribution 3 (from 1.38 to 0.21) has a higher variation than the default distribution (from 1.38 to 0.21), which is considered to be distribution 2. As Figure 3-8 (b) shows, in all three days, as the distribution variance increases, the

congestion level network-wide slightly decreases. At the bottlenecks, the duration of the breakdown increases, as the variability decreases.

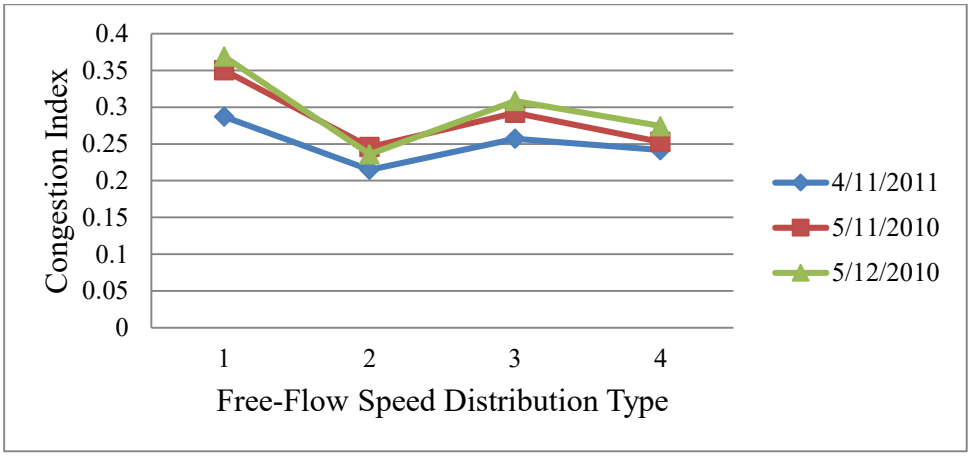

(a) Congestion Index network-wide for different free-flow distributions

Figure 3-8. Congestion Index network-wide for different types of drivers

(Continued on next page).

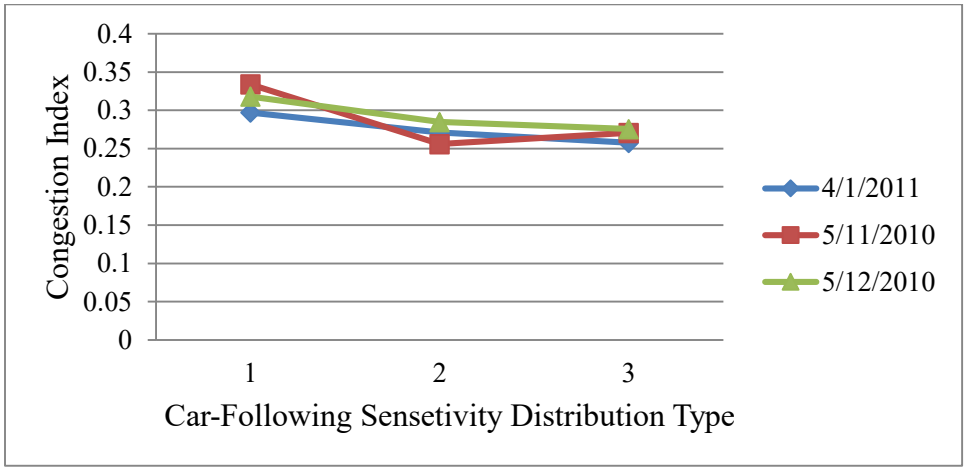

(b) Congestion Index network-wide for different car-following sensitivity distributions

Figure 3-8. Congestion Index network-wide for different types of drivers.

As described in the methodology section, these parameters were modified, taking into consideration characteristics such as capacity, traffic flows, flow-occupancy fundamental diagram, breakdown characteristics, travel times, and extents of queues, Tables 3-5 to 3-7 present the breakdown characteristics at the three bottlenecks based on the calibrated network results. In addition to presenting the results for each run, the results based on the average traffic data are also presented. Furthermore, the average and standard deviation of each measurement are presented, based on outputs of the 10 runs.

As the results indicate, the breakdown characteristics estimated based on the average results are smoothed compared to the results from individual runs, and the average conditions are less congested than most of the runs. This confirms that each run should be considered individually, in addition to averaging the results.

Table 3-5. Breakdown Characteristics at First Bottleneck Based on Simulation Results

Run #	Starting time (hh:mm)	Duration (hh:mm)	Speed before breakdown (mph)	Pre-breakdown flow (vph)	breakdown speed (mph)	Queue Discharge (vph)	Speed after breakdown (mph)	Recovery flow after breakdown (vph)
1	15:55	0:30	43.83	7476	33.23	7358	47.30	7128
2	16:00	1:20	48.51	7344	34.67	7306.4	49.88	6756
3	-	-	-	-	-	-	-	-
4	15:45	0:35	46.77	7392	31.33	7320	44.79	6864
5	15:30	2:05	50.77	7428	32.68	7302	49.53	6888

6	15:30	0:50	48.31	7488	32.65	7296	44.58	7344
7	16:25	1:00	48.64	7428	34.21	7340	49.27	7032
8	15:55	0:35	47.87	7572	32.64	7248	47.96	7056
9	-	-	-	-	-	-	-	-
10	-	-	-	-	-	-	-	-
Average traffic data	16:00	1:00	44.67	7314	38.16	7252.2	44.69	7108.8
Average	15:51	0:59	47.81	7447	33.06	7310	47.61	7010
Standard Deviation	0:17	0:31	1.97	68	1.03	33	2.04	181

Table 3-6. Breakdown Characteristics at Second Bottleneck Based on Simulation Results

Run #	Starting time (hh:mm)	Duration (hh:mm)	Speed before breakdown (mph)	Pre-breakdown flow (vph)	breakdown speed (mph)	Queue Discharge (vph)	Speed after breakdown (mph)	Recovery flow after breakdown (vph)
1	-	2:10	-	-	36.62	7233	47.15	6912
2	15:25	1:45	51.47	7248	36.84	7229	48.01	7212
3	15:25	1:50	46.55	7164	36.69	7201	46.11	6984
4	15:25	2:10	52.56	7332	37.48	7184	47.78	6684

5	15:30	2:20	46.75	7236	37.83	7174	48.39	6876
6	15:40	1:30	47.23	7320	36.74	7282	50.15	7032
7	15:35	1:55	49.98	7368	38.15	7251	51.20	6636
8	15:30	1:50	47.28	7248	37.69	7219	48.91	7152
9	15:25	2:10	48.38	7224	36.50	7160	49.58	6984
10	15:15	1:00	49.73	7296	33.93	7203	49.25	7080
Average traffic data	15:30	1:15	46.65	7237	38.79	7220	41.11	7172
Average	15:27	1:52	48.88	7271	36.85	7214	48.65	6955
Standard Deviation	0:06	0:22	2.05	60	1.12	35	1.41	176

Table 3-7. Breakdown Characteristics at Second Bottleneck Based on Simulation Results

Run #	Starting time (hh:mm)	Duration (hh:mm)	Speed before breakdown (mph)	Pre-breakdown flow (vph)	breakdown speed (mph)	Queue Discharge (vph)	Speed after breakdown (mph)	Recovery flow after breakdown (vph)
1	17:02	0:53	50.1	7920	21.11	7758	51.35	6520
2	16:53	0:55	51.17	8196	20.83	7894	52.39	7192
3	17:03	0:27	52.04	8081	23.38	7986	51.53	7155

4	16:59	1:01	48.58	8115	19.36	7505	-*	-
5	17:05	0:55	51.71	7950	19.6	7649	-	-
6	17:02	0:58	50.06	7960	19.77	7614	-	-
7	16:56	1:04	50.71	8200	19.01	7427	-	-
8	16:53	0:55	51.11	8160	21.86	7857	50.67	7011
9	16:49	1:03	52.2	8025	21.95	7816	51.96	7080
10	17:02	0:45	51.43	7960	22.17	7773	52.63	6900
Average traffic data	17:02	0:50	39.98	7819	22.64	7676	39.12	7214
Average	16:58	0:53	50.91	8057	20.90	7728	51.76	6976
Standard Deviation	0:05	0:09	1.04	102	1.37	168	0.66	225

When examining the probability of breakdown in Tables 3-1 to 3-3 and 3-5 to 3-7, it should be noted that the variations in day-to-day real-world performance in event-free days are due to the breakdown stochasticity mentioned earlier, but can also be due to variations in traffic demands between days. The variation in the simulation seed numbers between runs only addresses the variations in the stochasticity of the breakdown. Further analysis is needed if demand variations are to be considered, in addition to varying the seed numbers to account for the capacity stochasticity. Another consideration in the calibration is that the stochasticity between runs can be influenced by changing the variances of different distributions in the model, including those related to vehicle and driver characteristics.

The results show that different simulation runs may be able to represent the stochastic nature of breakdown. For instance, at the first bottleneck, some of runs did not show traffic breakdown occurrence, as is the case with other runs, which were also observed in real-word

conditions. Table 4-8 presents breakdown characteristics and comparisons of real-world data and simulation outcome. For this purpose, the breakdown characteristics of a specific date (May 12, 2010) and the average and standard deviation of different days are compared with the average and standard deviation of different runs.

The results in Table 3-8 indicate that the main difference between the real-world and simulation outcomes is the capacity drop phenomenon, which can be calculated as the difference between pre-breakdown flow and queue discharge rate. During this research, it was observed that although CORSIM microscopic simulation is capable of showing the drop in speed after breakdown, it fails to capture the capacity drop. This points out that the modeling of traffic behavior in CORSIM during breakdown conditions may need to be improved. In the interim, using the rubbernecking factor in CORSIM, which drops the capacity of the freeway at a specific time window, could be considered one solution to simulate the 5-10% drop in capacity due to breakdown that is observed in the real-world.

Table 3-8. Breakdown Characteristics Comparison

Bottleneck			Starting time (hh:mm)	Duration (hh:mm)	Speed before breakdown (mph)	Pre-breakdown flow (vph)	breakdown speed (mph)	Queue Discharge (vph)	Speed after breakdown (mph)	Recovery flow after breakdown (vph)
#1	Real-World	5/12/10	15:35	1:00	55.43	7672	30.38	6794	56.95	6888
		Average	15:37	2:14	55.67	7522	30.46	6721	54.36	6816
		Standard	0:36	0:41	2.01	143	1.50	105	3.01	85

		Deviation								
	Simulation	Average	15:51	0:59	47.81	7447	33.06	7310	47.62	7010
		standard deviation	0:17	0:31	1.97	68	1.03	33	2.03	181
#2	Real-World	5/12/10	15:25	2:35	59.48	7380	36.69	6840	-	-
		Average	15:47	2:30	56.49	7299	34.78	6727	50.29	6768
		Standard Deviation	0:33	0:35	3.80	152	1.53	95	0*	0
	Simulation	Average	15:27	1:52	48.88	7271	36.85	7214	48.65	6955
		standard deviation	0:06	0:22	2.05	60	1.12	35	1.41	176
#3	Real-World	5/12/10	17:00	1:00	55.43	9192	23.03	7596	-	-
		Average	16:32	1:27	55.67	8880	24.60	7773	56.39	7632
		Standard Deviation	0:17	0:17	2.01	251	1.33	108	0*	0
	Simulation	Average	16:58	0:53	50.91	8057	20.90	7728	51.76	6976
		standard deviation	0:05	0:09	1.04	102	1.37	168	0.66	225

The results in Table 3-8 indicate that the main difference between the real-world and simulation outcomes is the capacity drop phenomenon, which can be calculated as the difference between the pre-breakdown flow and queue discharge rate. During this research, it was observed that although CORSIM microscopic simulation is capable of showing the drop in speed after breakdown, it fails to capture the capacity drop. This points out that the modeling of traffic behavior in CORSIM during breakdown conditions may need to be improved. In the interim, using the rubbernecking factor in CORSIM, which drops the capacity of the freeway at a specific time

window, could be considered one solution to simulate the 5-10% drop in capacity due to breakdown that is observed in the real-world.

In addition to pre-breakdown flow and queue discharge, the fundamental diagram is considered in the calibration process. Fundamental diagrams are constructed from both simulated and real-world data to present the flow-occupancy relationship at the bottleneck. In addition to capacity and capacity stochasticity, the diagram also shows the critical density, at which the flow reaches capacity. Figure 3-9 compares the occupancy-flow relationships for the three bottlenecks based on real-world and simulated data. As these figures show, the calibrated model is successful in replicating capacity and the related critical occupancy. It is interesting to note, however, that the traffic flow during congested conditions is a little higher in the simulation, compared to real-world conditions, possibly reflecting the drop in maximum throughput due to breakdown that was observed in the real-world, but not in the simulation.

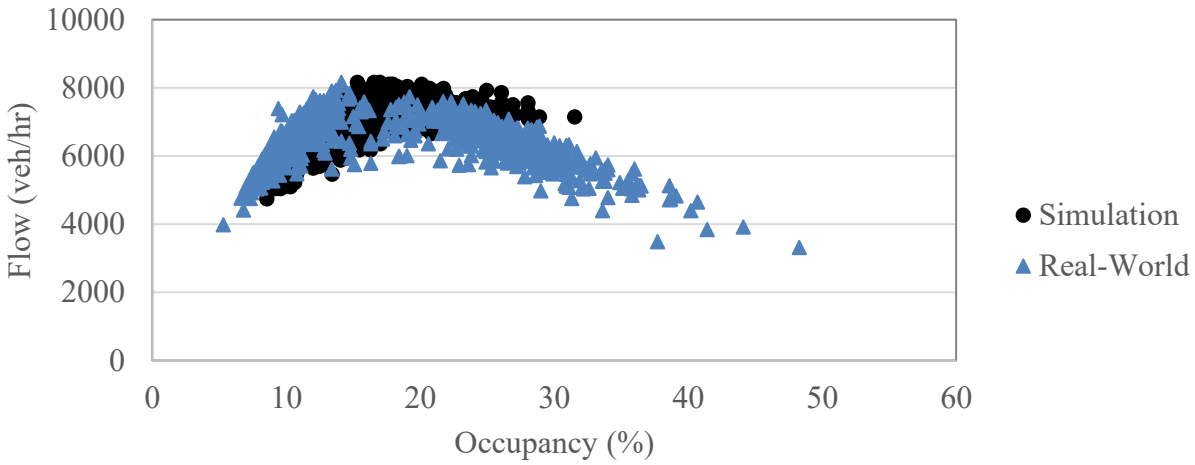

(a) Comparison of flow-occupancy relationship at first bottleneck

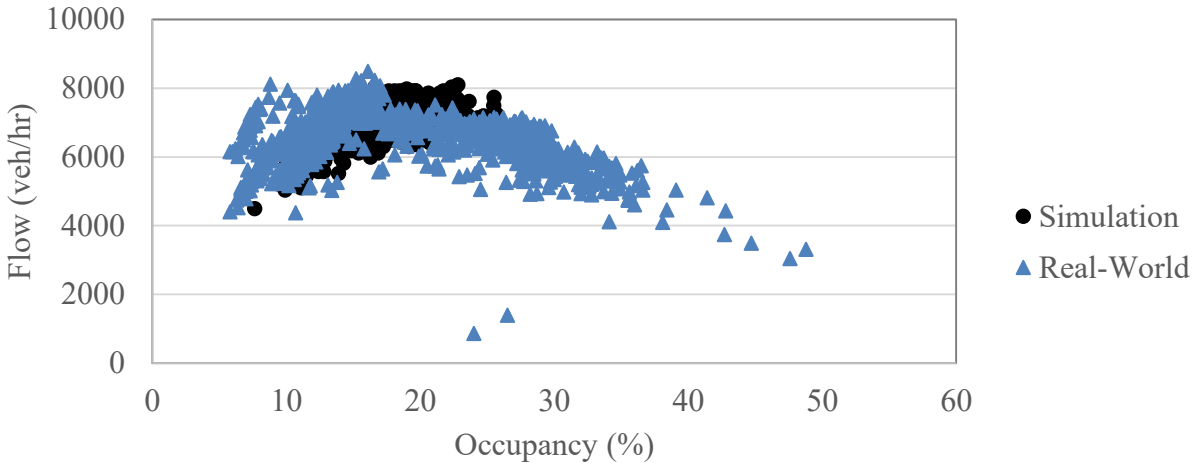

(b) Comparison of flow-occupancy relationship at second bottleneck

Figure 3-9. Comparison of flow-occupancy relationship between real-world and simulation

(Continued on next page).

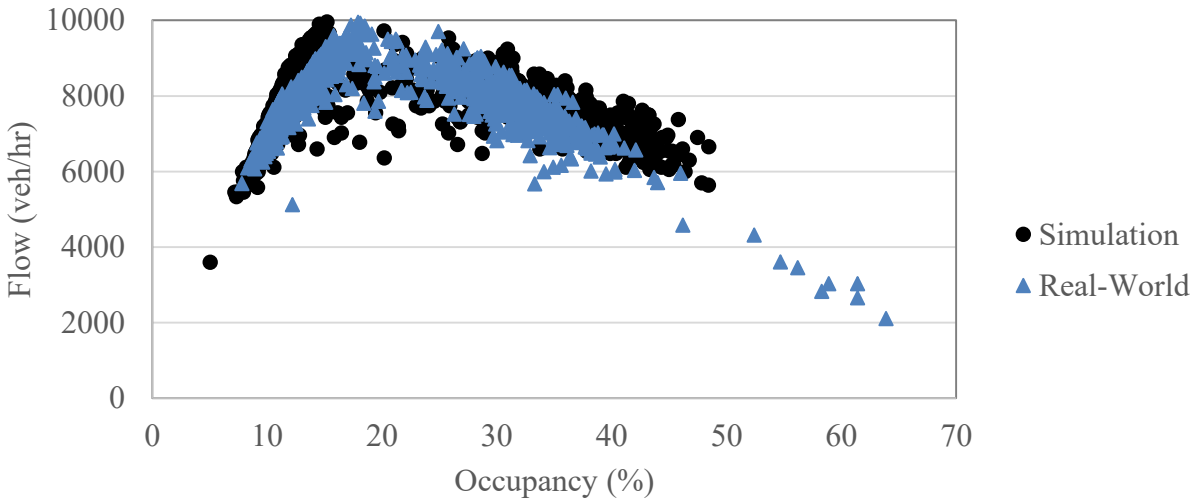

(c) Comparison of flow-occupancy relationship at third bottleneck

Figure 3-9. Comparison of flow-occupancy relationship between real-world and simulation.

Another part of the breakdown characteristics calibration step is to examine the capability of the simulation model to replicate breakdown probability. Breakdown probability models were developed based on detector measurements at three bottleneck locations from different normal days using Equation 3-5. These models were compared with the breakdown probability models based on simulation runs with different seed numbers. The comparisons are shown in Figure 3-10.

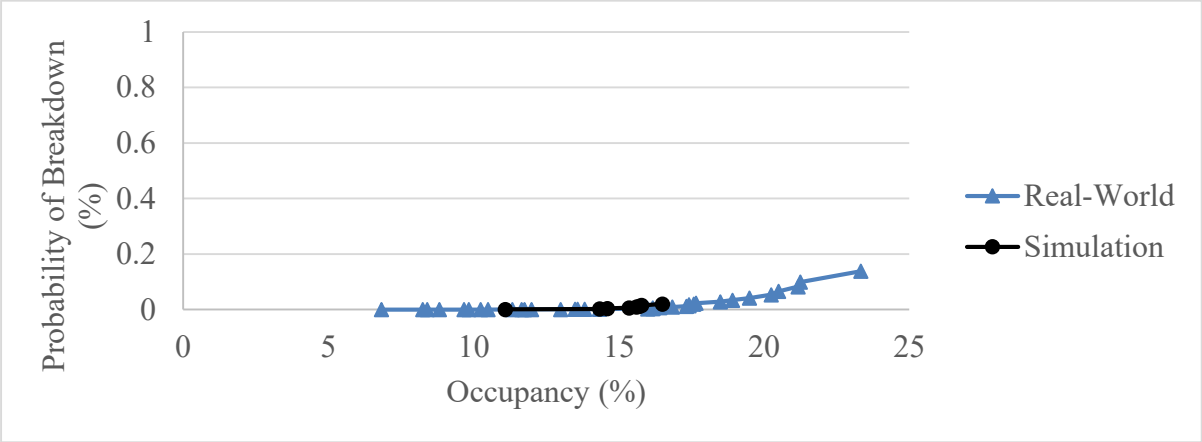

(a) Comparison of breakdown probability at first bottleneck

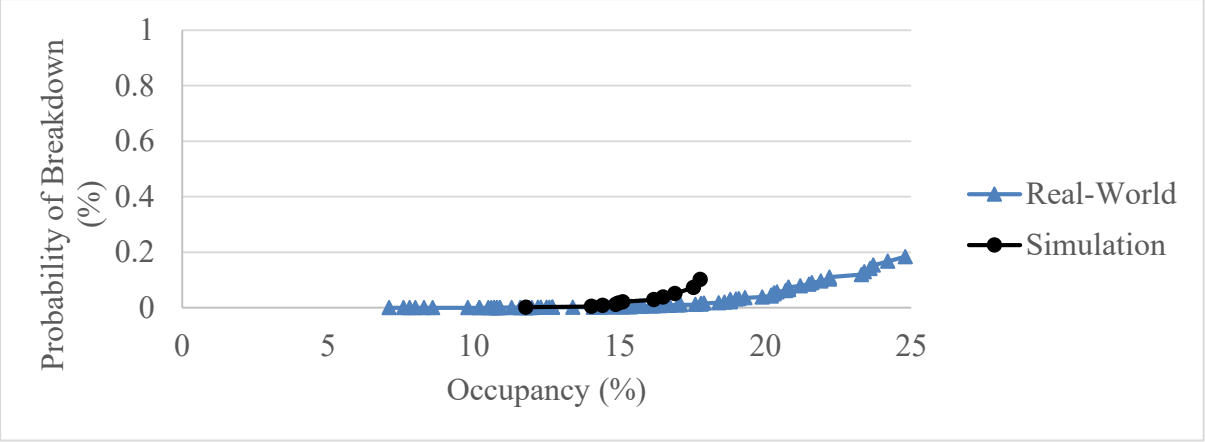

(b) Comparison of breakdown probability at second bottleneck

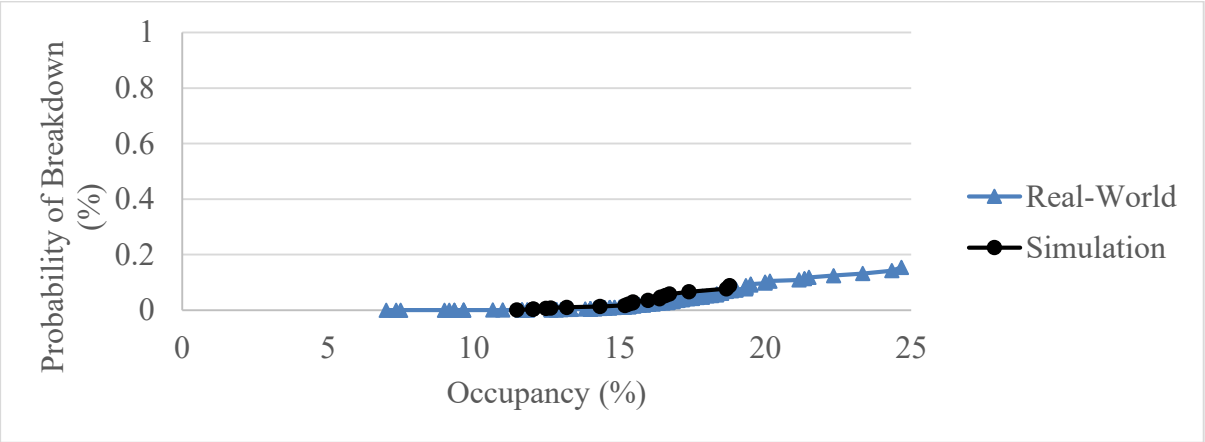

(c) Comparison of breakdown probability at third bottleneck

Figure 3-10. Comparison of breakdown probability between real-world and simulation.

Figure 3-10 indicates that since the simulation results are based on only a 3-hour PM peak period, the range of data based on the real-world is wider than the simulation data since a longer period is represented by the real-world model. However, it appears, particularly at the first and third bottleneck, that the simulation model thoroughly replicates the real-world breakdown probability. Even at the second bottleneck, the results of the real-world and simulation breakdown probabilities appear to be similar. Table 3-9 presents the system performance measurements, mean absolute error, mean absolute normalized error, Theil's Inequality Coefficient, and root mean squared normalized percent error on volume and speed results of the calibrated model in different runs. In addition, the congestion index is calculated for each run to show how well the congestion network-wide is replicated. It should be noted that congestion index based on field data is 0.232. This table also shows the correlation coefficient of volume.

Table 3-9. Goodness-of-fit Assessment of MOEs

Run #	Congestion Index	MAE		MANE		Theil's Inequality Coefficient		RMSNPE		Correlation Coefficient
		speed	volume	speed	volume	speed	volume	speed	volume	volume
1	0.212	5.898	368.04	0.119	0.061	0.089	0.039	31.573	8.617	0.939
2	0.209	6.179	367.987	0.125	0.061	0.095	0.038	34.001	8.342	0.939
3	0.195	6.227	376.76	0.126	0.063	0.096	0.04	36.195	8.738	0.935
4	0.229	5.974	364.947	0.121	0.061	0.093	0.038	27.846	8.237	0.942
5	0.246	6.066	354.813	0.123	0.059	0.097	0.037	27.824	8.185	0.943
6	0.216	6.151	391.867	0.124	0.065	0.092	0.04	30.481	9.003	0.934
7	0.232	6.105	378.853	0.123	0.063	0.093	0.039	28.74	8.795	0.939
8	0.211	6.213	366.56	0.126	0.061	0.095	0.039	33.64	8.336	0.939
9	0.224	6.62	359.64	0.134	0.06	0.105	0.038	34.031	8.323	0.94
10	0.199	6.482	365.72	0.131	0.061	0.098	0.038	36.065	8.33	0.941
Average traffic data	0.217	5.898	353.676	0.119	0.059	0.085	0.037	29.505	8.155	0.944

Visual validation is another tool that is used to validate the calibrated model. Figure 3-11 shows the speed counter map based on simulation results. A comparison between the speed counter map of simulated results and field data shows that the calibrated model adequately replicated the bottleneck location, shockwave, congestion in different locations of the network during different time intervals, and the speed pattern in general.

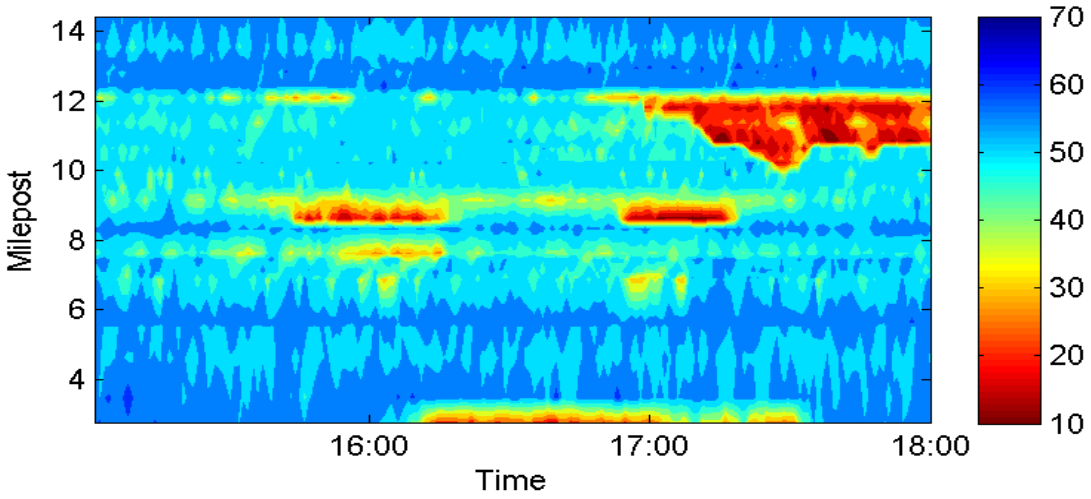

Figure 3-11. Speed contour map – simulation results.

SUMMARY

The ATMS strategies considered in this study were assessed using CORSIM, a microscopic simulation tool. It is known that without calibration of simulation models, there is no assurance that the model's outputs are reliable and that the model will correctly predict the traffic performance for the projects as a result of improvements. The state of the practice in calibrating simulation models is based on the capacity, volume and system performance values. Since the proposed ATMS strategies are mainly investigated as countermeasures to the impacts of breakdown conditions, the examination of the breakdown characteristics in the calibration procedure of traffic simulation models is important to ensure that simulation models can produce a reliable assessment. In this study, the wavelet transform was used to determine the start and end times of breakdown occurrence. Then, the breakdown characteristics as measured at the bottleneck

locations were used as inputs to the calibration process. The calibrated simulation model was used in assessing the ramp metering and VSL strategies considered in this study.

CHAPTER 4

INCORPORATION OF THE PROBABILITY OF BREAKDOWN CONCEPT INTO THE I-95 RAMP METERING OPERATION

This chapter describes the research efforts to incorporate probability of breakdown into the ramp metering operations on I-95 in Miami, FL. The scenarios evaluated pertain to changes in the activation process of the ramp meters, and changes to the fuzzy logic ramp metering algorithm. The outcome of this task is an assessment of the effectiveness of these ramp metering strategies through simulation.

Section 4.1 describes the freeway facility examined and the current ramp metering operations, followed by the development of probability of breakdown curves at selected recurring bottleneck locations. The third subsection discusses the simulation scenarios tested along with the respective results and findings. Conclusions and recommendations are provided in the final section.

OVERVIEW OF CURRENT I-95 RAMP METERING OPERATIONS

In February, 2009 the Florida Department of Transportation (FDOT) installed a ramp metering system on I-95 in Miami, FL. Eight meters were installed in the northbound direction from NW 62 Street to NW 2 Ave. In April, 2010 two more ramp meters were installed in the northbound direction, along with twelve new ramp meters in the southbound direction from Ives Dairy Rd to NW 62 Street. The focus of this study is the northbound direction, and the locations of the ramp meters are shown in Table 4-1 and Figure 4-1.

Table 4-10. Ramp Meter Locations and Metering Information in the Northbound Direction

Site	Location	Minimum Metering Rate (vpm)	Maximum Metering Rate (vpm)	Vehicles/Green
1	I-95 NB ramp from NW 62nd St	13	20	1
2	I-95 NB ramp from NW 69th St	6	20	1
3	I-95 NB ramp from NW 81st St	13	20	1
4	I-95 NB ramp from 95th St	6	20	1
5	I-95 NB ramp from 103rd St	8	20	1
6	I-95 NB ramp from NW 125th St	12	20	1
7	I-95 NB ramp from Opa Locka Blvd	12	24	2
8	I-95 NB ramp from NW 2nd Ave	N/A	24	2
9	I-95 NB ramp from Miami Gardens Dr	N/A	24	2
10	I-95 NB ramp from Ives Dairy Rd	N/A	24	2

The northbound ramp meter system operates in the afternoon peak period from approximately 3:00 pm to 7:00 pm, while individual ramp time of day settings vary by location and day of the week. All ramps employ a fuzzy logic metering algorithm. The time of day schedule is used with operator discretion to override metering operation. Ramp sites 8, 9 and 10 are only activated during non-recurring congestion, or based on operator discretion. It is estimated that these ramps are activated for approximately 20% of the time during the peak period. These ramps are considered non active for the purposes of this study.

Fuzzy Logic Ramp Metering

The fuzzy logic ramp metering algorithm is a rule-based algorithm designed to incorporate operator expertise while automating the metering rate selection process. Rather than employ strict rules such as yes/no or on/off, the algorithm allows every input to contribute to a varying degree *(113)*.

Detector Associations and Inputs

Detector information is taken from different locations relative to the ramp, and these serve as inputs to the fuzzy logic algorithm. While the exact locations of the detectors vary for every individual ramp setup, the same general framework is used. Figure 4-2 shows the detector configuration for the ramp meter located at the northbound ramp from NW 103rd St.

Detector information is relayed every 20 seconds to a fuzzy logic controller for each metered ramp. This information is processed by the controller and serves as an input to the fuzzy logic algorithm. The metering rate is updated every 20 seconds using 1-minute averages of the previous three samples. The inputs to the metering algorithm and the detector associations are shown in Table 4-2.

Table 4-11. Fuzzy Logic Ramp Metering Algorithm Inputs

Input	Typical Detector Locations
Local Occupancy	Mainline station just upstream of merge
Local Speed	Mainline station just upstream of merge
Upstream Occupancy	Next upstream mainline station
Downstream Occupancy	Multiple downstream stations
Downstream Speed	Multiple downstream stations
Queue Occupancy	Queue detector on the ramp
Advance Queue Occupancy	Tail end of the available queue storage
HOV Volume	HOV bypass passage loop

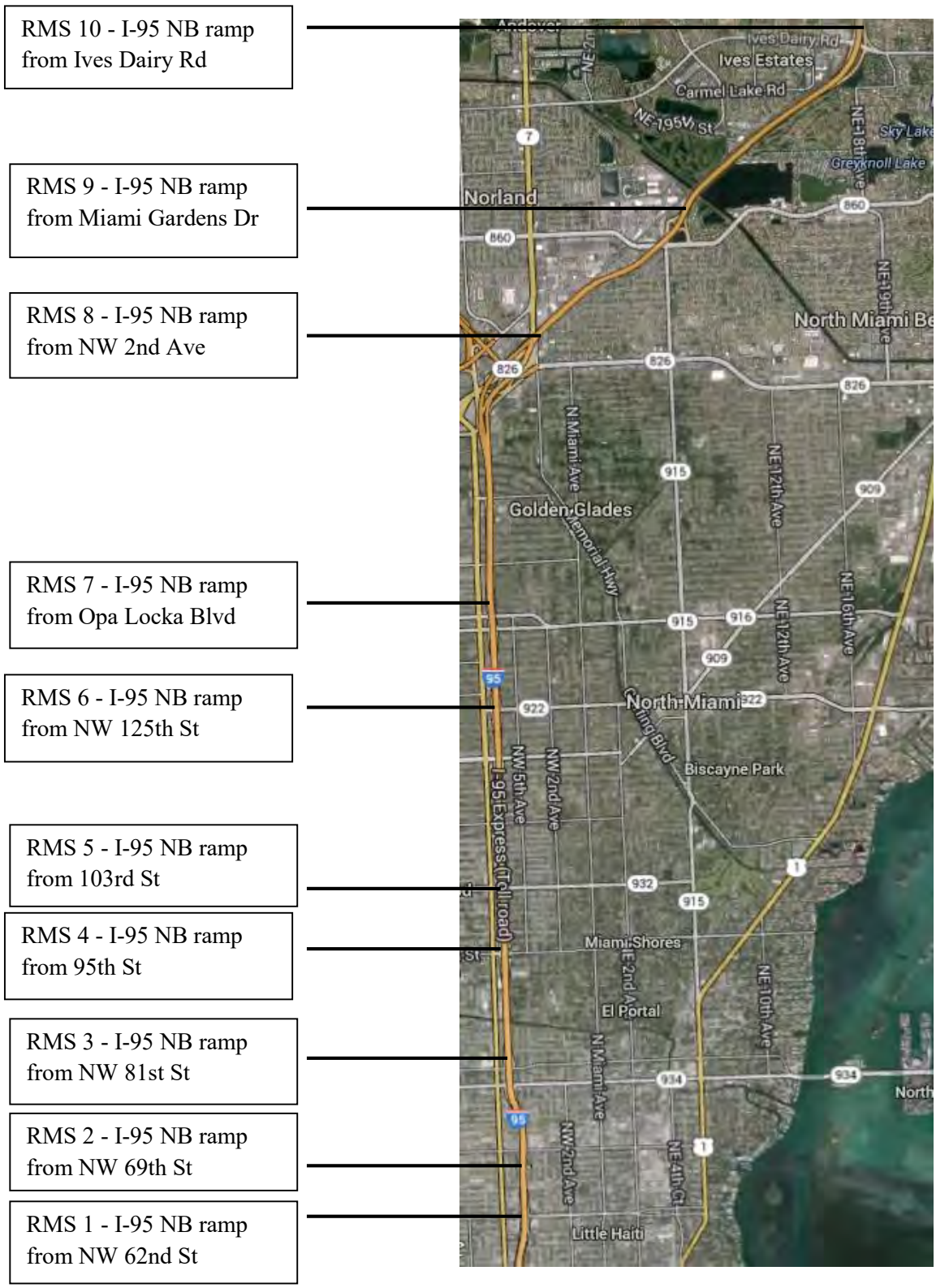

Figure 4-12. Location of ramp meters throughout the study site.

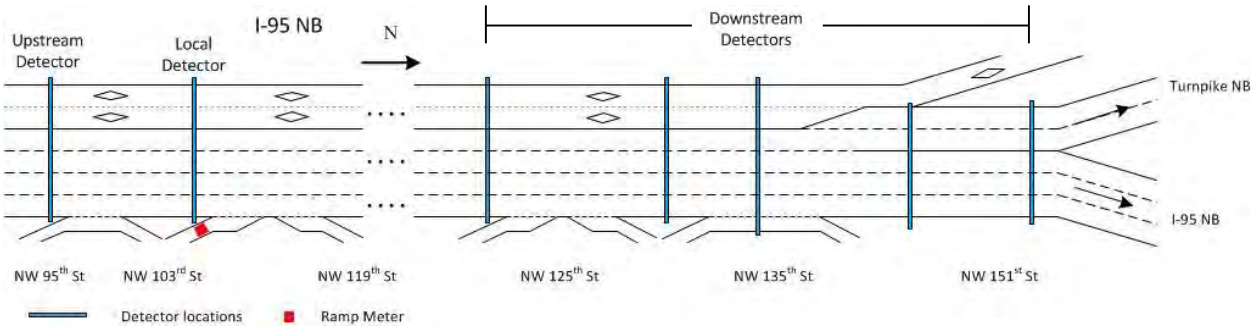

Figure 4-13. Detector configuration at NW 62nd St.

Fuzzification

Once the inputs are received by the controller they are "fuzzified", by converting them into different fuzzy class membership values. Membership in each fuzzy class ranges from 0 to 1, and classes of very small (VS), small (S), medium (M), big (B), and very big (VB) are used *(1)*. The fuzzy classes and associated parameters are shown in Figures 4-3 through 4-8.

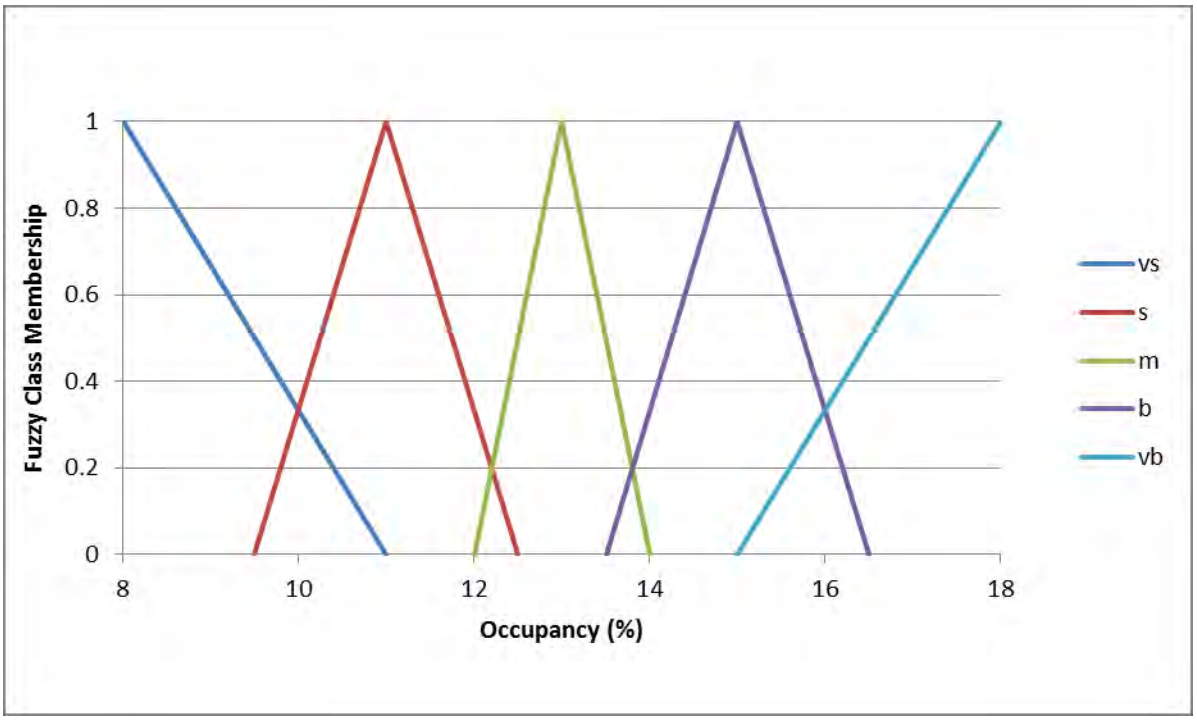

Figure 4-14. Fuzzy classes for local occupancy.

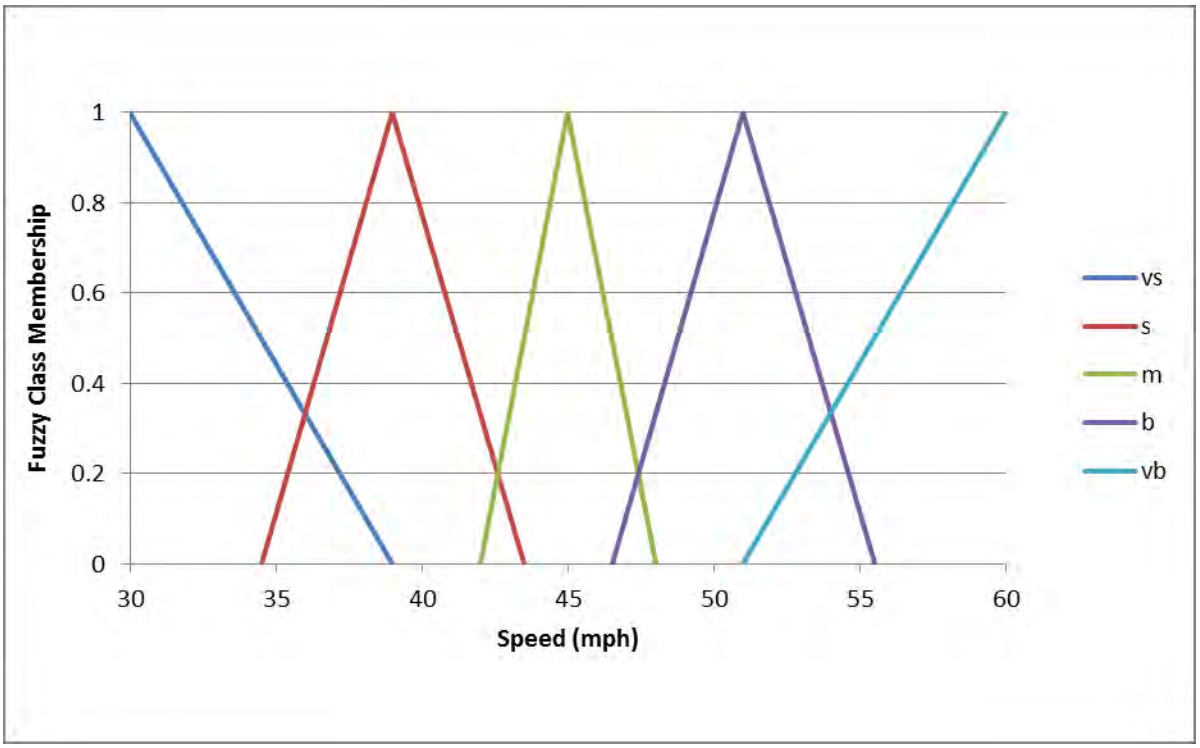

Figure 4-15. Fuzzy classes for local speed.

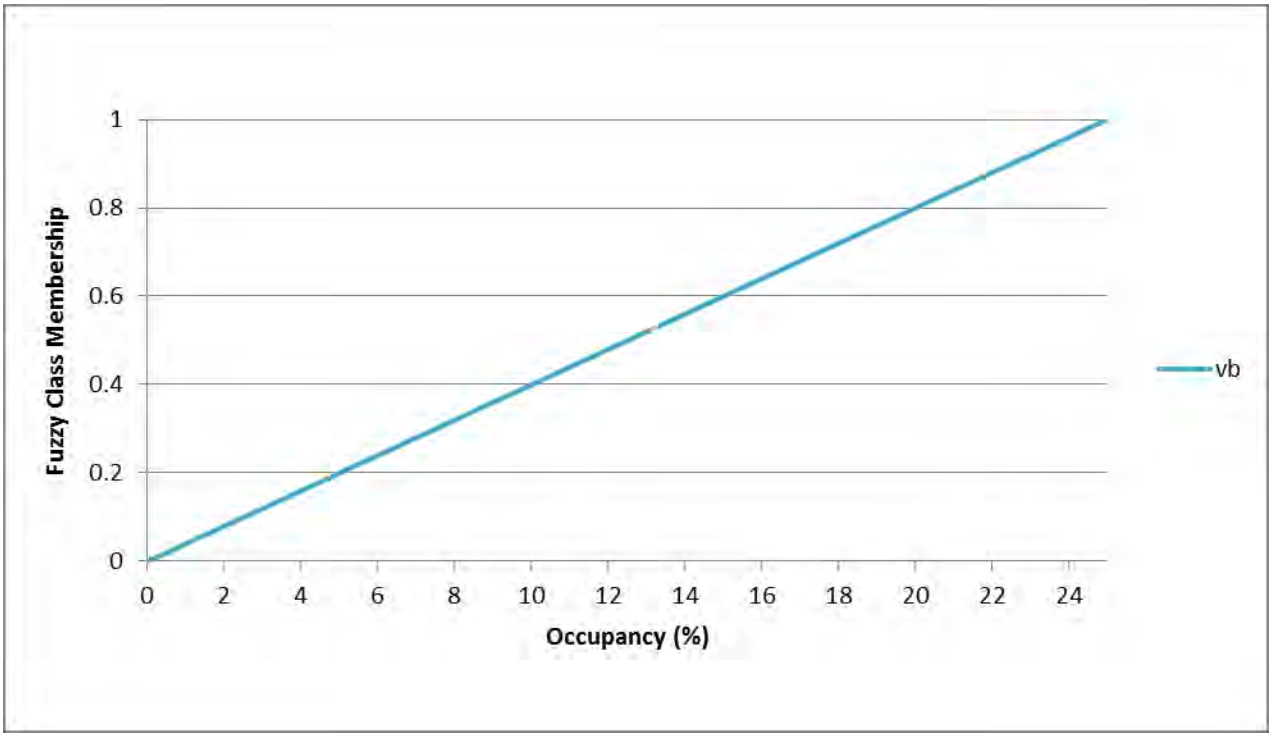

Figure 4-16. Fuzzy class for downstream occupancy.

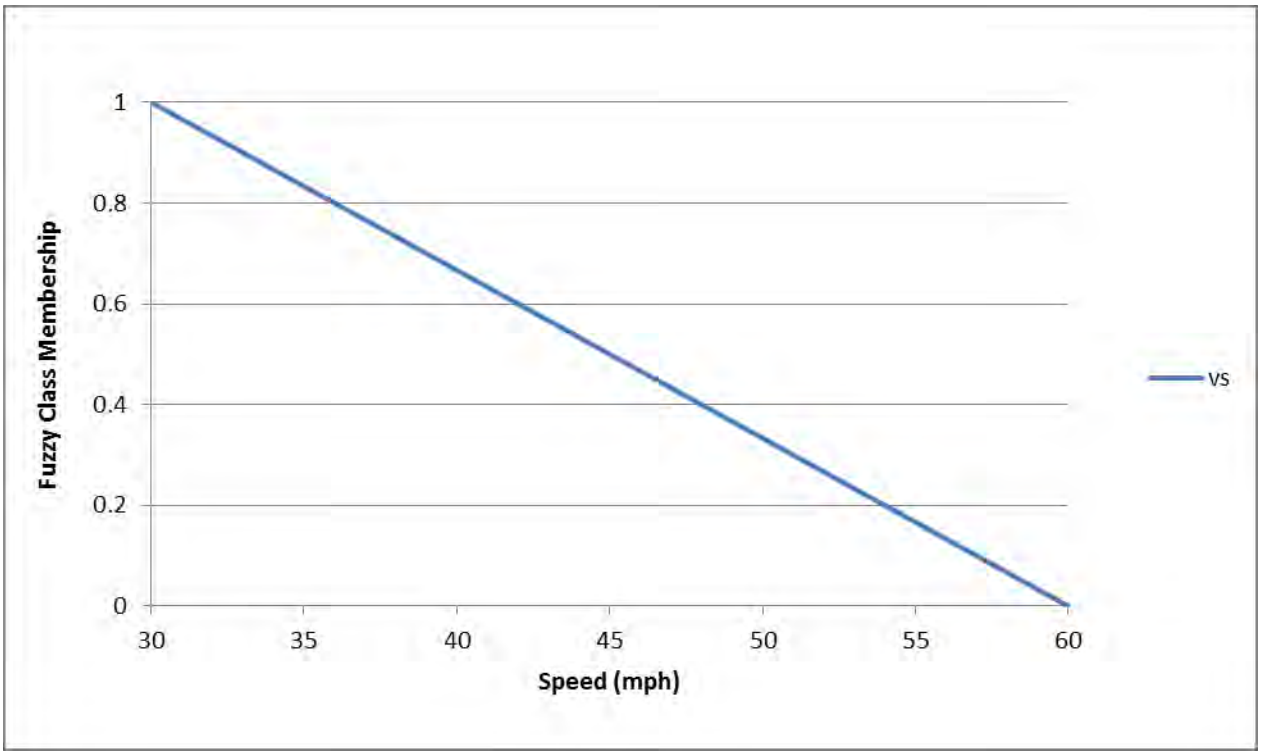

Figure 4-17. Fuzzy class for downstream speed.

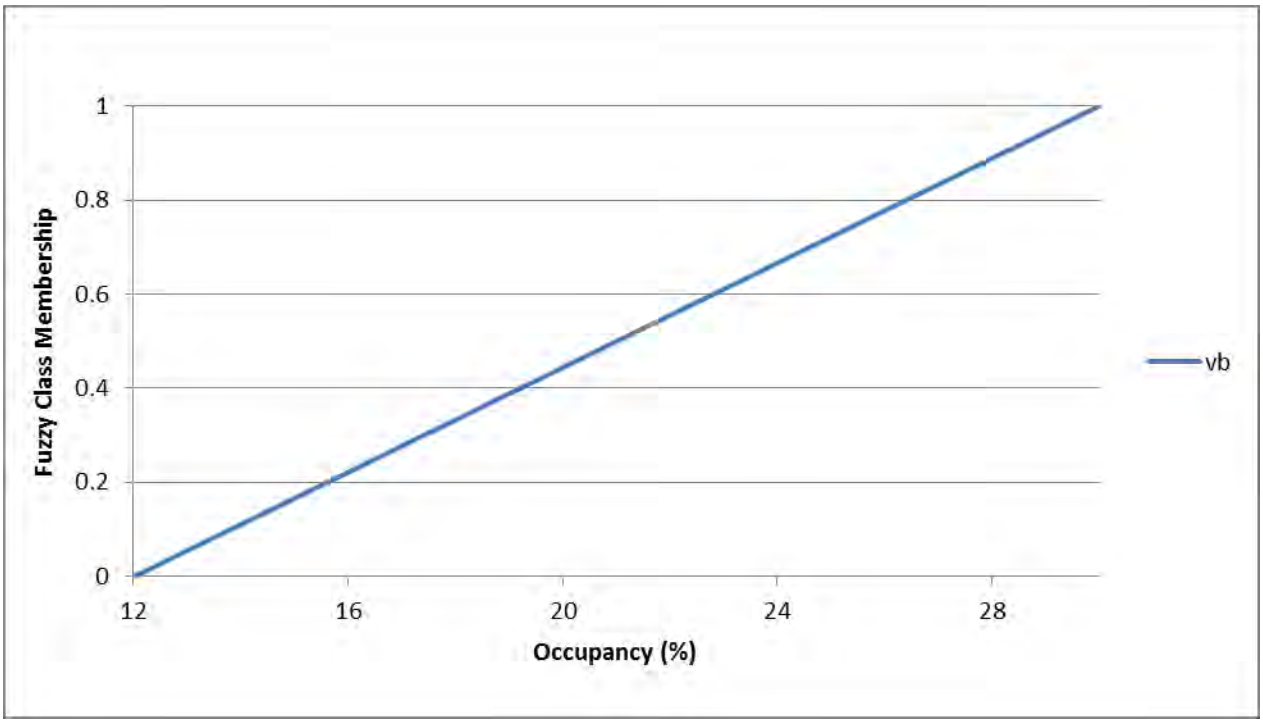

Figure 4-18. Fuzzy class for queue occupancy

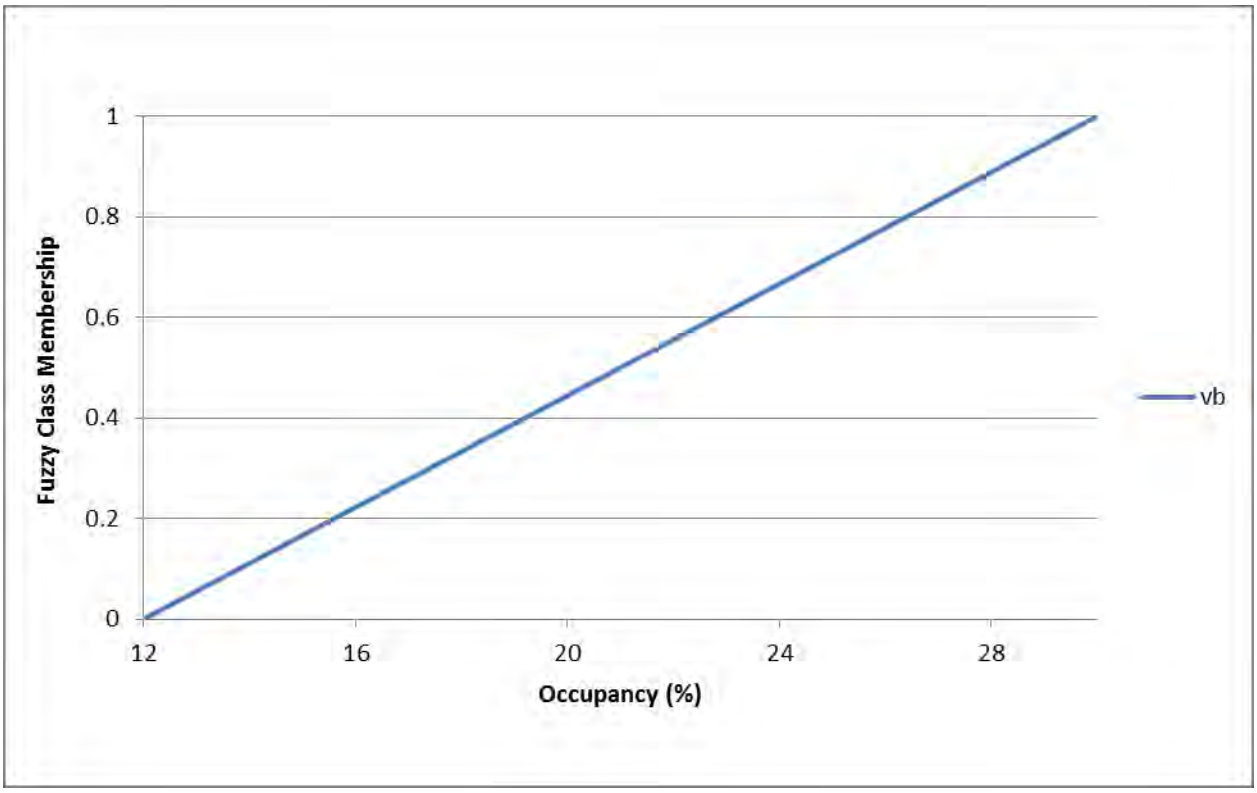

Figure 4-19. Fuzzy class for advance queue occupancy.

Fuzzy Rules

Once the inputs are converted into their respective fuzzy classes, a set of rules is used to convert the data into metering rate output classes. A weighting value is provided which is factored in when calculating the output metering rate *(113)*. The set of fuzzy rules is shown in Table 4-3.

Table 4-12. Fuzzy Logic Rules

Rule	Logic	Value
1	If Local Occ is VB, MR is VS	2.5
2	If Local Occ is B, MR is S	1
3	If Local Occ is M, MR is M	1
4	If Local Occ is S, MR is VB	1
5	If Local Occ is VS, MR is VB	2.5
6	If Local Spd is VS & Local Occ is VB, MR is VS	3
7	If Local Spd is S, MR is S	1

Rule	Logic	Value
8	If Local Spd is B, MR is B	1
9	If Local Spd is VB & Local Occ is VS, MR is VB	1
10	If Downstream Spd is VS & Downstream Occ is VB, MR is VS	4
11	If Queue Occ is VB, MR is VB	2
12	If Advance Q Occ is VB, MR is VB	4

Defuzzification and Calculation of the Metering Rate

Defuzzification involves converting the fuzzy rule outcomes into a single metering rate. The output metering rate is determined by converting the set of metering rate fuzzy variables to a single quantitative metering rate *(113)*. Each ramp has a specific set of metering rate fuzzy classes. These differ slightly by the ranges of the fuzzy variables. The output fuzzy class for ramp site 1 is shown in Figure 4-9.

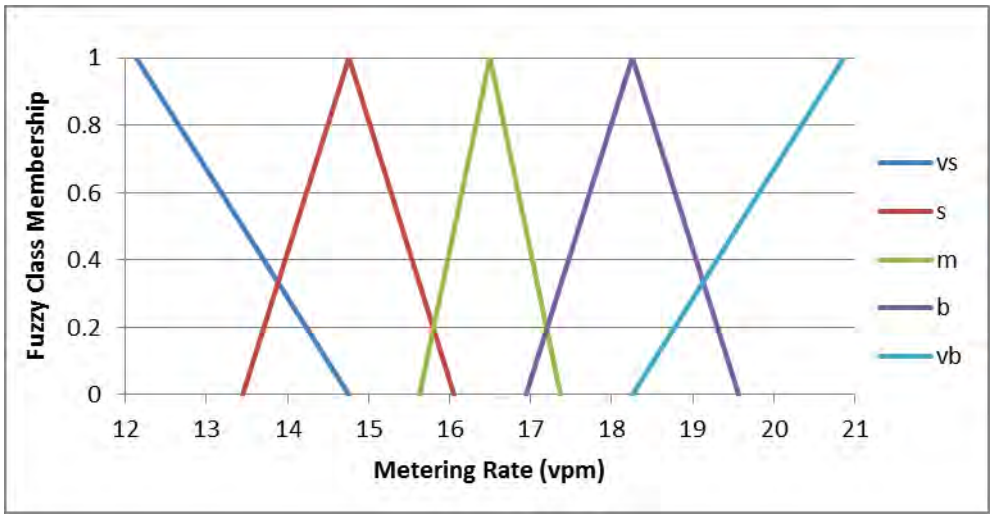

Figure 4-20. Fuzzy Classes for Metering Rates at Ramp Site 1.

The output metering rate can be calculated by using the following equation:

$$Metering\ Rate = \frac{\sum_{i=1}^{N} w_i c_i I_i}{\sum_{i=1}^{N} w_i I_i} \quad (4\text{-}1)$$

w_i = the weighting of the ith rule
c_i = the centroid of the output class
I_i = the implicated area of the output class

The implicated area of each rule outcome can be found by multiplying the fuzzy metering class by its activation degree *(113)*. For example, if the following rules are active during a given time period:

Rule 1: Metering Rate is very small to a degree of 1.0, weighted by 2.5

Rule 6: Metering Rate is very small to a degree of 0.7, weighted by 1.0

Rule 11: Metering Rate is very big to a degree of 0.84, weighted by 2.0

Rule 12: Metering rate is very big to a degree of 0.33, weighted by 4.0

The metering rate is calculated as:

$$metering\ rate = \frac{(2.5)(13.87)(1) + (1)(13.87)(0.7) + (2)(20)(0.84) + (4)(20)(0.33)}{(2.5)(1) + (1)(0.7) + (2)(0.84) + (4)(0.33)} = 17.4\ vpm$$

DEVELOPMENT OF PROBABILITY OF BREAKDOWN CURVES

This section describes the research effort to develop the probability of breakdown models, which includes the data collection, the methodology used to develop the models as well as the final developed models.

Data Collection

For the purposes of this research, traffic data were obtained at two bottleneck locations along the study site, as these locations were found to be active bottlenecks (i.e., freeway flow breaks down due to merging or diverging operations). The first location is the merge junction at NW 103rd Street and the second location is also a merge junction at NW 81st Street. Of course,

other bottlenecks within the study corridor experience congestion as well; however, this is primarily caused by the spillback from the two active bottlenecks, rather than excess demand. It should be noted that the bottleneck at NW 81st Street is upstream, but initial analysis has shown that this bottleneck breaks down earlier, before the NW 103rd Street bottleneck is activated.

The main data collection sources and requirements used for this project are as follows:

- Freeway volume, occupancy and/or speed data at the detector station upstream and downstream of each junction (if available);
- Ramp volumes;
- Data collection period for over an entire calendar year (weekdays only, excluding holidays).
- Days with adverse weather (precipitation greater than 0.20 inches, fog or hail) were removed from the data set.
- Days where incidents occurred at the sites during the time period of interest were also removed from the data set.
- Traffic data were obtained for operationally similar conditions. For the purposes of this research, the breakdown probability models were developed by analyzing the data for periods when ramp metering was in operation.
- Traffic data were obtained in 1-minute intervals to capture the abrupt oscillations of traffic.

Traffic data were available through the Statewide Transportation Engineering Warehouse for Archived Regional Data (STEWARD) database in intervals less than 1 minute but were aggregated to 1-minute intervals. Counts (or volumes) were averaged across all lanes, and converted to total hourly flows (veh/h). Speeds were calculated as the volume-weighted average

across all lanes, in mi/h. Occupancies were averaged to obtain average occupancy (in %) across all lanes for each 1-minute interval. Weather-related data were obtained through the http://www.weather.gov/climate website. The incident data were obtained through FDOT's CARS database. The entire data collection period ranged from May 2010 to March 2012. Lastly, information on the ramp metering activation and termination times were available through SunGuide.

A schematic of the two freeway-ramp merge sites with the detector locations is presented in Figure 4-10.

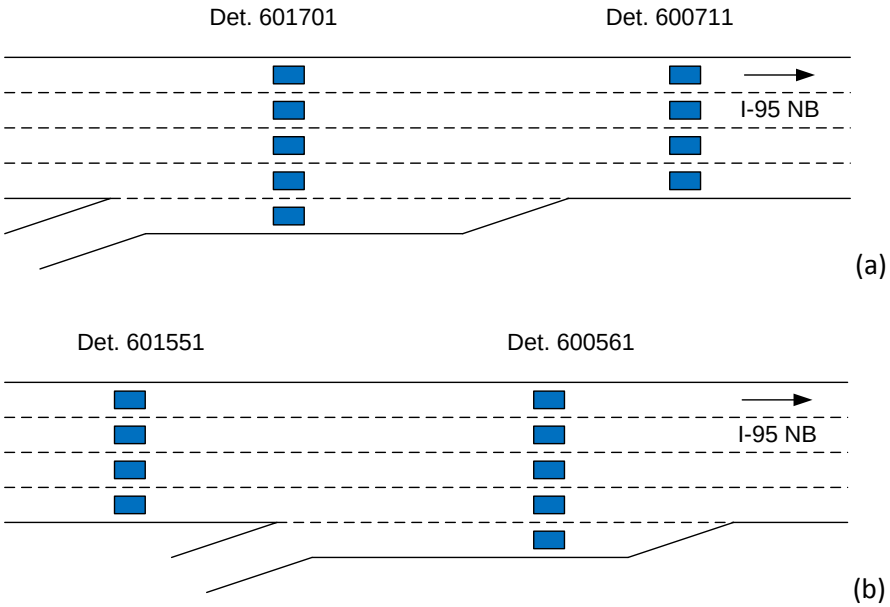

Figure 4-21. Freeway-ramp junctions and detector stations at (a) NW 103rd Street and (b) 81st Street.

Methodology

The traffic data collected at the two active bottlenecks were used to identify breakdown events at those sites during the data collection period of interest and construct the probability of

breakdown curves. Breakdown events were identified as sharp speed drops at the vicinity of the bottlenecks. A speed-based algorithm was applied, that identifies the minute prior to the breakdown event and the recovery back to pre-breakdown conditions (*28*). The speed-based algorithm is described in the following steps:

1. Calculate speed difference between two consecutive minutes:

$$\Delta S_i = S_{i+1} - S_i \tag{4-2}$$

2. For $\Delta Si < 0$, consider the threshold of X mi/h for determining the following:

$$Avg\ \{S_{i-4},\ \ldots,\ S_i\} > Avg\{S_{i+1},\ \ldots,\ S_{i+5}\} + X\ mi/h \tag{4-3}$$

3. Determine whether the maximum speed during the following Y minutes (minimum duration) is less than S_i.

$$Max\ \{S_{i+1},\ \ldots\ ,\ S_{i+Y}\} < S_i \tag{4-4}$$

4. The breakdown time is identified at $t = i$, i.e., before the speed drop (or the occupancy increase).

A recovery is assumed to occur when the following criteria are met:

1. Positive speed difference between two consecutive minutes:

$$S_j - S_{j-1} > 0 \tag{4-5}$$

2. The minimum speed during the following Y minutes is greater than the average speed before and after congestion has occurred.

$$Min\ \{S_j, \ldots, S_{j+Y-1}\} > Avg\ \{S_{i+1}, S_i\} \quad (4\text{-}6)$$

The recovery is identified as occurring at time tj, with the speeds before and after the recovery being Sj-1 and Sj respectively. The parameters X and Y are user-defined parameters. For the purposes of this research, we selected a speed drop magnitude of 10 mi/h and a minimum duration of congestion/ recovery of 10 minutes. Following this process, all breakdown times and recovery periods were identified at the two bottleneck locations.

The methodology used for the estimation of the distribution of the breakdown volume, is based on lifetime data analysis statistics (*9*). The breakdown volume (q) is the volume that triggers the abrupt speed drop and the queue formation observed at the merge area. The distribution function is obtained by applying the non-parametric Product-Limit Method (PLM) (*109*). An advantage of this method is that it is not necessary to assume a distribution of breakdown volumes. The distribution function of the breakdown volume considering the PLM (*9*) is given by:

$$F(q) = 1 - \prod_{i:q_j \le q} \frac{k_i - 1}{k_i}; i \in \{B\} \quad (4\text{-}7)$$

Where:

$F(q)$ = distribution function of breakdown volume

q = traffic volume (veh/h/ln)

q_i = traffic volume in interval i, which is the one prior to the drop in speeds, i.e., the breakdown flow (veh/h/ln)

k_i = number of intervals with a traffic volume of $q \geq q_i$

$\{B\}$ = set of breakdown intervals (1-minute observations)

A breakdown probability model as a function of the freeway occupancy can be developed using a similar formulation. In this case, the corresponding occupancies and breakdown occupancies are used in Equation 4-7. According to Brilon et al. (*9*), the observed volumes or occupancies to be used, are classified into:

B: Breakdown Set: Traffic is non-congested at interval i but the observed volume (or occupancy) causes a breakdown at interval i+1. This category includes all breakdown events (non-censored data).

F: Non- Breakdown Set: Traffic is uncongested at interval i and the following interval i+1. This category includes all intervals preceding the breakdown event and following the recovery (censored data).

Once the breakdown probability model was constructed using the Product-Limit Method a parametric analysis was performed to investigate whether the model follows a particular distribution, such as the normal, Lognormal, Weibull, and Logistic distributions. The Maximum Likelihood Estimation (MLE) method was used to estimate the distribution parameters for each of the candidate distributions. The log-likelihood function and the Anderson-Darling statistic (*113*) were used to show how well the data follow a particular distribution.

Breakdown Probability Models

This section presents the final models developed for the NW 103rd Street and the NW 81st Street bottlenecks. Generally, two types of models were developed: occupancy-based models and flow-based models. For the development of these models the method described in the previous section was undertaken, which is non-parametric. It is possible to perform a parametric analysis to investigate whether the model follows a particular distribution, such as the normal, Lognormal, Weibull, and Logistic distributions. The Maximum Likelihood Estimation (MLE) method can be used to estimate the distribution parameters for each of the candidate distributions. The log-likelihood function and the Anderson-Darling statistic (*113*) show how well the data follow a particular distribution.

I-95 NB at NW 103rd Street Models

A total of 98 breakdown events were identified at this location. The occupancy-based breakdown probability model at the NW 103rd Street bottleneck is presented in Figure 4-11. Data obtained at the detector downstream of the merge were used to develop the curve.

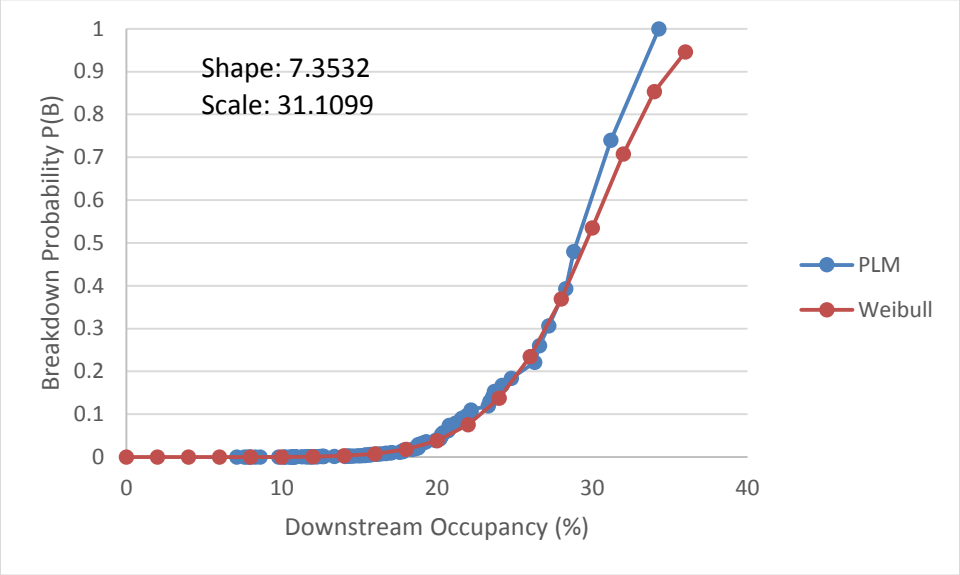

Figure 4-22. Breakdown probability model at NW 103rd Street based on downstream detector occupancy.

As this figure shows, the probability of breakdown curve based on the field data (PLM) reaches 100%, which suggests that the highest observed occupancy also resulted in a breakdown event. Although it is desirable to obtain a curve that reaches 100%, it is not always feasible to do so, as there are cases where the absolute maximum occupancies (or volumes) are not always followed by breakdown events.

As it was also discussed earlier, the PLM curve shown in Figure 4-11 is non-parametric. However, a parametric analysis was also performed, and it was found that the Weibull distribution produces an acceptable fit to the PLM curve. The Weibull model parameters (shape and scale) are given in Figure 4-11.

In addition to the occupancy-based model, a volume-based model was also developed. This model also utilizes information obtained from the detector located downstream of the merge junction. The breakdown probability model using the downstream data is shown in Figure 4-12.

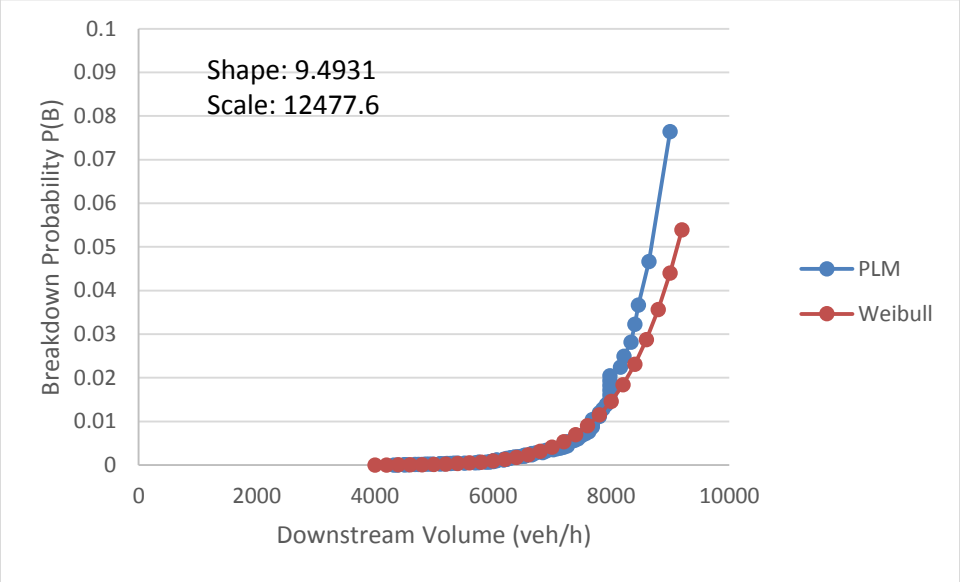

Figure 4-23. Breakdown probability model at NW 103rd Street based on downstream detector volume.

The probability of breakdown curve only reaches to 8% in this case, which suggests that higher volumes observed did not contribute to a breakdown event. A parametric analysis was performed and it was found that the Weibull distribution provided an acceptable fit to the data, compared to the other distributions. The Weibull distribution parameters (shape and scale) are given in Figure 4-12.

I-95 NB at NW 81st Street Models

A total of 37 breakdown events were identified at this location. The occupancy-based breakdown probability model at the NW 81st Street bottleneck is presented in Figure 4-13. Data obtained at the detector downstream of the merge were used to develop the curve.

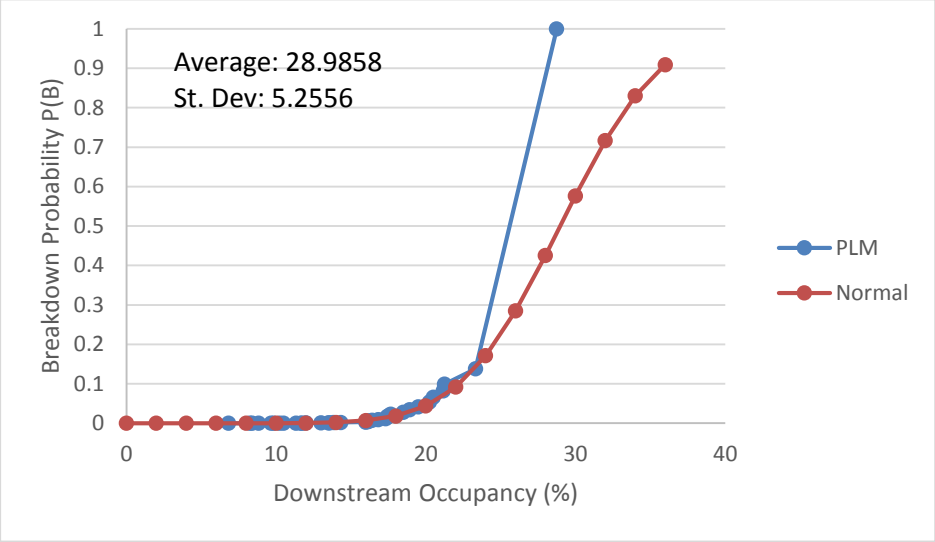

Figure 4-24. Breakdown probability model at NW 81st Street based on downstream detector occupancy.

In this case, it was found that the Normal distribution provides the best fit to the PLM curve. The specifications of this distribution (average, standard deviation) are shown in Figure 4-13.

Next, the PLM model using the downstream volume data was developed. This model, along with the fitted curve, is shown in Figure 4-14 that follows.

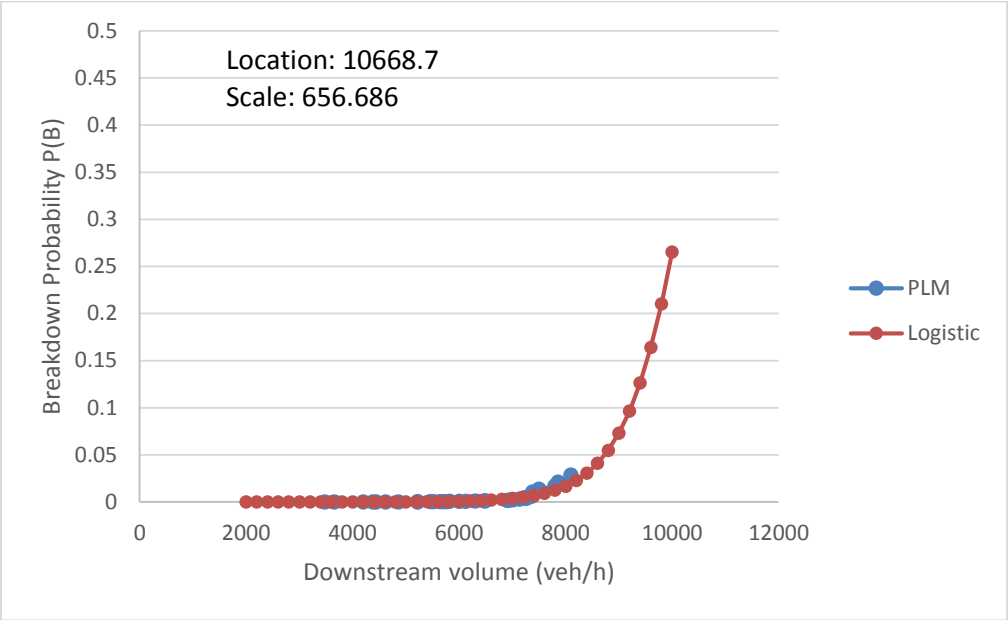

Figure 4-25. Breakdown probability model at NW 81st Street based on downstream detector volume.

A parametric analysis was performed and it was found that the Logistic distribution provided an acceptable fit to the data, compared to the other distributions. The Logistic distribution parameters (location and scale) are given in Figure 4-14.

ENHANCEMENTS TO THE METERING ALGORITHM

This section provides an overview of modifications made to the current I-95 fuzzy logic ramp metering algorithm. Each proposed modification is presented, and the simulation results are discussed in detail.

Addition of Ramp Metering Activation Threshold

The current ramp metering operation on I-95 in Miami, FL uses a combination of operator judgment and time of day operation to determine the start of the metering period. Based on our field data observations, ramp metering may often start after the beginning of congestion. The objective of this enhancement is to automate this process allowing the ramp metering activation to be responsive to varying traffic demands, and to initiate ramp metering operation before congestion starts.

To automate the metering activation process the probability of breakdown curves developed in the previous were used. From the probability of breakdown curves the lowest value at which a breakdown had occurred was selected as the activation threshold. At the 81st street on-ramp the lowest breakdown occurs at 6.83% occupancy (Figure 4-15). This value was rounded up to 7% occupancy. Therefore in our simulations, the ramp metering operation will begin at this ramp when the average occupancy rises above 7% for at least 5 minutes.

At the 103rd street on-ramp the lowest breakdown occurs at 7.1% occupancy (Figure 4-16), in our simulations the ramp metering operation will begin at this ramp when the average occupancy rises above 7% for at least 5 minutes.

The two initialization thresholds were tested in conjunction, and all other ramp meters remain operating under standard time of day procedure. The simulation was run a total of ten times, and performance measures were averaged over the ten runs. The total travel time over the entire network is shown in Table 4-4. The total travel time on the mainline is shown in Table 4-5, and the total travel time on the ramp segments is shown in Table 4-6.

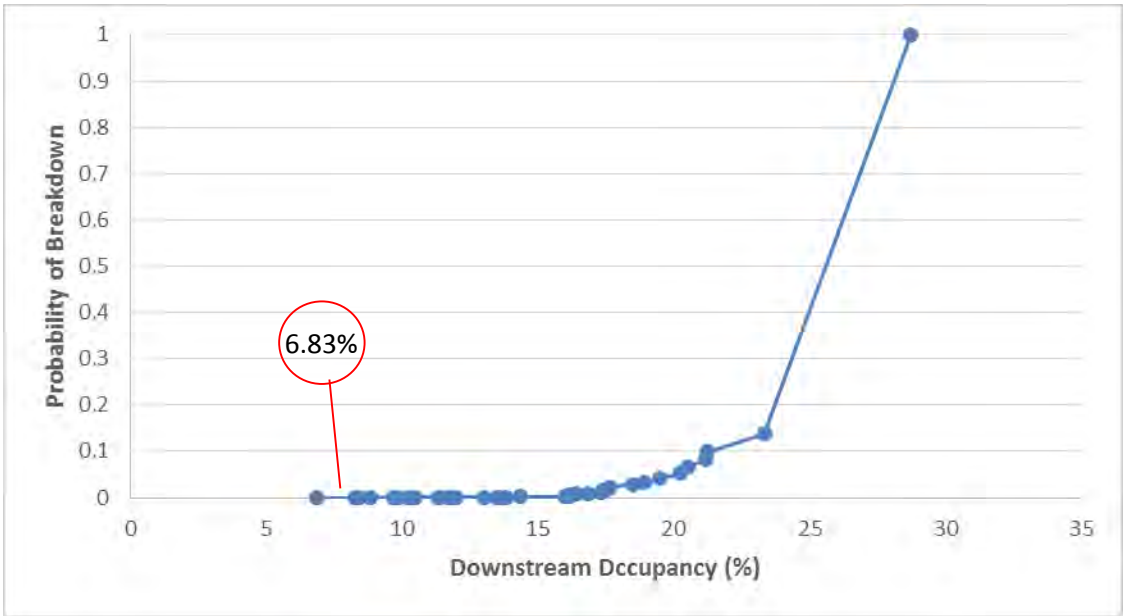

Figure 4-26. Breakdown occupancies at the 81st street on-ramp

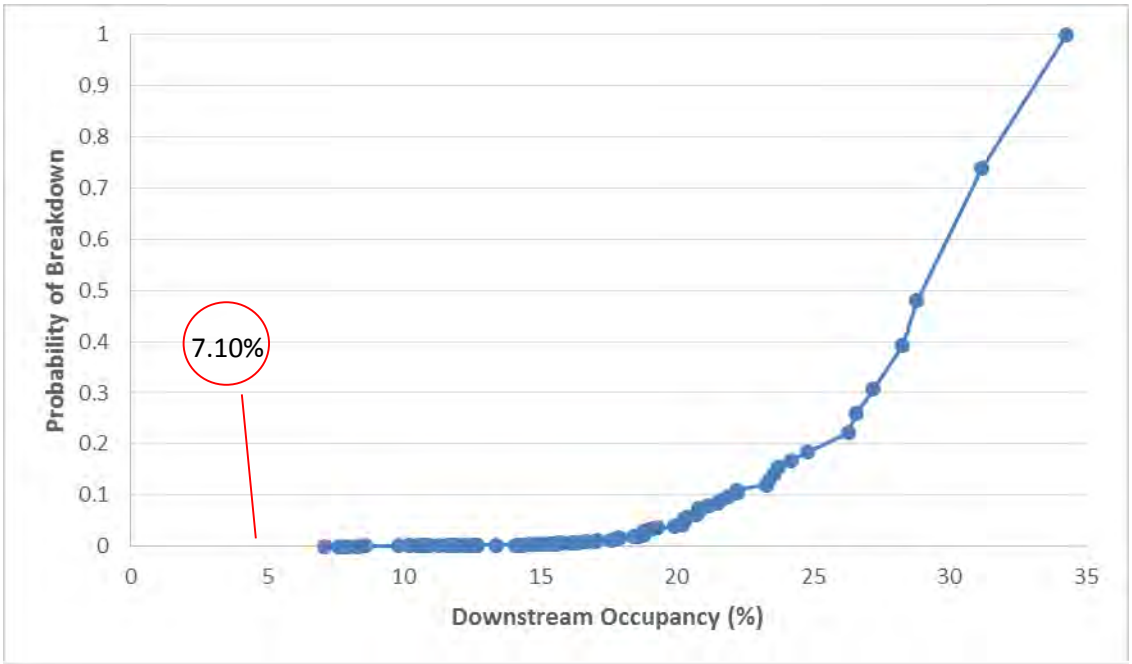

Figure 4-27. Breakdown occupancies at the 103rd street on-ramp

The total travel time improved for seven of the ten runs, and on average improved by 139.1 hours (2%). The mainline travel times showed a similar change, however the ramp travel time was

shown to increase by 3.1 hours (0.7 %) on average. This is due to the ramp meters being activated earlier than during the time of day operation. For example in Run 6, ramp site 3 (on-ramp from 81st St.) is activated at 3:09 pm, and ramp site 5 (on-ramp from 103rd St.) is activated at 3:07 pm. The standard time of day operation for these ramps is 3:30 pm. This longer ramp metering period will cause longer ramp vehicle delays.

Table 4-13. Total Travel Time over the Entire Network

Travel Time (hours)	Run 1	Run 2	Run 3	Run 4	Run 5	Run 6	Run 7	Run 8	Run 9	Run 10	Avg	Pct Diff
Base	7050.1	7216.6	6741.4	7444.7	7193.8	6922.1	6744.1	7081.0	7013.2	6969.0	7037.6	
Modified	7139.0	6821.7	7277.4	6642.1	6974.4	6741.8	6700.3	7013.1	7222.3	6452.5	6898.5	2.0

Table 4-14. Total Travel Time on the Mainline

Travel Time (hours)	Run 1	Run 2	Run 3	Run 4	Run 5	Run 6	Run 7	Run 8	Run 9	Run 10	Avg	Pct Diff
Base	6500.0	6660.4	6254.3	6851.4	6664.9	6429.6	6276.4	6553.7	6515.0	6460.1	6516.6	
Modified	6558.3	6315.9	6738.1	6165.2	6452.0	6262.6	6210.1	6481.0	6687.8	5971.1	6384.2	2.0

Table 4-15. Total Travel Time on the Ramps

Travel Time (hours)	Run 1	Run 2	Run 3	Run 4	Run 5	Run 6	Run 7	Run 8	Run 9	Run 10	Avg	Pct Diff
Base	422.8	418.2	432.1	418.9	440.2	432.0	415.4	430.6	442.1	438.7	429.1	
Modified	417.0	428.9	467.5	424.6	422.7	424.9	427.8	425.2	458.3	425.0	432.2	-0.7

A more detailed look at the ramp operations from Run 6 shows an earlier formation of the ramp queue in Figure 4-17. The maximum queue has also increased from 24 to 28 vehicles. This

earlier activation of the ramp meter temporarily reduces the throughput rate from the ramp shown in Figure 4-18. These observations are typical throughout all runs.

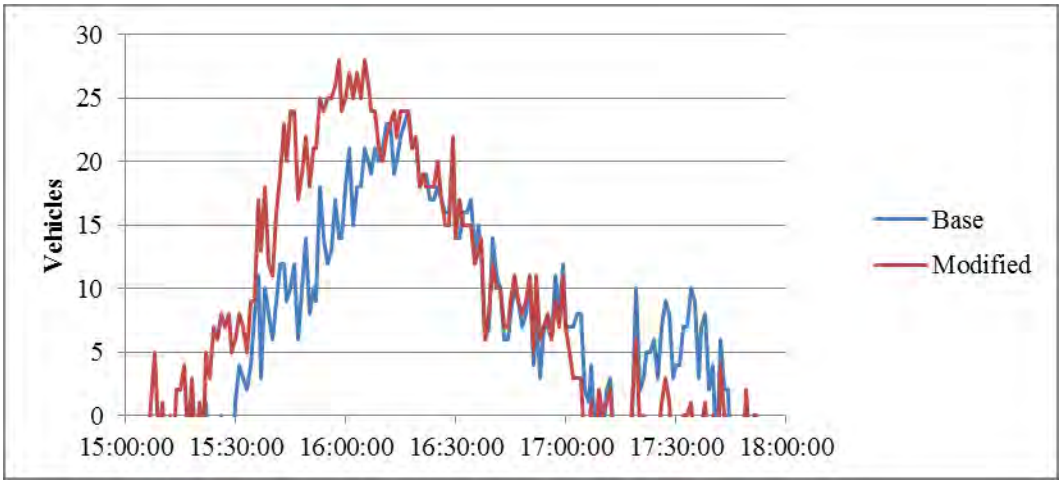

Figure 4-28. Ramp queue at the on-ramp from 81st St.

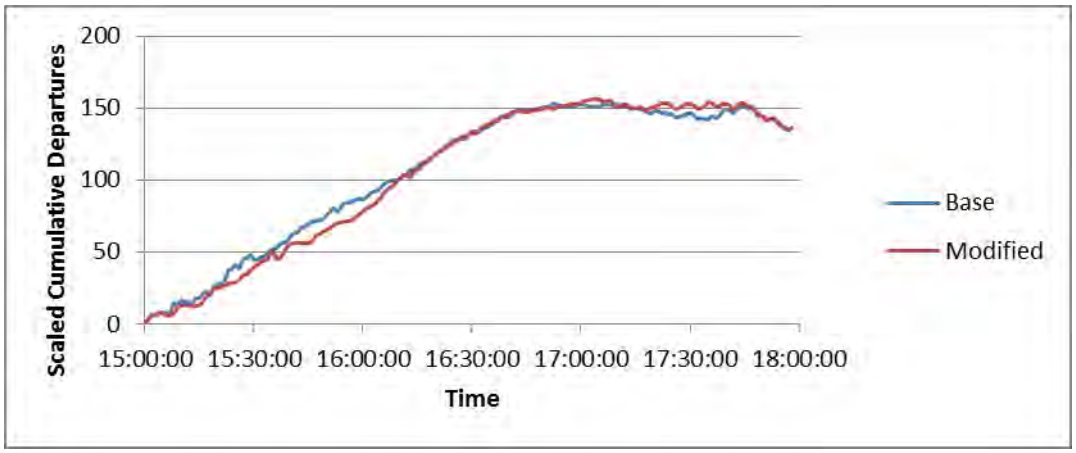

Figure 4-29. Plot of scaled cumulative departures at the on-ramp from 81st St.

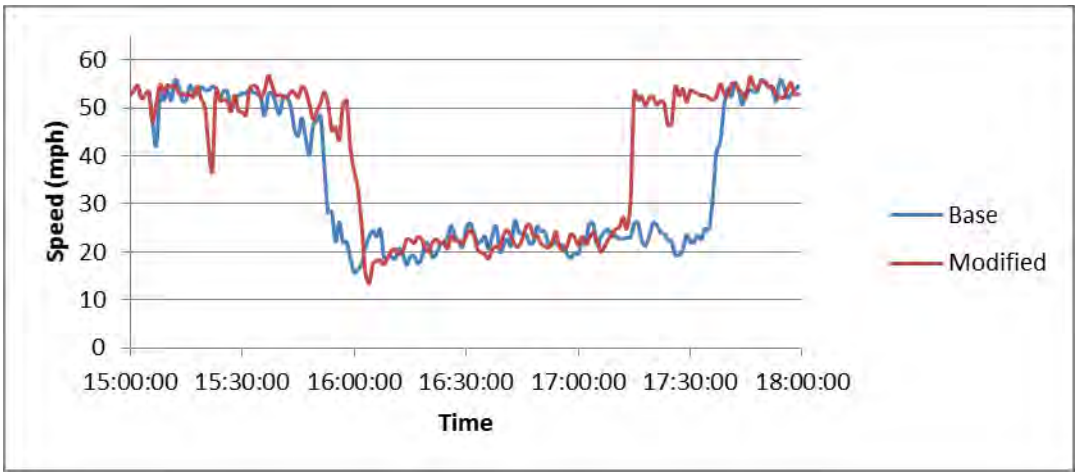

Figure 4-30. Speed profile at 81st St. over the entire duration of the simulation.

In the case of Run 6, the result on the mainline is a delayed time to breakdown at ramp site 3 shown in Figure 4-19. The mainline traffic at ramp site 5 seems largely unaffected. While the results of the metering activation are consistent with respect to the ramp operations, the effect on the mainline traffic is not consistent.

Additional testing was performed by increasing the initialization threshold from the original value upward to a maximum of 20%. This testing is aimed to evaluate the impact of a range of activation thresholds on the total travel time of the network. The total travel time results for the entire network, mainline and ramps are shown in Tables 4-7, 4-8, and 4-9 respectively.

Table 3-16. Total Travel Time over the Entire Network Varying the Activation Threshold

	Run 1	Run 2	Run 3	Run 4	Run 5	Run 6	Run 7	Run 8	Run 9	Run 10	Avg	Pct Diff
Base	7050.1	7216.6	6741.4	7444.7	7193.8	6922.1	6744.1	7081.0	7013.2	6969.0	7037.6	
7%	7139.0	6821.7	7277.4	6642.1	6974.4	6741.8	6700.3	7013.1	7222.3	6452.5	6898.5	2.0
8%	7139.0	6821.7	7277.4	6642.1	6974.4	6741.8	6700.3	7013.1	7222.3	6452.5	6898.5	2.0
9%	7139.0	6821.7	7277.4	6642.1	6974.4	6741.8	6700.3	7013.1	7222.3	6452.5	6898.5	2.0
10%	7139.0	6821.7	7277.4	6642.1	6974.4	6741.8	6700.3	7013.1	7222.3	6452.5	6898.5	2.0
11%	7064.0	6924.1	7277.4	7166.9	6974.4	6741.8	7015.6	7106.7	7104.5	6452.5	6982.8	0.8
12%	7072.5	6924.1	7139.0	6635.9	6974.4	6741.8	7015.6	6997.3	6730.6	6452.5	6868.4	2.4
13%	7063.9	6757.4	7538.5	6760.9	7163.1	6852.3	6881.5	7239.2	7064.0	6452.5	6977.3	0.9
14%	6772.1	6637.8	7134.2	6644.0	7310.0	7154.0	7482.7	6892.4	6713.3	6452.5	6919.3	1.7
15%	6991.0	7325.2	6951.5	7026.4	6997.9	6755.3	7247.4	6711.5	6950.5	6935.3	6989.2	0.7
16%	6516.3	7233.1	7627.3	7027.8	6756.5	7319.4	6892.7	6803.3	6583.6	6935.3	6969.5	1.0
17%	6671.6	7045.0	7274.6	6783.0	6767.5	6814.6	7025.5	7075.7	6988.2	7118.0	6956.4	1.2
18%	6671.6	7069.7	7150.6	6951.0	7007.2	6865.2	7030.0	7075.7	6910.0	7118.0	6984.9	0.7
19%	7048.4	7069.7	7202.8	6748.2	7189.1	6865.2	6516.5	7304.7	6756.2	7138.5	6983.9	0.8
20%	6960.4	6913.4	7131.6	6793.3	7231.4	6620.8	7096.6	6795.7	6810.7	6967.5	6932.1	1.5

Table 4-17. Total Travel Time on the Mainline Varying the Activation Threshold

	Run 1	Run 2	Run 3	Run 4	Run 5	Run 6	Run 7	Run 8	Run 9	Run 10	Avg	Pct Diff
Base	6500.0	6660.4	6254.3	6851.4	6664.9	6429.6	6276.4	6553.7	6515.0	6460.1	6516.6	
7%	6558.3	6315.9	6738.1	6165.2	6452.0	6262.6	6210.1	6481.0	6687.8	5971.1	6384.2	2.0
8%	6558.3	6315.9	6738.1	6165.2	6452.0	6262.6	6210.1	6481.0	6687.8	5971.1	6384.2	2.0
9%	6558.3	6315.9	6738.1	6165.2	6452.0	6262.6	6210.1	6481.0	6687.8	5971.1	6384.2	2.0
10%	6558.3	6315.9	6738.1	6165.2	6452.0	6262.6	6210.1	6481.0	6687.8	5971.1	6384.2	2.0
11%	6551.0	6414.2	6738.1	6612.7	6452.0	6262.6	6475.8	6563.6	6551.0	5971.1	6459.2	0.9
12%	6533.6	6414.2	6601.9	6156.2	6452.0	6262.6	6475.8	6486.9	6241.3	5971.1	6359.6	2.4
13%	6542.6	6266.9	6975.4	6262.8	6626.3	6362.0	6408.8	6696.1	6507.0	5971.1	6461.9	0.8
14%	6246.5	6146.0	6588.8	6167.9	6722.1	6626.1	6894.2	6376.9	6228.8	5971.1	6396.9	1.8
15%	6448.8	6797.1	6458.2	6495.8	6506.0	6264.9	6695.9	6233.2	6419.0	6440.4	6475.9	0.6
16%	6068.4	6703.5	7013.0	6519.1	6269.6	6749.3	6404.0	6301.0	6126.4	6440.4	6459.5	0.9
17%	6170.4	6536.1	6690.1	6321.6	6301.0	6343.3	6497.9	6603.0	6469.5	6558.3	6449.1	1.0
18%	6170.4	6581.5	6597.4	6482.3	6492.7	6382.6	6511.7	6603.0	6430.6	6558.3	6481.0	0.5
19%	6531.7	6581.5	6640.9	6255.6	6666.9	6382.6	6052.6	6769.6	6292.9	6619.0	6479.3	0.6
20%	6453.9	6430.7	6636.8	6311.1	6691.9	6182.3	6599.4	6336.7	6336.0	6438.8	6441.8	1.1

Table 4-18. Total Travel Time on the Ramps Varying the Activation Threshold

	Run 1	Run 2	Run 3	Run 4	Run 5	Run 6	Run 7	Run 8	Run 9	Run 10	Avg	Pct Diff
Base	422.8	418.2	432.1	418.9	440.2	432.0	415.4	430.6	442.1	438.7	429.1	
7%	417.0	428.9	467.5	424.6	422.7	424.9	427.8	425.2	458.3	425.0	432.2	-0.7
8%	417.0	428.9	467.5	424.6	422.7	424.9	427.8	425.2	458.3	425.0	432.2	-0.7
9%	417.0	428.9	467.5	424.6	422.7	424.9	427.8	425.2	458.3	425.0	432.2	-0.7
10%	417.0	428.9	467.5	424.6	422.7	424.9	427.8	425.2	458.3	425.0	432.2	-0.7
11%	435.4	454.2	467.5	426.0	422.7	424.9	424.5	432.1	444.6	425.0	435.7	-1.5
12%	427.4	454.2	443.2	426.4	422.7	424.9	424.5	437.8	436.8	425.0	432.3	-0.7
13%	458.0	440.9	485.5	437.0	464.4	440.4	417.2	431.4	421.6	425.0	442.1	-3.0
14%	414.1	407.1	454.8	413.2	431.4	443.5	460.2	427.6	426.9	425.0	430.4	-0.3
15%	402.6	456.1	441.1	406.9	436.5	436.9	453.0	414.3	446.4	442.8	433.7	-1.1
16%	397.3	430.7	424.5	426.1	425.0	407.8	426.2	423.3	411.4	442.8	421.5	1.8
17%	399.7	439.9	414.2	405.6	417.1	416.1	427.3	412.5	399.4	417.8	415.0	3.3
18%	399.7	428.8	418.6	413.6	425.6	401.2	418.7	412.5	432.8	417.8	416.9	2.8
19%	416.0	428.8	412.1	370.9	432.3	401.2	408.4	435.7	412.3	440.6	415.8	3.1
20%	399.1	383.4	427.4	371.7	450.7	378.0	429.4	399.5	430.4	413.3	408.3	4.8

The results show that on average the travel time has been reduced for all of the activation threshold levels tested. Activation set at 12% occupancy produced the best results with a reduction in total network travel time of 2.4%. The initial testing used an activation threshold of 7% for both ramps. The thresholds that were set below 11% occupancy produced identical results for every scenario. This is due to the freeway occupancy being above 10% during the beginning of the simulation. The ramp meters are activated immediately when the simulation starts.

There is no noticeable trend when increasing the activation threshold, and an inconsistency is observed between the ten individual runs for a given activation level. The results on the mainline are consistent with the total network results. On the ramps the travel time has increased on average until 16% occupancy, then the ramp travel time has been reduced. This likely represents the point corresponding to current time of day operations.

Enhancements to the Fuzzy Logic Ramp Metering Algorithm

The enhancements presented in this section are direct alterations to the fuzzy logic control, and are specific to the identified ramps on I-95 in Miami, FL. All enhancements are tested in conjunction with the metering initialization enhancement.

Replacing the Downstream Occupancy Curve with the Probability of Breakdown Curve Based on Downstream Occupancy

Rule 10 of the fuzzy logic algorithm contains a class for downstream occupancy. The proposed modification involves replacing this linear curve with the probability of breakdown curve based on downstream occupancy. In this way probability of breakdown is directly input as the fuzzy class membership. Figures 4-20 and 4-21 show the conversion from the linear input fuzzy class, to the probability of breakdown based on downstream occupancy at 81st St., and 103rd St. respectively. The travel time results for the testing are shown in Table 4-10, 4-11, and 4-12 respectively.

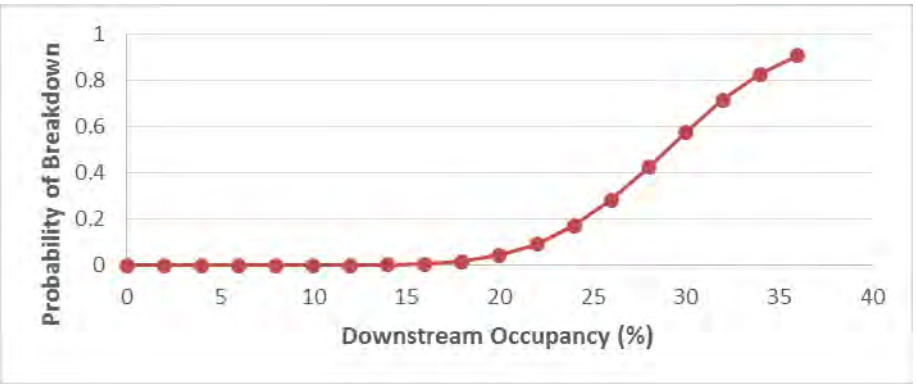

Figure 4-31. Conversion of the downstream occupancy fuzzy class at 81st St.

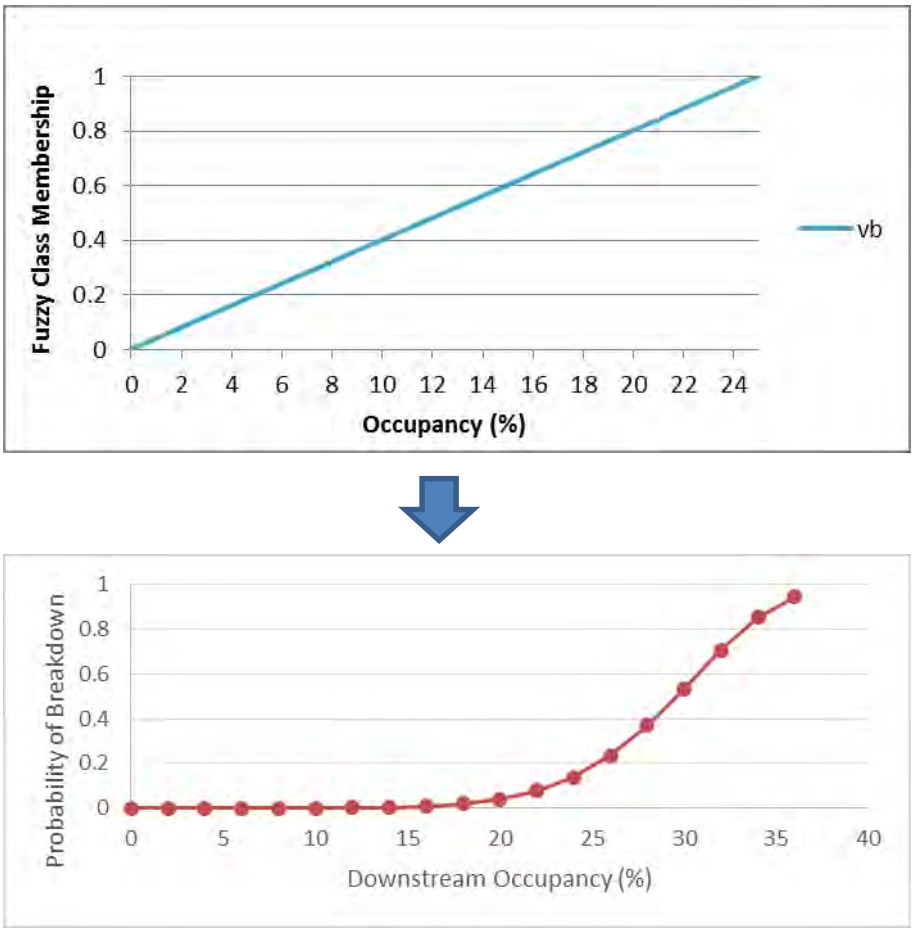

Figure 4-32. Conversion of the downstream occupancy fuzzy class at 103rd St.

Table 4-19. Total Travel Time over the Entire Network

Travel Time (hours)	Run 1	Run 2	Run 3	Run 4	Run 5	Run 6	Run 7	Run 8	Run 9	Run 10	Avg	Pct Diff
Base	7050.1	7216.6	6741.4	7444.7	7193.8	6922.1	6744.1	7081.0	7013.2	6969.0	7037.6	
Modified	6916.1	7179.3	7214.4	6795.6	6947.2	6912.4	7330.3	6936.0	7081.7	6898.1	7021.1	0.2

Table 4-20. Total Travel Time on the Mainline

	Run 1	Run 2	Run 3	Run 4	Run 5	Run 6	Run 7	Run 8	Run 9	Run 10	Avg	Pct Diff
Base	6500.0	6660.4	6254.3	6851.4	6664.9	6429.6	6276.4	6553.7	6515.0	6460.1	6516.6	
Modified	6436.9	6648.4	6721.8	6313.6	6448.2	6413.9	6783.8	6430.9	6528.9	6404.2	6513.1	0.1

Table 4-21. Total Travel Time on the Ramps

Travel Time (hours)	Run 1	Run 2	Run 3	Run 4	Run 5	Run 6	Run 7	Run 8	Run 9	Run 10	Avg	Pct Diff
Base	422.8	418.2	432.1	418.9	440.2	432.0	415.4	430.6	442.1	438.7	429.1	
Modified	422.1	434.0	435.8	424.2	435.2	399.0	420.4	406.4	413.8	428.4	421.9	1.7

The results show an average of 0.2% improvement over the entire network versus the base scenario. Most of this improvement is observed on the ramps. This is due to the shape of the probability of breakdown curve. For every input value of occupancy, the modified algorithm will provide a less restrictive metering rate.

Replacing the Downstream Occupancy Curve with a Transformed Probability of Breakdown Curve Based on Downstream Occupancy

In this modification the downstream occupancy is used as an input and converted to probability of breakdown. A linear relationship between probability of breakdown and fuzzy class membership is established. Due to the flat shape of the probability of breakdown curve at lower

occupancies, the range used for the fuzzy class is restricted to a range of 0.006 to 0.1. The idea is to provide a less restrictive metering rate for lower occupancies, but provide a more restrictive rate at higher occupancy levels. The travel time results for the testing are shown in Table 4-13, 4-14, and 4-15 respectively. The results show on average, no improvement over the entire network versus the base scenario. While there is a 0.7% improvement observed on the ramps, this impact becomes negligible when averaged into the entire network.

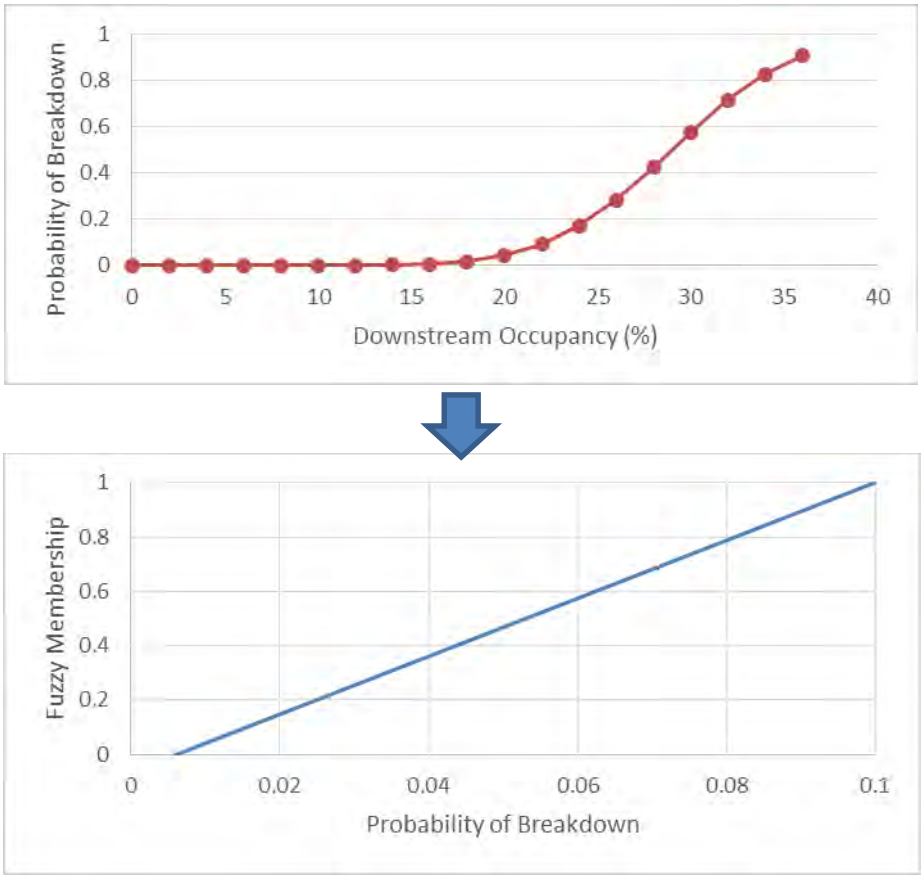

Figure 4-33. Conversion of the downstream POB curve at 81st St.

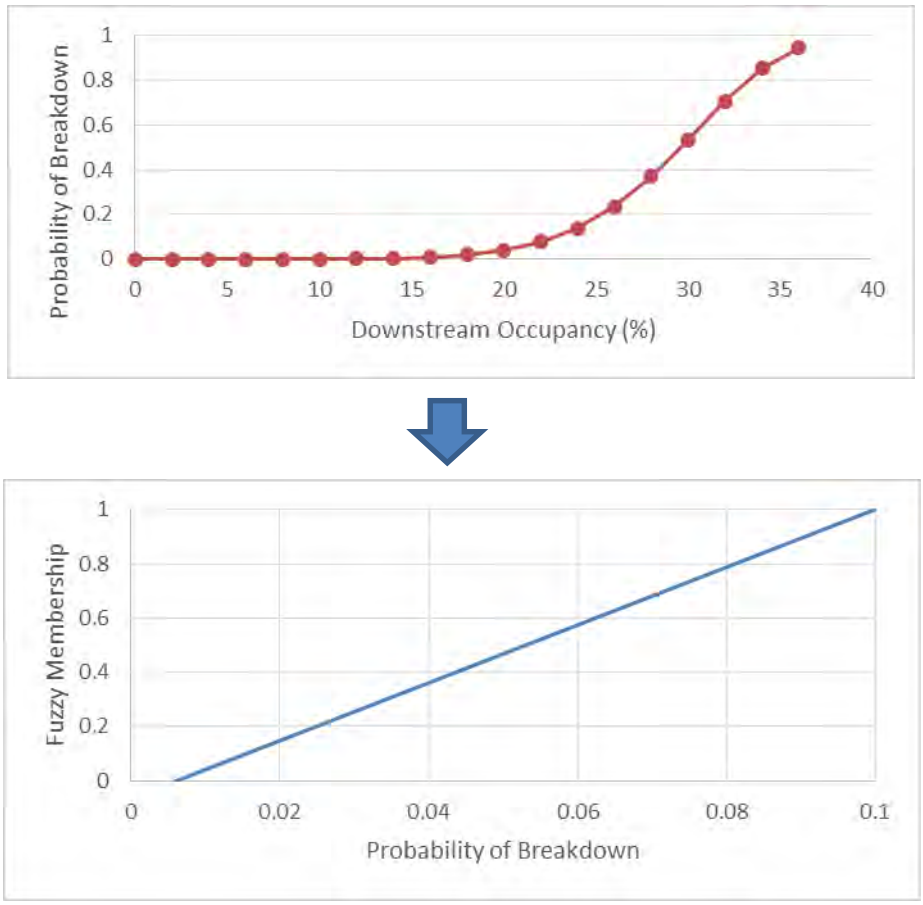

Figure 4-34. Conversion of the downstream POB curve at 103rd St.

Table 4-22. Total Travel Time over the Entire Network

Travel Time (hours)	Run 1	Run 2	Run 3	Run 4	Run 5	Run 6	Run 7	Run 8	Run 9	Run 10	Avg	Pct Diff
Base	7050.1	7216.6	6741.4	7444.7	7193.8	6922.1	6744.1	7081.0	7013.2	6969.0	7037.6	
Modified	6862.3	6933.1	6697.6	7056.9	7320.0	7333.4	7060.1	7031.8	7003.0	7076.6	7037.5	0.0

Table 4-23. Total Travel Time on the Mainline

Travel Time (hours)	Run 1	Run 2	Run 3	Run 4	Run 5	Run 6	Run 7	Run 8	Run 9	Run 10	Avg	Pct Diff
Base	6500.0	6660.4	6254.3	6851.4	6664.9	6429.6	6276.4	6553.7	6515.0	6460.1	6516.6	
Modified	6355.0	6426.1	6232.9	6557.3	6738.1	6763.2	6546.4	6528.5	6491.7	6555.0	6519.4	0.0

Table 4-24. Total Travel Time on the Ramps

Travel Time (hours)	Run 1	Run 2	Run 3	Run 4	Run 5	Run 6	Run 7	Run 8	Run 9	Run 10	Avg	Pct Diff
Base	422.8	418.2	432.1	418.9	440.2	432.0	415.4	430.6	442.1	438.7	429.1	
Modified	422.5	425.3	395.1	442.2	428.7	463.6	442.6	409.7	407.5	425.0	426.2	0.7

Replacing the Local Occupancy Fuzzy Set with Transformed Probability of Breakdown Curves Based on Local Occupancy

A probability of breakdown curve was generated for each ramp based on local occupancy. In the normal fuzzy logic metering operation there is currently a set of fuzzy rules based on local occupancy. The local occupancy is classified by 5 fuzzy sets as very small (VS), small (S), medium (M), big (B), and very big (VB). The probability of breakdown plot was used to re-classify the fuzzy sets. Because the range of values is restricted due to the shape of the probability of breakdown curve, the intervals are not evenly distributed. The range for each fuzzy class are as follows: VS (0.00005 – 0.002), S (0.0001 – 0.025), M (0.002 – 0.1), B (0.05 – 0.2), VB (0.1 – 0.2).

The creation of the fuzzy class sets for 81st St., is shown in Figure 4-19. The travel time results for the testing are shown in Table 4-16, 4-17, and 4-18 respectively.

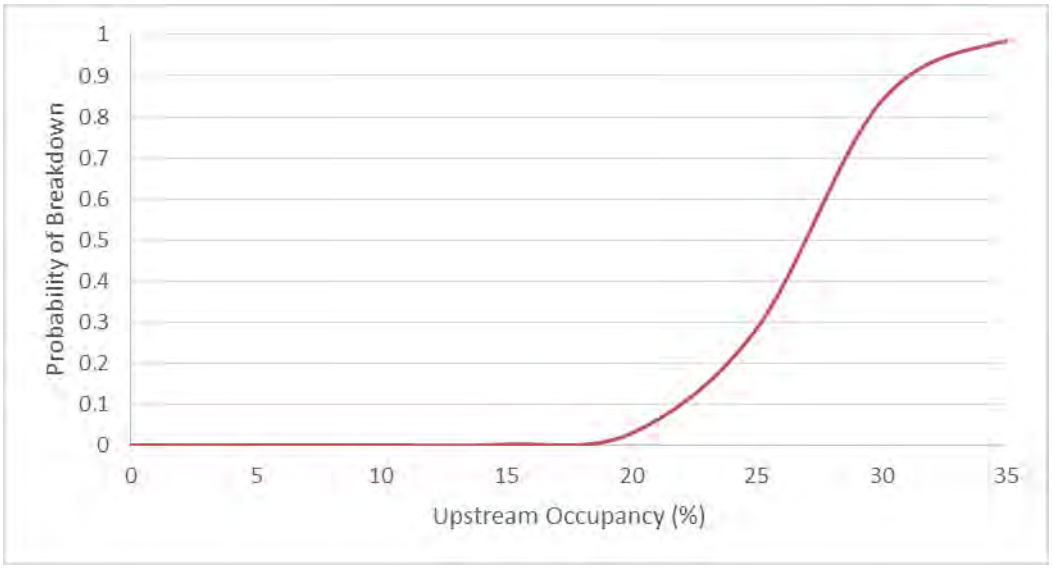

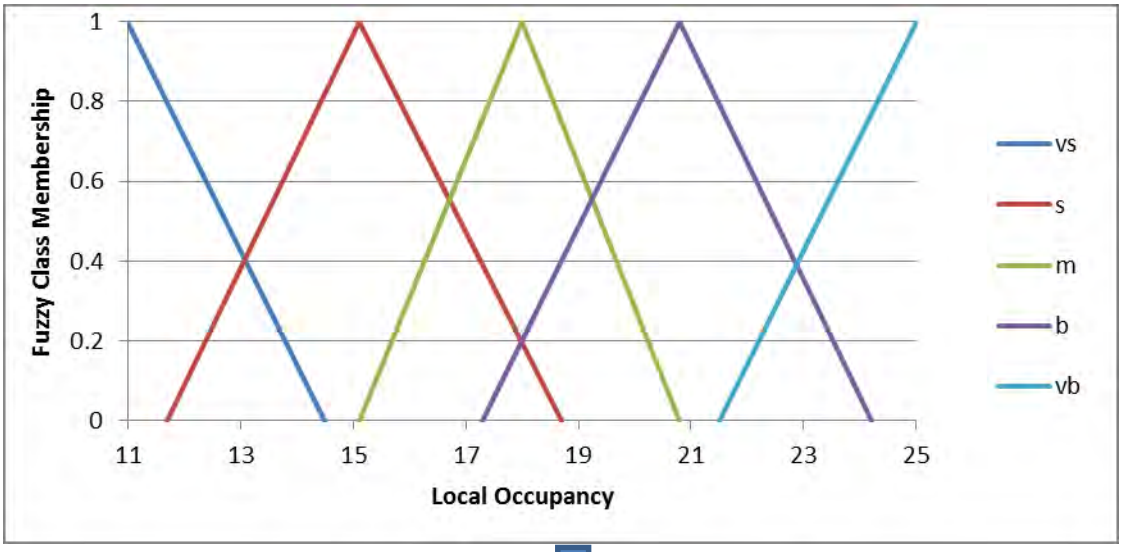

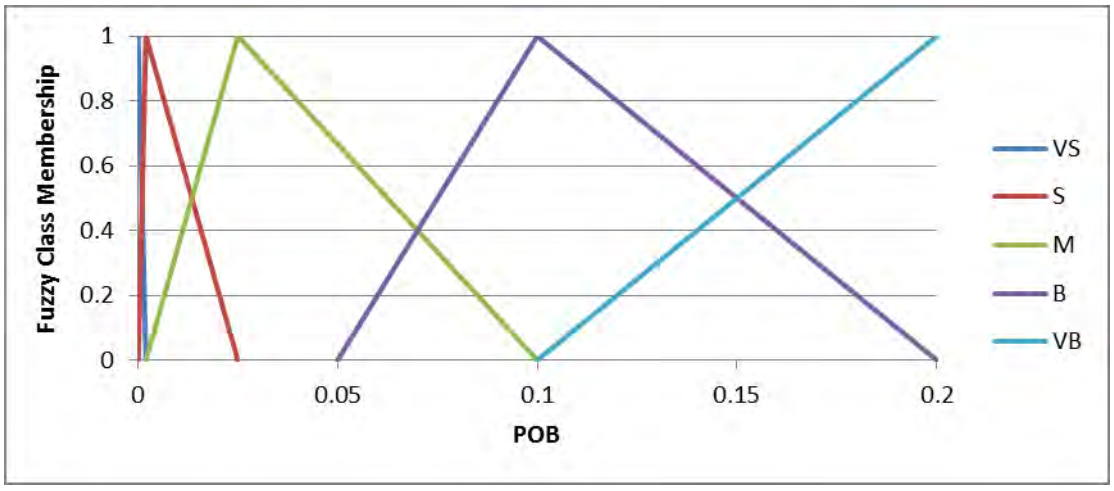

Figure 4-35. Creation of the Fuzzy Sets based on Local Occupancy at 81st Street.

Table 4-25. Total Travel Time over the Entire Network

Travel Time (hours)	Run 1	Run 2	Run 3	Run 4	Run 5	Run 6	Run 7	Run 8	Run 9	Run 10	Avg	Pct Diff
Base	7050.1	7216.6	6741.4	7444.7	7193.8	6922.1	6744.1	7081.0	7013.2	6969.0	7037.6	
Modified	6957.6	7261.7	6950.0	6571.0	7143.9	6985.1	7029.4	7167.2	6958.4	7233.8	7025.8	0.2

Table 4-26. Total Travel Time on the Mainline

Travel Time (hours)	Run 1	Run 2	Run 3	Run 4	Run 5	Run 6	Run 7	Run 8	Run 9	Run 10	Avg	Pct Diff
Base	6500.0	6660.4	6254.3	6851.4	6664.9	6429.6	6276.4	6553.7	6515.0	6460.1	6516.6	
Modified	6397.7	6437.4	6583.0	6441.5	6295.3	6376.8	6724.1	6269.9	6703.2	6403.2	6463.2	0.8

Table 4-27. Total Travel Time on the Ramps

	Run 1	Run 2	Run 3	Run 4	Run 5	Run 6	Run 7	Run 8	Run 9	Run 10	Avg	Pct Diff
Base	422.8	418.2	432.1	418.9	440.2	432.0	415.4	430.6	442.1	438.7	429.1	
Modified	437.2	425.5	447.3	449.1	442.8	433.5	432.8	436.4	466.8	443.7	441.5	-2.9

The results show an average of 0.2% improvement over the entire network versus the base scenario. This improvement is only observed on the mainline while the ramp segments are negatively affected. This is due to the selection of threshold values in the probability of breakdown curve. Because the probability of breakdown curve is flat during under-critical conditions, the range of the S and VS classes is limited. This algorithm has the ability to distribute delay to either the ramp or the mainline through selection of the threshold values. With this flexibility also comes added complexity, as there are numerous possible variations on the selection of thresholds.

Determine a metering rate based on probability of breakdown external to the fuzzy logic ramp metering process. Then select the most restrictive metering rate

For this modification a probability of breakdown curve is created based on downstream volume, and a critical probability of breakdown threshold is selected. Each minute the average volumes are relayed to the controller. If the critical probability of breakdown has been exceeded, the current metering rate is reduced to bring the total volume below critical level. Based on the shape of the probability of breakdown curve, the critical breakdown probability threshold is set to 0.01. The metering rate reduction is set to reduce the total volume to a level 100 vph below the critical value. After this calculation, the most restrictive metering rate is selected between the calculated and the fuzzy logic recommended rates. Based on the recommendations from the Sunguide Center, the maximum and minimum metering rates for the two ramps are: 81st St.(13 vpm, 20 vpm), 103rd St. (8 vpm, 20 vpm). The probability of breakdown curves showing the selected critical value are seen in Figures 4-25 and 4-26. The travel time results are shown in Tables 4-19, 4-20, and 4-21.

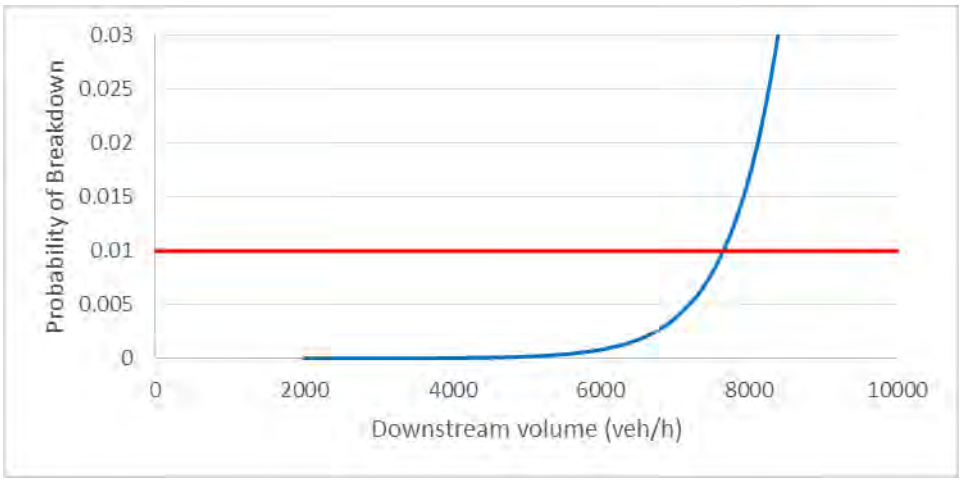

Figure 4-36. Probability of breakdown curve based on downstream volume with critical POB value at 81st Street

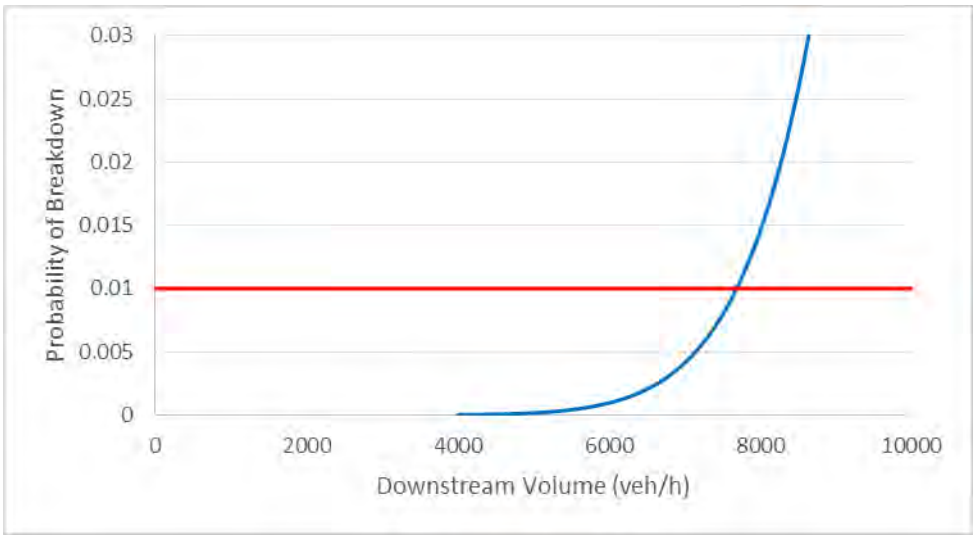

Figure 4-37. Probability of Breakdown curve based on downstream volume with critical POB value at 103rd Street.

Table 4-28. Total Travel Time over the Entire Network

Travel Time (hours)	Run 1	Run 2	Run 3	Run 4	Run 5	Run 6	Run 7	Run 8	Run 9	Run 10	Avg	Pct Diff
Base	7050.1	7216.6	6741.4	7444.7	7193.8	6922.1	6744.1	7081.0	7013.2	6969.0	7037.6	
Modified	6901.2	6951.1	7147.3	6965.9	6787.0	6931.5	7325.9	6773.3	7266.5	6947.9	6999.7	0.5

Table 4-29.Total Travel Time on the Mainline

	Run 1	Run 2	Run 3	Run 4	Run 5	Run 6	Run 7	Run 8	Run 9	Run 10	Avg	Pct Diff
Base	6500.0	6660.4	6254.3	6851.4	6664.9	6429.6	6276.4	6553.7	6515.0	6460.1	6516.6	
Modified	6482.4	6744.2	6465.3	6117.2	6608.5	6477.0	6491.9	6609.9	6461.2	6685.6	6514.3	0.0

Table 4-30. Total Travel Time on the Ramps

Travel Time (hours)	Run 1	Run 2	Run 3	Run 4	Run 5	Run 6	Run 7	Run 8	Run 9	Run 10	Avg	Pct Diff
Base	422.8	418.2	432.1	418.9	440.2	432.0	415.4	430.6	442.1	438.7	429.1	
Modified	407.8	417.5	417.1	402.1	418.1	409.9	409.8	414.3	421.5	419.5	413.8	3.6

The results show an average of 0.5% improvement over the entire network versus the base scenario. The impact on the mainline appears to minimal, but individual runs show both a positive and negative impact. The travel time on the ramps has improved for every scenario, and on average by 3.6%.

Create a New Fuzzy Class and Rule Based on Probability of Breakdown

A new fuzzy class and rule set are created based on the probability of breakdown. The probability of breakdown curve is based on the local occupancy just upstream of the merge. The range of the fuzzy class was scaled to account for the flattened portion of the probability of breakdown curve at lower occupancies. The fuzzy classes generated for 81st St. and 103rd St. are

shown in Figure 4-27 and Figure 4-28 respectively. A general weighting of 3.0 is used, and each value is converted to a VS metering output class. This new rule is added to the fuzzy rule set:

Rule 13 – If probability of breakdown is VB, metering rate is VS 3.0

The travel time results for the testing are shown in Table 4-22, 4-23, and 4-24 respectively.

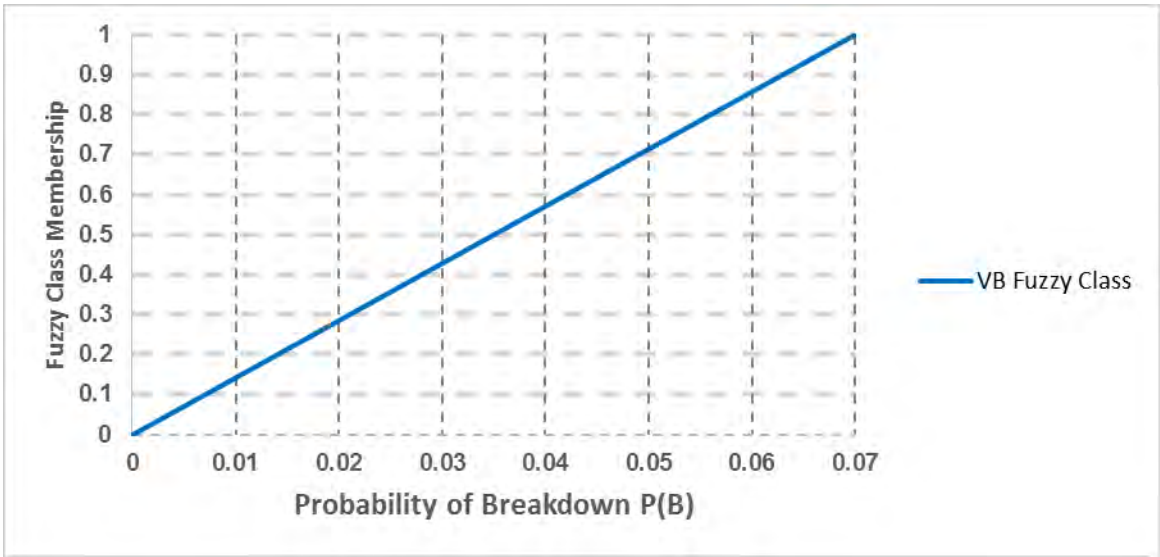

Figure 4-38. Fuzzy Class for POB Based on Local Occupancy at 81st Street

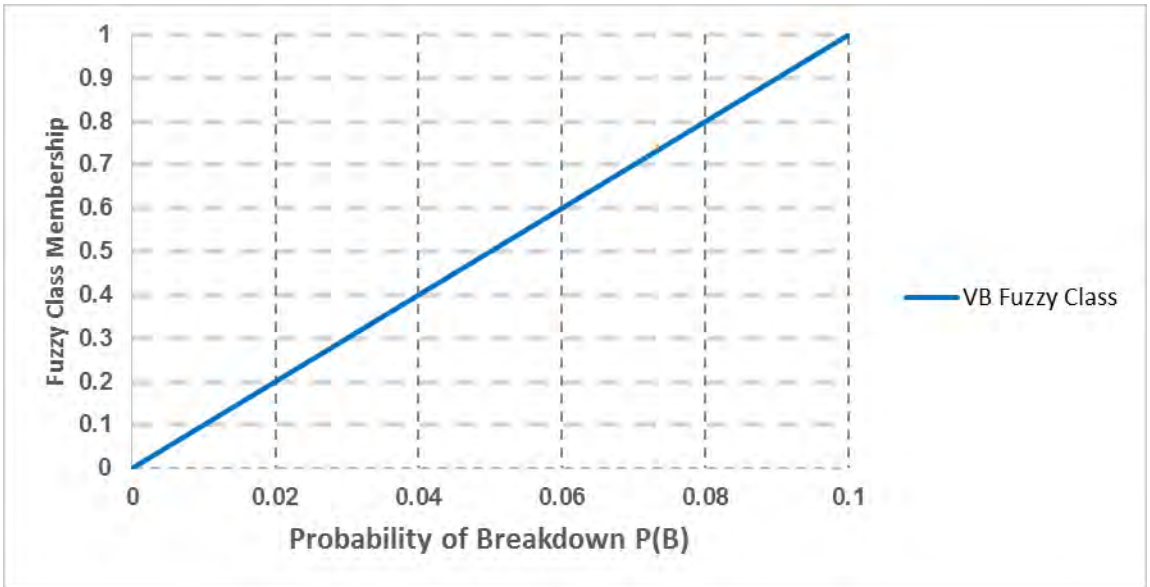

Figure 4-39. Fuzzy Class for POB Based on Local Occupancy at 103rd Street.

Table 4-31. Total Travel Time over the Entire Network

Travel Time (hours)	Run 1	Run 2	Run 3	Run 4	Run 5	Run 6	Run 7	Run 8	Run 9	Run 10	Avg	Pct Diff
Base	7050.1	7216.6	6741.4	7444.7	7193.8	6922.1	6744.1	7081.0	7013.2	6969.0	7037.6	
Modified	6957.6	7261.7	6950.0	6571.0	7143.9	6985.1	7029.4	7167.2	6958.4	7233.8	7025.8	0.2

Table 4-32. Total Travel Time on the Mainline

Travel Time (hours)	Run 1	Run 2	Run 3	Run 4	Run 5	Run 6	Run 7	Run 8	Run 9	Run 10	Avg	Pct Diff
Base	6500.0	6660.4	6254.3	6851.4	6664.9	6429.6	6276.4	6553.7	6515.0	6460.1	6516.6	
Modified	6537.8	6245.9	6683.5	6405.5	6457.8	6597.8	6564.2	6254.4	6404.7	6496.2	6464.8	0.8

Table 4-33. Total Travel Time on the Ramps

Travel Time (hours)	Run 1	Run 2	Run 3	Run 4	Run 5	Run 6	Run 7	Run 8	Run 9	Run 10	Avg	Pct Diff
Base	422.8	418.2	432.1	418.9	440.2	432.0	415.4	430.6	442.1	438.7	429.1	
Modified	416.0	408.8	458.0	433.0	452.9	467.8	448.7	436.6	435.9	446.7	440.4	-2.6

The results show an average of 0.2% improvement over the entire network versus the base scenario. The impact on the mainline appears positive, but the individual runs do not show a consistent improvement. The travel time on the ramps has increased on average by 2.6%.

Continued Testing

Based on the testing performed, a more detailed testing procedure was performed on one algorithm modification. The modified algorithm from the previous section was selected for further testing. This modification creates a new fuzzy class and rule based on probability of breakdown. The probability of breakdown curve was generated using local occupancy data.

Increased Demand

The first variation on the testing was to increase the demand in the network. The demand was increased by 5% for all on ramps and entry nodes. The travel time results are shown in Tables 4-25, 4-26, and 4-27.

Table 4-34. Total Travel Time over the Entire Network

Travel Time (hours)	Run 1	Run 2	Run 3	Run 4	Run 5	Run 6	Run 7	Run 8	Run 9	Run 10	Avg	Pct Diff
Base	9139.8	9298.0	9366.6	8897.6	9127.1	9355.6	9183.9	9113.0	9502.0	9201.2	9218.5	
Modified	8877.1	8902.3	9419.7	9359.3	8749.7	9292.3	9068.1	9473.0	9695.2	9155.2	9199.2	0.2

Table 4-35. Total Travel Time on the Mainline

Travel Time (hours)	Run 1	Run 2	Run 3	Run 4	Run 5	Run 6	Run 7	Run 8	Run 9	Run 10	Avg	Pct Diff
Base	9139.8	9298.0	9366.6	8897.6	9127.1	9355.6	9183.9	9113.0	9502.0	9201.2	9218.5	
Modified	8877.1	8902.3	9419.7	9359.3	8749.7	9292.3	9068.1	9473.0	9695.2	9155.2	9199.2	0.2

Table 4-36. Total Travel Time on the Ramps

Travel Time (hours)	Run 1	Run 2	Run 3	Run 4	Run 5	Run 6	Run 7	Run 8	Run 9	Run 10	Avg	Pct Diff
Base	786.4	732.4	757.4	792.1	747.8	788.6	809.4	799.7	760.2	770.4	774.4	
Modified	796.4	788.0	762.8	772.8	788.0	818.7	755.7	777.7	797.0	785.5	784.2	-1.3

The results show an average of 0.2% improvement over the entire network versus the base scenario. This is the same improvement observed in the previous demand scenario. However, there was a shift of delay from the ramps to the mainline. This may be due to ramp queue lengths becoming large. In the fuzzy logic algorithm when queue lengths reach a maximum fuzzy value, the metering rate is relaxed allowing dissipation of this queue.

Variation of Thresholds for Algorithm 5 Using Downstream Occupancy

Testing was performed varying the value that the probability of breakdown curve was scaled to. Each ramp was tested separately from the other to ensure the only variable was the scaling factor for each ramp. The value of the scaling factor for each ramp varied from 0.00625 to 0.871. The results are shown in Table 4-28 through Table 4-33.

From the results it is shown that on average the total travel time is reduced for most scenarios, but this trend is not observed through all ten runs. There is no obvious trend that would suggest one weighting strategy over the other. Between both 81st St. and 103rd St. the travel time on the ramps has increased relative to the base scenario.

Table 4-37.Total Travel Time over the Entire Network with Modification at 81st St.

	Run 1	Run 2	Run 3	Run 4	Run 5	Run 6	Run 7	Run 8	Run 9	Run 10	Avg	Pct Diff
Base	7050.1	7216.6	6741.4	7444.7	7193.8	6922.1	6744.1	7081.0	7013.2	6969.0	7037.6	
0.85	7375.0	6748.4	6806.4	6820.5	7063.1	7132.4	6782.6	6843.7	7381.8	7048.3	7000.2	0.5
0.75	7053.4	6610.0	7105.9	6856.4	7367.6	6856.2	7235.7	6703.9	7054.5	7112.4	6995.6	0.6
0.65	6798.9	7100.7	7644.0	7506.4	7276.0	6892.3	7022.0	6827.7	6494.7	7202.6	7076.5	-0.6
0.55	6462.6	6688.5	6645.6	7028.0	7587.8	7026.6	6896.5	7130.1	6793.5	7034.3	6929.3	1.5
0.482	6836.6	7142.2	7440.7	6717.6	7332.8	6883.1	6724.7	7008.4	6836.2	7011.4	6993.4	0.6
0.4	6530.7	6993.3	7464.4	7308.2	7212.5	6718.8	6906.4	7389.1	6830.7	7076.2	7043.0	-0.1
0.3	6991.8	6843.7	6782.0	6585.7	6909.6	7006.4	7162.0	6826.3	6954.2	6769.0	6883.1	2.2
0.2	6865.2	6631.0	6640.9	6795.5	7119.1	6813.5	6748.2	6883.8	7038.2	7083.3	6861.9	2.5
0.1	6998.3	6772.4	6989.2	6820.1	7363.8	7214.3	7027.5	7159.9	7082.5	6839.6	7026.8	0.2
0.05	6858.8	7196.0	7134.1	7028.5	7221.5	6540.6	6779.1	6854.3	6914.8	7058.8	6958.7	1.1
0.025	6665.8	7128.1	6956.9	6878.6	7308.3	6838.2	7063.3	6866.6	6829.8	6892.0	6942.8	1.3
0.0125	7144.6	6735.4	7274.8	6976.2	7233.7	6757.6	7169.7	7135.5	6607.5	7291.8	7032.7	0.1
0.00625	6790.6	6949.5	7131.7	6963.6	7268.6	6743.1	6869.6	7095.3	6910.5	6540.6	6926.3	1.6

Table 4-38. Total Travel Time on the Mainline with Modification at 81st St.

	Run 1	Run 2	Run 3	Run 4	Run 5	Run 6	Run 7	Run 8	Run 9	Run 10	Avg	Pct Diff
Base	6500.0	6660.4	6254.3	6851.4	6664.9	6429.6	6276.4	6553.7	6515.0	6460.1	6516.6	
0.85	6791.4	6272.2	6312.9	6343.4	6485.9	6603.8	6286.9	6349.6	6784.5	6529.2	6476.0	0.6
0.75	6551.2	6136.7	6575.1	6352.9	6844.7	6374.9	6693.5	6218.2	6514.4	6602.1	6486.4	0.5
0.65	6308.0	6519.9	7027.9	6951.3	6731.6	6399.8	6489.8	6349.6	6037.0	6655.2	6547.0	-0.5
0.55	6016.2	6205.6	6182.5	6504.7	7003.8	6488.9	6404.0	6557.9	6289.3	6488.2	6414.1	1.6
0.482	6332.3	6615.1	6873.8	6247.0	6772.2	6394.6	6243.6	6472.5	6351.7	6512.0	6481.5	0.5
0.4	6075.0	6503.0	6892.7	6711.0	6678.4	6210.2	6408.8	6794.7	6315.2	6582.2	6517.1	0.0
0.3	6547.0	6407.2	6351.9	6174.5	6480.2	6546.4	6714.5	6405.6	6515.0	6344.8	6448.7	1.0
0.2	6333.9	6159.9	6174.7	6305.6	6619.3	6319.9	6260.5	6406.1	6521.8	6571.0	6367.3	2.3
0.1	6447.5	6305.8	6440.9	6334.8	6795.7	6667.1	6474.8	6636.0	6570.4	6361.7	6503.5	0.2
0.05	6331.5	6616.1	6573.5	6485.5	6694.3	6083.7	6284.9	6374.0	6408.4	6530.4	6438.2	1.2
0.025	6173.8	6583.3	6419.1	6387.2	6751.5	6339.0	6523.4	6378.6	6344.7	6391.1	6429.2	1.3
0.0125	6562.6	6258.2	6667.0	6471.1	6680.5	6247.3	6642.6	6622.8	6139.8	6724.8	6501.7	0.2
0.00625	6263.1	6453.8	6587.6	6447.7	6716.8	6268.1	6388.9	6574.4	6405.4	6065.4	6417.1	1.5

Table 4-39. Total Travel Time on the Ramps with Modification at 81st St.

	Run 1	Run 2	Run 3	Run 4	Run 5	Run 6	Run 7	Run 8	Run 9	Run 10	Avg	Pct Diff
Base	422.8	418.2	432.1	418.9	440.2	432.0	415.4	430.6	442.1	438.7	429.1	
0.85	456.8	422.5	418.4	421.7	447.6	430.9	422.5	442.6	428.6	439.0	433.1	-0.9
0.75	430.5	412.3	441.3	416.8	464.0	430.3	444.3	404.4	433.3	447.6	432.5	-0.8
0.65	403.4	411.3	436.2	443.4	467.9	419.2	448.5	418.5	409.3	435.2	429.3	0.0
0.55	393.0	423.0	415.5	415.8	464.7	422.9	430.3	418.1	415.8	413.6	421.3	1.8
0.482	437.9	447.3	431.0	419.9	457.5	416.2	431.0	414.1	436.7	433.5	432.5	-0.8
0.4	405.2	433.3	436.4	419.4	435.1	403.3	430.1	431.1	419.2	445.7	425.9	0.8
0.3	438.2	426.9	424.4	403.1	423.6	453.0	441.1	413.4	436.6	417.2	427.7	0.3
0.2	400.7	410.2	413.2	430.1	449.8	407.5	427.7	422.5	421.7	453.9	423.7	1.3
0.1	396.7	408.8	433.8	423.8	479.1	419.5	417.3	434.1	453.8	427.2	429.4	-0.1
0.05	402.1	417.1	412.5	445.3	436.6	407.6	437.8	423.6	417.6	445.7	424.6	1.0
0.025	400.9	441.4	407.2	418.0	466.3	409.3	430.9	426.3	431.6	410.1	424.2	1.1
0.0125	402.5	426.9	412.3	442.8	463.7	401.6	455.1	449.9	406.4	433.4	429.5	-0.1
0.00625	392.4	439.9	423.8	452.9	476.7	423.7	428.3	445.7	440.9	409.7	433.4	-1.0

Table 4-40. Total Travel Time over the Entire Network with Modification at 103rd St.

	Run 1	Run 2	Run 3	Run 4	Run 5	Run 6	Run 7	Run 8	Run 9	Run 10	Avg	Pct Diff
Base	7050.1	7216.6	6741.4	7444.7	7193.8	6922.1	6744.1	7081.0	7013.2	6969.0	7037.6	
0.871	6836.6	7142.2	7440.7	6717.6	7332.8	6883.1	6724.7	7008.4	6836.2	7011.4	6993.4	0.6
0.75	6624.8	6692.6	6652.3	7089.1	7124.2	6625.9	6803.4	7034.3	6907.8	6844.5	6839.9	2.8
0.65	6603.5	6704.7	6932.7	7379.3	7245.8	7002.5	7187.2	6925.5	6836.1	6805.8	6962.3	1.1
0.55	6942.8	6963.3	6866.5	7165.2	7129.1	6873.6	6827.1	7016.4	6831.2	6977.4	6959.3	1.1
0.45	7014.8	6946.4	7070.5	7314.0	7191.8	6973.9	6997.7	6731.2	6836.6	7244.5	7032.1	0.1
0.35	6886.5	7064.0	6888.3	7350.2	7108.9	7071.9	7038.4	6849.8	6914.1	7045.9	7021.8	0.2
0.25	6687.9	6712.9	6861.5	7042.3	7042.4	7124.1	7169.8	7115.1	6809.4	6767.8	6933.3	1.5
0.15	7053.6	6897.2	6897.4	7064.7	7064.0	6916.2	7048.7	7091.7	6731.7	7166.2	6993.1	0.6
0.1	7125.6	6712.5	6742.5	7230.7	7205.8	7168.8	7229.2	6610.4	6829.3	7141.8	6999.7	0.5
0.05	6997.1	7085.8	6908.6	6901.1	7014.2	6684.4	7315.5	6767.0	6615.3	6911.8	6920.1	1.7
0.025	6794.1	7338.4	7297.0	6766.8	7639.9	6529.9	7215.8	6662.3	6961.0	7264.0	7046.9	-0.1
0.0125	7271.4	7047.9	6756.2	7063.5	7188.8	6738.0	7083.8	6961.0	6669.4	7285.0	7006.5	0.4
0.00625	6840.3	6645.5	6820.6	7060.7	7216.3	6577.3	6995.1	7317.3	7001.6	7094.9	6957.0	1.1

Table 4-41. Total Travel Time on the Mainline with Modification at 103rd St.

	Run 1	Run 2	Run 3	Run 4	Run 5	Run 6	Run 7	Run 8	Run 9	Run 10	Avg	Pct Diff
Base	6500.0	6660.4	6254.3	6851.4	6664.9	6429.6	6276.4	6553.7	6515.0	6460.1	6516.6	
0.871	6332.3	6615.1	6873.8	6247.0	6772.2	6394.6	6243.6	6472.5	6351.7	6512.0	6481.5	0.5
0.75	6123.7	6231.8	6403.2	6811.8	6722.2	6450.1	6637.7	6415.5	6342.3	6292.5	6443.1	1.1
0.65	6123.7	6231.8	6403.2	6811.8	6722.2	6450.1	6637.7	6415.5	6342.3	6292.5	6443.1	1.1
0.55	6413.6	6465.9	6353.0	6668.7	6619.6	6357.3	6343.4	6536.4	6310.9	6435.9	6450.5	1.0
0.45	6512.0	6424.7	6553.6	6750.3	6645.8	6448.4	6485.9	6227.4	6344.6	6717.1	6511.0	0.1
0.35	6391.5	6536.4	6409.0	6769.0	6588.0	6532.0	6507.6	6360.1	6431.8	6555.8	6508.1	0.1
0.25	6625.3	6236.7	6262.9	6660.9	6699.6	6607.3	6682.1	6136.3	6333.7	6609.0	6485.4	0.5
0.15	6625.3	6236.7	6262.9	6660.9	6699.6	6607.3	6682.1	6136.3	6333.7	6609.0	6485.4	0.5
0.1	6625.3	6236.7	6262.9	6660.9	6699.6	6607.3	6682.1	6136.3	6333.7	6609.0	6485.4	0.5
0.05	6466.5	6559.4	6426.1	6373.5	6523.5	6203.7	6771.4	6266.7	6136.5	6405.3	6413.3	1.6
0.025	6310.0	6759.0	6748.3	6264.5	7016.5	6061.5	6676.2	6187.2	6442.8	6711.8	6517.8	0.0
0.0125	6693.6	6509.5	6269.6	6509.0	6662.9	6255.8	6571.1	6452.2	6204.8	6750.3	6487.9	0.4
0.00625	6326.7	6162.5	6335.1	6516.5	6655.2	6124.0	6470.3	6713.0	6474.8	6549.6	6432.8	1.3

Table 4-42. Total Travel Time on the Ramps with Modification at 103rd St.

	Run 1	Run 2	Run 3	Run 4	Run 5	Run 6	Run 7	Run 8	Run 9	Run 10	Avg	Pct Diff
Base	422.8	418.2	432.1	418.9	440.2	432.0	415.4	430.6	442.1	438.7	429.1	
0.871	437.9	447.3	431.0	419.9	457.5	416.2	431.0	414.1	436.7	433.5	432.5	-0.8
0.75	405.2	407.8	422.3	459.3	463.5	439.6	445.4	412.4	425.8	443.3	432.5	-0.8
0.65	405.2	407.8	422.3	459.3	463.5	439.6	445.4	412.4	425.8	443.3	432.5	-0.8
0.55	392.4	419.0	398.9	443.1	453.4	425.2	434.2	427.7	428.2	410.6	423.3	1.4
0.45	430.4	434.9	433.8	438.0	440.7	402.2	451.7	403.3	422.7	443.1	430.1	-0.2
0.35	424.0	438.0	422.0	421.7	458.4	415.9	417.5	431.3	429.1	436.8	429.5	-0.1
0.25	453.1	422.4	431.3	435.4	453.7	408.1	434.1	414.1	408.0	452.4	431.3	-0.5
0.15	453.1	422.4	431.3	435.4	453.7	408.1	434.1	414.1	408.0	452.4	431.3	-0.5
0.1	453.1	422.4	431.3	435.4	453.7	408.1	434.1	414.1	408.0	452.4	431.3	-0.5
0.05	429.7	443.5	434.2	426.6	423.8	398.9	456.3	417.3	391.2	438.1	426.0	0.7
0.025	425.1	416.8	451.3	412.6	450.3	400.0	441.4	423.3	423.2	462.8	430.7	-0.4
0.0125	416.9	429.2	436.0	425.8	469.5	429.6	446.8	430.9	411.8	433.7	433.0	-0.9
0.00625	432.5	416.0	433.5	427.2	463.2	400.6	442.7	425.0	417.4	428.5	428.7	0.1

Weighting Testing

The weighting of the new fuzzy class rule described in the previous section was varied to test the impact different weightings would have on network performance. The modifications to the algorithm at 81st St. and 103rd St. were tested independently to evaluate their impact. Based on the results of the threshold scaling testing, the fuzzy classes at 81st St. and 103rd St. were scaled to 0.3 and 0.75 respectively. The results of the testing are shown in Table 4-34 through 4-39.

Table 4-43. Total Travel Time over the Entire Network with Modification at 81st St.

	Run 1	Run 2	Run 3	Run 4	Run 5	Run 6	Run 7	Run 8	Run 9	Run 10	Avg	Pct Diff
Base	7050.1	7216.6	6741.4	7444.7	7193.8	6922.1	6744.1	7081.0	7013.2	6969.0	7037.6	
Wt 3	6991.8	6843.7	6782.0	6585.7	6909.6	7006.4	7162.0	6826.3	6954.2	6769.0	6883.1	2.2
Wt 4	6903.8	7059.0	6750.6	6998.9	7094.5	6830.7	7355.0	6798.1	7314.0	7185.5	7029.0	0.1
Wt 5												
Wt 6	6788.2	6921.5	7153.4	7105.8	7132.9	6767.5	6962.3	7102.8	7113.5	7181.9	7023.0	0.2
Wt 7	6866.9	6694.1	6750.4	6736.2	7121.3	6836.0	7107.0	6893.7	6845.2	6842.5	6869.3	2.4
Wt 8	6719.8	6828.4	7020.6	6897.2	7086.8	7212.9	7207.6	7189.6	6781.0	7247.3	7019.1	0.3
Wt 9	6735.2	6853.5	7126.1	7012.3	7521.3	6860.3	7035.5	6917.3	6699.8	6905.0	6966.6	1.0
Wt 10	6951.6	7130.4	7261.2	6688.7	7238.2	7063.9	6966.7	6689.9	6863.4	7145.9	7000.0	0.5

Table 4-44. Total Travel Time on the Mainline with Modification at 81st St.

	Run 1	Run 2	Run 3	Run 4	Run 5	Run 6	Run 7	Run 8	Run 9	Run 10	Avg	Pct Diff
Base	6500.0	6660.4	6254.3	6851.4	6664.9	6429.6	6276.4	6553.7	6515.0	6460.1	6516.6	
Wt 3	6547.0	6407.2	6351.9	6174.5	6480.2	6546.4	6714.5	6405.6	6515.0	6344.8	6448.7	1.0
Wt 4	6391.4	6514.9	6270.0	6444.3	6578.6	6324.9	6792.9	6307.8	6766.5	6686.3	6507.8	0.1
Wt 5												
Wt 6	6301.6	6396.9	6564.7	6569.4	6617.4	6299.2	6456.9	6550.3	6582.5	6643.7	6498.3	0.3
Wt 7	6360.7	6228.4	6261.6	6231.5	6598.4	6361.5	6586.3	6380.3	6376.9	6360.4	6374.6	2.2
Wt 8	6252.6	6301.8	6467.7	6400.2	6565.1	6658.7	6671.4	6675.2	6262.9	6709.5	6496.5	0.3
Wt 9	6231.2	6361.9	6593.8	6489.8	6931.0	6344.8	6475.2	6412.5	6176.7	6417.4	6443.4	1.1
Wt 10	6443.3	6581.9	6707.2	6198.0	6723.0	6545.3	6473.1	6216.5	6376.5	6631.8	6489.7	0.4

Table 4-45. Total Travel Time on the Ramps with Modification at 81st St.

	Run 1	Run 2	Run 3	Run 4	Run 5	Run 6	Run 7	Run 8	Run 9	Run 10	Avg	Pct Diff
Base	422.8	418.2	432.1	418.9	440.2	432.0	415.4	430.6	442.1	438.7	429.1	
Wt 3	438.2	426.9	424.4	403.1	423.6	453.0	441.1	413.4	436.6	417.2	427.7	0.3
Wt 4	418.4	417.0	408.7	420.5	459.8	408.9	445.7	432.3	418.6	446.7	427.7	0.3
Wt 5												
Wt 6	435.7	398.3	407.6	426.0	433.8	415.3	457.7	452.6	450.5	425.0	430.3	-0.3
Wt 7	398.9	413.0	433.6	414.6	448.1	420.8	465.8	436.5	412.9	426.5	427.1	0.5
Wt 8	408.5	407.8	403.6	425.2	456.0	427.5	452.5	436.9	412.4	450.9	428.1	0.2
Wt 9	414.1	424.3	435.6	429.8	460.0	420.9	425.4	405.1	398.1	436.3	425.0	1.0
Wt 10	414.1	408.1	431.5	427.1	465.4	432.4	435.1	422.2	428.1	432.9	429.7	-0.1

Table 4-46. Total Travel Time over the Entire Network with Modification at 103rd St.

	Run 1	Run 2	Run 3	Run 4	Run 5	Run 6	Run 7	Run 8	Run 9	Run 10	Avg	Pct Diff
Base	7050.1	7216.6	6741.4	7444.7	7193.8	6922.1	6744.1	7081.0	7013.2	6969.0	7037.6	
Wt 3	6624.8	6692.6	6652.3	7089.1	7124.2	6625.9	6803.4	7034.3	6907.8	6844.5	6839.9	2.8
Wt 4	6804.5	6957.6	6708.7	6670.6	7111.5	6672.6	6972.0	7049.9	7126.6	7691.0	6976.5	0.9
Wt 5	6926.6	6943.8	7269.0	6627.2	7493.3	6689.8	6816.4	6838.9	7046.0	7339.8	6999.1	0.5
Wt 6	6726.0	6926.5	6801.0	6589.0	7141.8	7251.4	6948.1	6736.0	6964.0	7147.2	6923.1	1.6
Wt 7	6680.5	6989.1	7322.6	6762.3	7416.0	6601.5	7356.5	6990.0	7029.0	7087.4	7023.5	0.2
Wt 8	6774.7	6704.7	6928.9	6781.7	7284.2	6644.1	6843.2	6902.3	6634.6	7190.0	6868.8	2.4
Wt 9	6769.5	6765.4	6836.8	6758.2	7117.7	6912.4	6987.0	6904.1	7123.8	6788.3	6896.3	2.0
Wt 10	6524.9	6880.1	7031.1	7044.8	6862.5	6577.9	7070.2	7105.8	6657.3	7298.0	6905.3	1.9

Table 4-47. Total Travel Time on the Mainline with Modification at 103rd St.

	Run 1	Run 2	Run 3	Run 4	Run 5	Run 6	Run 7	Run 8	Run 9	Run 10	Avg	Pct Diff
Base	6500.0	6660.4	6254.3	6851.4	6664.9	6429.6	6276.4	6553.7	6515.0	6460.1	6516.6	
Wt 3	6123.7	6231.8	6403.2	6811.8	6722.2	6450.1	6637.7	6415.5	6342.3	6292.5	6443.1	1.1
Wt 4	6316.3	6455.7	6234.8	6185.1	6584.2	6213.5	6418.2	6559.0	6559.2	7099.8	6462.6	0.8
Wt 5	6416.5	6428.3	6659.4	6154.9	6950.0	6187.7	6314.7	6340.0	6524.7	6789.1	6476.5	0.6
Wt 6	6248.6	6375.6	6304.3	6123.9	6601.2	6686.3	6430.7	6270.0	6462.9	6599.5	6410.3	1.6
Wt 7	6196.8	6452.3	6758.0	6287.8	6876.4	6132.3	6834.4	6486.4	6530.5	6544.7	6510.0	0.1
Wt 8	6274.6	6198.7	6434.5	6301.9	6729.1	6159.3	6342.2	6411.9	6157.5	6643.8	6365.4	2.3
Wt 9	6267.9	6285.6	6358.0	6293.8	6596.4	6396.0	6459.6	6386.6	6584.0	6314.6	6394.3	1.9
Wt 10	6072.6	6359.4	6497.2	6547.6	6361.5	6112.3	6564.1	6595.2	6170.7	6735.7	6401.6	1.8

Table 4-48. Total Travel Time on the Ramps with Modification at 103rd St.

	Run 1	Run 2	Run 3	Run 4	Run 5	Run 6	Run 7	Run 8	Run 9	Run 10	Avg	Pct Diff
Base	422.8	418.2	432.1	418.9	440.2	432.0	415.4	430.6	442.1	438.7	429.1	
Wt 3	405.2	407.8	422.3	459.3	463.5	439.6	445.4	412.4	425.8	443.3	432.5	-0.8
Wt 4	430.5	446.1	420.5	423.6	450.7	406.0	412.4	436.4	408.5	465.7	430.0	-0.2
Wt 5	412.6	417.5	426.7	417.2	481.6	405.0	448.8	418.2	434.4	445.7	430.8	-0.4
Wt 6	406.5	394.4	423.4	404.9	451.6	420.4	440.9	417.2	420.9	424.3	420.4	2.0
Wt 7	420.0	410.7	430.5	413.1	487.6	409.7	463.8	430.7	429.3	453.0	434.8	-1.3
Wt 8	409.9	419.8	429.2	414.9	457.5	395.4	436.6	437.0	400.6	438.4	423.9	1.2
Wt 9	418.6	426.3	432.0	414.2	448.5	419.5	420.5	418.4	432.9	425.8	425.7	0.8
Wt 10	404.1	422.7	423.7	434.2	449.0	414.9	449.1	433.0	401.4	420.8	425.3	0.9

Best Scenario Testing

From the sensitivity testing that was performed, the best performing alternatives were chosen to be tested in conjunction with each other. Based on the sensitivity analysis, the activation threshold is set to 12% for both ramp locations. The enhancement used is Algorithm 5 based on downstream occupancy. The scaling factors for the 81st Street, and 103rd Street locations are 0.2 and 0.75 respectively, and the weighting for both rules is set to 3.0. Table 4-40, 4-41, and 4-42 show the travel time results from the testing compared to the base fuzzy logic implementation.

Table 4-49. Total Travel Time over the Entire Network

Travel Time (hours)	Run 1	Run 2	Run 3	Run 4	Run 5	Run 6	Run 7	Run 8	Run 9	Run 10	Avg	Pct Diff
Base	7050.1	7216.6	6741.4	7444.7	7193.8	6922.1	6744.1	7081.0	7013.2	6969.0	7037.6	
Enhanced	6965.3	6842.2	6660.8	7188.1	7053.5	6953.0	6949.0	6812.0	6830.2	7014.4	6926.8	1.6

Table 4-50. Total Travel Time on the Mainline

Travel Time (hours)	Run 1	Run 2	Run 3	Run 4	Run 5	Run 6	Run 7	Run 8	Run 9	Run 10	Avg	Pct Diff
Base	6500.0	6660.4	6254.3	6851.4	6664.9	6429.6	6276.4	6553.7	6515.0	6460.1	6516.6	
Enhanced	6462.2	6292.4	6168.8	6616.8	6507.6	6448.3	6446.5	6304.2	6328.3	6484.7	6406.0	1.7

Table 4-51.Total Travel Time on the Ramps with Modification at 103rd St.

Travel Time (hours)	Run 1	Run 2	Run 3	Run 4	Run 5	Run 6	Run 7	Run 8	Run 9	Run 10	Avg	Pct Diff
Base	422.8	418.2	432.1	418.9	440.2	432.0	415.4	430.6	442.1	438.7	429.1	
Enhanced	444.8	418.7	423.1	416.9	453.9	432.7	444.6	427.8	449.6	434.4	434.6	-1.3

SUMMARY

This study investigated the probability of breakdown in ramp meter activation decision and also in metering rate determination, as explained next. The probability of breakdown was incorporated directly in the fuzzy logic ramp metering control algorithm to allow the algorithm to better react to potential traffic breakdown conditions. A series of simulation experiments were designed in this study to assess the modifications to the fuzzy logic ramp metering system on I-95 in Miami, FL. The northbound I-95 segment that is currently controlled by the fuzzy logic algorithm was first modeled in CORSIM and calibrated to replicate the existing operations. The modifications were tested at two ramp metering locations identified as recurring sources of congestion.

It was concluded that incorporating an activation threshold in the metering operation has the potential to improve or at least replace the current time of day activation. On average, the metering operations with the activation threshold outperformed the current time of day operations

by as much as 2.4% in terms of total network travel time. However, the results were inconsistent between individual runs, and the system was sometimes shown to experience increase in the total travel time. However, an advantage of linking ramp metering rate to breakdown probability is making metering more reactive to non-typical traffic congestion.

A number of different modifications were made to the fuzzy logic ramp metering algorithm to include the probability of breakdown. It was concluded that the effect of these changes on the ramp metering operations is to cause a slightly more strict metering strategy. The mainline showed some travel time improvement, but with more strict metering rates some delay was shifted toward the ramp vehicles. While the modifications showed some potential to improve traffic operations, the overall impact on the network performance was minimal. The total travel time showed improvement on the average, but was inconsistent when analyzing individual runs. Varying traffic demands between individual simulation runs causes the roadway to break down at slightly different locations and times. Based on the location of the source of congestion, the enhanced metering strategy may not be enough to handle congestion resulting from specific mainline and ramp demands. Further exploration of ramp metering combined with other ATDM strategies may prove to result in a more robust control strategy.

Overall, it was concluded that the probability of breakdown inclusion in ramp metering may be able to provide some limited operational improvement at specific bottlenecks and/or along the entire network. However, there was no clear pattern regarding when these improvements are expected, and how different traffic demand levels can affect these impacts. Using an activation threshold to turn on ramp meters seems to be a viable alternative to time of day operation. This would allow less operator involvement and allow the activation process to become demand sensitive.

CHAPTER 5

VARIABLE SPEED LIMIT

BACKGROUND

This research focuses on developing VSL strategies that address congestion caused by recurrent bottlenecks. Figure 5-1 shows how congestion starts at the bottleneck, as breakdown occurs, and how it propagates upstream of the bottleneck. As time passes, the traffic demand decreases and the bottleneck capacity (supply) surpasses demand, resulting in the dissipation of congestion.

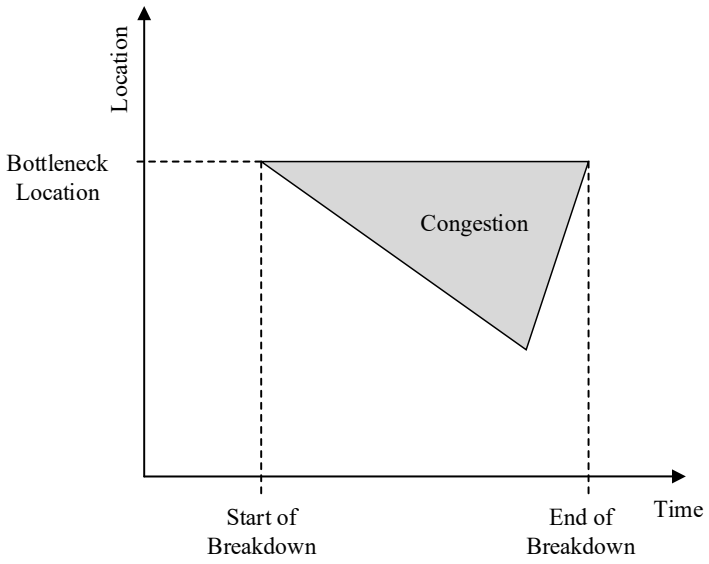

Figure 5-40. Traffic congestion build up and dissipation.

During the development and testing of VSL strategies in this study, results showed that the mobility benefits from VSL can arise from two different mechanisms for the under-saturated and over-saturated regimes. This section presents an overview of the VSL operations during these two different traffic regimes.

Before breakdown occurs, the benefit of VSL is to eliminate or delay traffic breakdown. VSL reduces the average speed and increases travel time as the posted speed limit decreases. The amount of speed reduction depends on the driver compliance rate and the posted dynamic speed limit. At this stage, with VSL, the same traffic flow moves at lower speeds and higher occupancies than the non-VSL state, as shown in Figure 5-2. Although travel time increases due to lower speeds, the VSL can decrease travel time by avoiding or postponing breakdown occurrence.

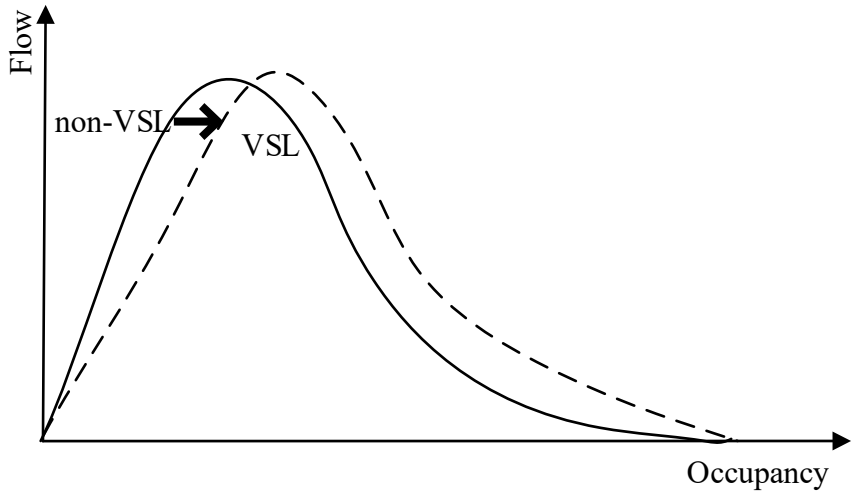

Figure 5-41. VSL impact on fundamental traffic diagram

Freeway capacity has a stochastic nature, which may cause different traffic patterns for the same demand levels. Field study results indicate two days with very similar traffic demands, but significantly different congestion levels and traffic conditions. This shows that breakdown occurrence has a stochastic nature as well. Analysis of field data has shown that breakdown could occur at different traffic flow levels. There has been a considerable amount of research and effort to find the probability of breakdown based on different indices, such as downstream volume and occupancy or the combination of on-ramp and upstream mainline volumes (*23*). Three traffic flow states are considered:

- Free-flow conditions: In this state, the traffic flow is low enough that the probability of breakdown occurrence is zero.
- Light congestion conditions: In this state, traffic flow is low enough such that small disturbances vanish without impacts on traffic, but it is high enough that large disturbances result in breakdown occurrence. In other words, there is a probability of breakdown.
- Heavy congestion conditions: In this state, traffic flow is high enough that breakdown could occur any time if it has not already occurred. In other words, the probability of breakdown is close to one.

At low congestion levels, with zero or very low probability of breakdown, and at heavy congestion conditions, with a breakdown probability close to 1, the VSL system has no room to reduce the probability of breakdown. However, in lower congestion conditions with moderate breakdown probability, the VSL is expected to reduce the probability of breakdown by reducing traffic flow disturbances through the decreasing of the input flow to the bottleneck location and achieving a more homogeneous distribution of speed.

The fundamental diagram of traffic flow shows the relationship between traffic flow and traffic density, and helps to better understand the traffic system's behavior. Figure 3-6 shows that when the VSL is applied prior to breakdown, it reduces the slope of the speed-occupancy relationship. The lower the posted speed limit, the larger the reduction in this slope. In addition, the VSL shifts the critical occupancy to higher values in the diagram, which means that the unstable region of the fundamental diagram shifted to the right. This indicates that the unstable region will start at a higher density with the VSL. While this shift in the fundamental diagram may result in an increase in freeway throughput, if the posted VSL is set too low, it may decrease

freeway capacity since the free-flow speed and capacity are related. This may result in traffic demands exceeding the capacity of the VSL influence area upstream of the bottleneck location. The above discussion indicates that there is a site-specific optimal speed limit to balance the different speed limit effects prior to breakdown.

After the occurrence of traffic breakdown, not only does the traffic speed decrease and congestion increases, but the freeway maximum possible throughput can drop as well. The average traffic speed in the congested area is significantly less than the posted speed limit, which means that lowering the speed limit in the congested segments has no effect on traffic performance. However, the VSL system activated ahead of the congested area can still influence the congestion after breakdown occurrence. During congestion, the VSL mobility benefits are estimated to be due to suppressing backward congestion shockwaves by reducing the inflow of traffic to the congested area. This is expected to result in reducing the growth of queues and thus the extents of traffic congestion. To achieve this goal, as the congested area propagates upstream, the VSL location should be pushed upstream as well.

It has also been suggested that at the head of the queue, specifically around the location of queue discharge, the vehicles should accelerate to increase throughputs (*79*). Deactivation of the VSL at the head of congestion, upstream of the bottleneck, could help vehicle acceleration. Carlson (*81*) suggested that the deactivation of the VSL should be made 0.3 – 0.6 miles ahead of the bottleneck location. This will potentially increase capacity at the bottleneck since capacity is a function of the traffic flow speed. In addition, as HCM points out the higher free-flow speed (posted speed limits), results in a higher capacity of freeway, as shown in Figure 5-3.

In summary, after traffic breakdown, the VSL strategy can be implemented to: (1) reduce the inflow of traffic and thus reduce the propagation of the congestion shockwave; and (2) increase the bottleneck capacity by deactivating the VSL at the head of the congestion.

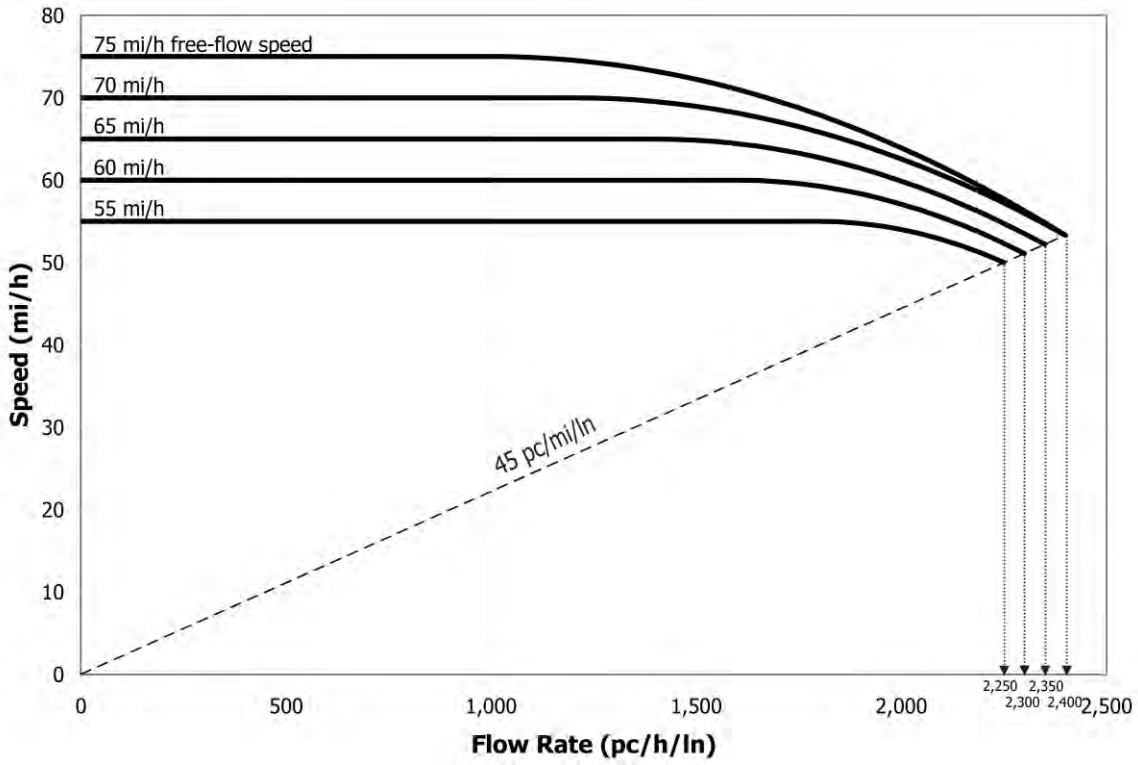

Figure 5-42. Speed-Flow curves for basic freeways segments under base conditions

VSL STRATEGY BASED ON INFRASTRUCTURE DATA

This research proposes a shockwave-based VSL strategy and assesses its ability to reduce the probability and impacts of traffic flow breakdown at bottlenecks. The term "shockwave strategies" indicates that the influence area of VSL signs are pushed upstream of the bottleneck as the probability of the breakdown increases before breakdown, and as the back of queue propagates

upstream after breakdown. The proposed system is based on recognizing the different influences of VSL before and after breakdown occurrence, as stated above.

This proposed VSL system is a reactive system that uses a heuristic switching logic-based controller with specified thresholds of prevailing traffic flow conditions. The logics used to switch the speed limits in the VSL systems, as reported in the literature, utilize thresholds based on occupancy, volume, speed, and combinations of these three variables. Based on simulation results, Elefteriadou et al. (*21*) emphasized that improper selection of the thresholds can cause negative impacts on traffic conditions. Thus, finding the best set of thresholds for setting the speed limits is important.

In this research, occupancy data from point detectors located at and upstream of the bottleneck is used in switching between dynamic speed limit values. By using the fundamental diagram, the breakdown probability model, it is possible to identify a range of potential occupancy thresholds that define the separation between different traffic regimes, which can be used as initial values for VSL switching thresholds. The traffic is categorized in three regimes based on the fundamental traffic breakdown and the probability of breakdown, as follows: free-flow conditions, light congestion conditions, and heavy congestion conditions. These regimes are then associated with different speed values, and as initial values to be displayed by the VSL system. Then, using the developed simulation model, these thresholds are further fine-tuned using an exhaustive enumeration on the threshold ranges to find the set of thresholds that produce the best results in terms of traffic mobility in the network. To prevent fluctuation of the posted speed limits, the switching thresholds that lower speed limits are set to be different from those that switch to higher speed limits.

In the proposed VSL system, the posted speed limits are discrete and are selected in increments of 5 mph, as normally implemented in the real-world. For safety and driver compliance reasons, the VSL system is constrained to maximum updating frequencies, both in time and space.

As stated earlier, the theory and application of VSL before and after breakdown are different, discussed separately in the following section. Before breakdown, the goal of the VSL is to postpone or avoid breakdown occurrence. The VSL system is activated upstream of a potential bottleneck, which is a location with a high probability of breakdown based on traffic detectors upstream of the bottleneck. In the initial implementation, the location of the VSL is set at fixed distances, resulting in a fixed length of the VSL influence areas. Many researchers, such as Talebpour et al. (*84*), indicated that finding the optimal location of the speed limit sign for this operation is important and has the most effect on system performance. In this study, an exhaustive enumeration is conducted to determine the optimal location of the fixed speed limit sign upstream of the bottleneck, taking into consideration the geometric constraints of the interchanges upstream of the bottleneck. When the VSL is placed further upstream of the potential bottleneck, the probability of breakdown is expected to further decrease. However, during uncongested conditions, this slows down vehicular speeds on longer sections of the freeway and can induce new bottlenecks due to lower capacities resulting from lower speeds. The optimal location is one that achieves the best balance between these two factors, which was obtained based on the simulation results. Based on sensitivity analysis, it was found that this location is a function of the static speed limit of the highway.

An extension of the above method was conducted to determine if activating the speed limit signs further upstream of the optimal sign location is beneficial when an increase in occupancy and thus an increase in the probability of breakdown, is detected prior to reaching the high

congestion levels that defines breakdown conditions. This approach is referred to as the "shockwave approach" and results in activating VSL signs further upstream when the traffic is recognized to have the potential to be on its way to breakdown. The proposed shockwave VSL system at this stage can analyze detector data from locations upstream of the bottleneck to determine if there is some increase in occupancy and will activate the upstream signs accordingly.

After breakdown, the VSL influence area should start at a sufficient distance upstream of the back of the queue to reduce shockwave propagation. In this study, the VSL influence extends from the first upstream VSL sign location to the location where the VSL is deactivated by a downstream VSL sign. When the VSL influence area is already congested, the reduction in speed limit by the VSL system has no effect on congestion. Thus, the proposed VSL system uses detector data upstream of the bottleneck to determine how far the congestion propagates upstream of the bottleneck, and furthermore, how far upstream of the back of queue the VSL signs need to be activated. In this approach, the location of the activated VSL sign is dynamic rather than static, with the location of the first activated sign pushed further upstream as the queue length grows; hence, it remains upstream of the back of the queue. This ensures that the VSL decreases the inflow traffic to the congested area in order to control the growth of the congestion. Again, this method of pushing the VSL location upstream is referred to as the shockwave approach in this study. In addition, the VSL system is deactivated within the congested area in order to encourage vehicles to accelerate if they can as they approach the head of the congested area.

The VSL system requires that traffic detector data be collected during short time intervals, such as 20-second to 1-minute intervals. Noise in the detector data causes fluctuation in the posted speed limit, which reduces the safety and compliance rates in real-world implementations, due to too many speed changes. These changes also lead to disturbance in traffic, which could result in

breakdown. To reduce and avoid the impacts of noise, detector data should be smoothed. Two smoothing methods are tested in this study: the simple moving average method, and the exponential moving average method. The simple moving average is the average of the previous "*m*" data points, where m specifies the length of the rolling period. The second type of smoothing, the exponential moving average method, is described in the following equation:

$$Y_t = \alpha X_t + (1 - \alpha) Y_{t-1} \quad (5\text{-}1)$$

where X_t represents the measurement t timestamp and Y_t is the smoothed traffic parameter at the t timestamp. The symbol α in Equation 5-1 refers to a smoothing factor. The expression for α is shown in Equation 5-2 below:

$$\alpha = 1 - e^{\frac{-\Delta t}{\tau}} \quad (5\text{-}2)$$

where Δt is the time interval between two consecutive records and τ is a time constant. The commonly used value of α is 0.4 (*114*).

VSL STRATEGY BASED ON CONNECTED VEHICLE DATA

With the fast-paced growth in technology, speed limit information can be disseminated to drivers by dynamic exchange of messages between vehicles and infrastructure utilizing Connected Vehicle technology. In this research, the effectiveness of VSL signs is compared with the use of V2I communications to inform drivers about speed limits.

In this research, the functions and goals of VSL strategies based on Connected Vehicle data are the same as the VSL strategies based on Infrastructure data. The differences are the source, details, and types of the collected traffic data and the flexibility of where specific information is provided to the vehicles without being constrained by the VSL sign locations. With Connected Vehicles, information from equipped vehicles provides trajectory speed and the location of the vehicle, at each time step.

Collected speed data from Connected Vehicles can be aggregated across any freeway segment in time and space based on the application requirements. Aggregated speed data across freeway segments can present a clear picture of the current traffic conditions at different locations of the freeway. In this research, speeds are aggregated to find the locations of congestion in the network using speed data to justify disseminating new speed limits at a given location. However, other than using the detailed collected data in this way, no attempts were made to utilize other types of collected parameters to enhance the algorithm developed based on infrastructure data.

The locations of congestion can be found using thresholds on speed. Whenever the speed at one segment is above a specific threshold and the speed upstream of the segment is less than the threshold, that point is determined to be at the end of queue or congestion. Having a threshold on the speed difference between two neighboring locations can be used for defining the beginning of the congested area. However, vehicle trajectories tend to be noisy due to various reasons, such as driver differences or the existence of traffic oscillations in congestion. Although this study uses aggregated speed data and has a lower amount of noise compared to individual vehicle data, as explained in Chapter 3, wavelet transform is used to automate the identification of breakdown occurrence, as well as the head and the tail of congestion. If the wavelet transform energy is not at

its peak at the bottleneck area, the breakdown has not occurred yet. After breakdown occurs, the wavelet transform energy's peak can be used to identify the tail of the congested area.

In Connected Vehicle based VSL, the VSL signs at different segments of the freeway are activated based on congestion location identified from speed trajectory data. Figure 5-4 shows the spatial distribution of aggregated trajectory data. As shown in this figure, using trajectory data, traffic regimes can be defined either based on predefined speed thresholds or sharp changes in speed data. The location of congestion can be further determined from these identified traffic regimes. As explained in VSL algorithm section, three different traffic regimes are considered to assign speed limit. It can be seen in Figure 5-4 that traffic is under free-flow conditions from the tail of the congested area to the tail of the VSL influence area, while traffic is in heavy congestion conditions from the bottleneck location to the location that speed begins to increase. The regime between these two locations is characterized as a light congestion condition.

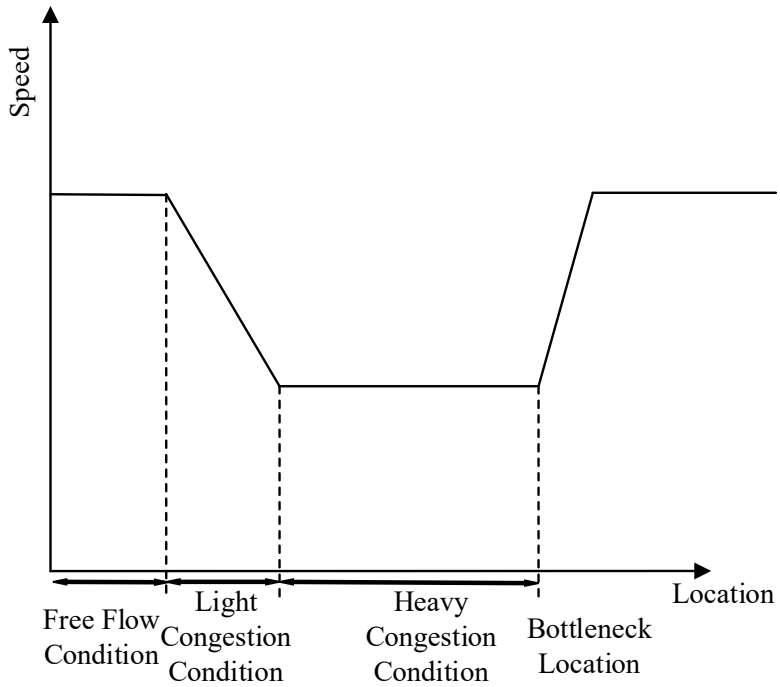

Figure 5-43. Traffic regimes at Congested area.

A shockwave-based VSL implementation is developed based on Connected Vehicle data, which is similar to the aforementioned VSL based on infrastructure data. Whenever the tail of congestion grows and gets close to the tail of the VSL influence area, one segment whose length is about one-third of a mile based on the geometric design of the facility is added to VSL influence area. Whenever the tail of the shrinking congestion and VSL influence area become far enough from each other, the VSL is deactivated for the last segment.

As mentioned before, for safety and driver compliance reasons, the VSL system is constrained to a maximum change of speed limit, both in time and space.

COMPLIANCE RATE

One of the most important issues in implementing VSL systems is driver behavior, and whether drivers will obey the speed limit signs. There have been VSL implementations such as the one on I-4 in Orlando, Florida that have not been successful and effective because drivers were not complying with the reduced speed limits (*66*). Most researchers have not considered the compliance rate when assessing the effectiveness of VSL in simulation models. However, the effectiveness of a VSL system is dependent on the driver's compliance with the system. In addition, low compliance rates may result in negative effects on traffic flow. Piao et al. (*75*) indicated that with low compliance rates, there is the possibility of large variations in speed. However, Talebpour et al. (*84*) indicated that 10% of compliance with the VSL is sufficient to achieve the desired outcomes.

For vehicles in congested sections, the compliance rate is expected to have less of an effect on system performance since there is less opportunity for vehicles desiring higher speeds to

overtake slower vehicles. However, when the posted speed limit changes at the less congested sections, some vehicles will comply with this new speed limit and decrease their speeds. The vehicles that do not comply with the VSL will continue at their speeds if they can. Otherwise, they follow the vehicles in front of them and decelerate like the leading vehicles. In this study, the impacts of compliance rates is investigated using the CORSIM Real-Time Extension (RTE) facility. A code was written in a format accepted by this this facility for this purpose.

EVALUATION OF VSL STRATEGIES

Traffic simulation is a valuable tool for analyzing and assessing ADTM strategies like VSL. The proposed VSL strategies are tested using a CORSIM model, with the VSL strategy logic incorporated in a dynamic link library (DLL). DLL is imported through the CORSIM Rear-Time Extension (RTE) facility. It interfaces with the CORSIM simulation in real simulation running time. A flowchart with the general logic of the program is shown in Figure 5-5.

Upon the initialization of the simulation, the DLL program identifies which detectors are used to control the VSL system and the links affected by the VSL system. In addition, it determines how data are aggregated from the detectors.

After the initialization is complete, the DLL is accessed at the call point PREFRESIMVEHICLE. This occurs every time-step (one second) during the simulation before vehicle movements take place. If the simulation is not at the initialization period, in which the simulated network is filled up with vehicles, the current VSL values at each location are determined based on the average occupancy value relayed from the specified detectors at the infrastructure based approach and trajectory speed data at specific segments upstream of the

bottleneck at the Connected Vehicle based approach. If it is determined that a speed change is to occur, the free-flow speed is updated on the simulated links in the VSL influence area.

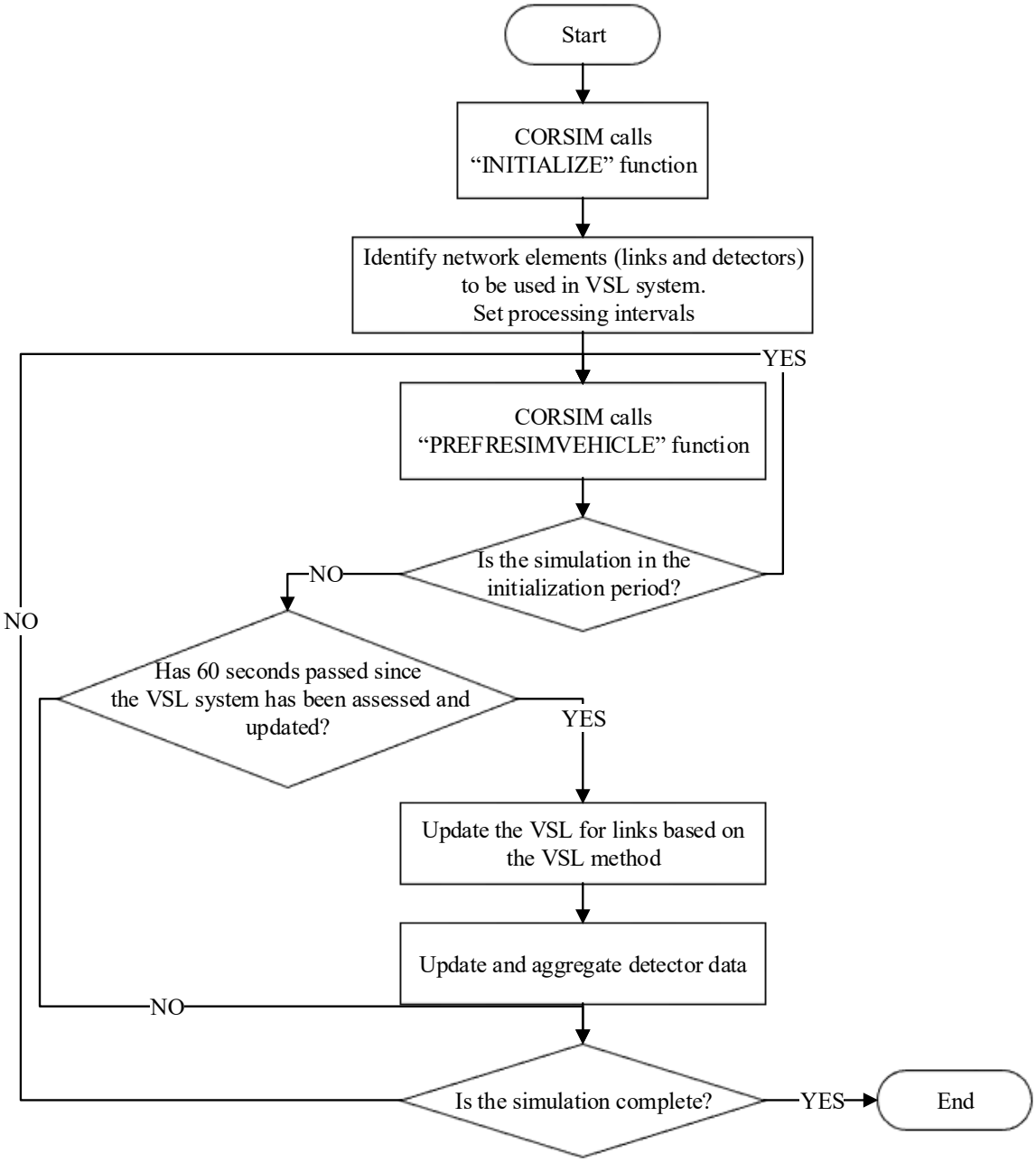

Figure 5-44. Flowchart of the RTE logic of VSL implementation

EVALUATION RESULTS

As stated in the methodology chapter, simulation modeling is used as a tool to evaluate the developed VSL strategies in this study. This chapter presents the findings from the evaluation. First, this chapter presents the results from the proposed model calibration procedure that considers breakdown characteristics, capacity, traffic volume, and system performance. This chapter then presents the results of the assessment of the impacts of various VSL strategies with different evaluated scenarios.

VSL Strategy Based on Infrastructure Data

The most severe bottleneck in the study area is the third bottleneck, as shown in Figure 5-6. This bottleneck is caused by spillback from an off-ramp. As congestion propagates, it reaches traffic volume entering from the managed lanes to the main lanes, which makes the speed at this location the lowest part of congested area. A lane-by-lane data analysis shows that the two left lanes that are affected by the spillback from the downstream off-ramp have significantly lower speeds and higher occupancies, compared to the three right lanes.

In this study, we only focused on investigating the effects of VSL alleviating the congestion caused by the third bottleneck. As field data have shown, this bottleneck is activated around 5:00 PM. This means that in the first two hours of the analysis, this bottleneck locations is uncongested, and during the last hour, it is congested. This condition provides a unique opportunity to analyze VSL effects both before and after breakdown occurrence.

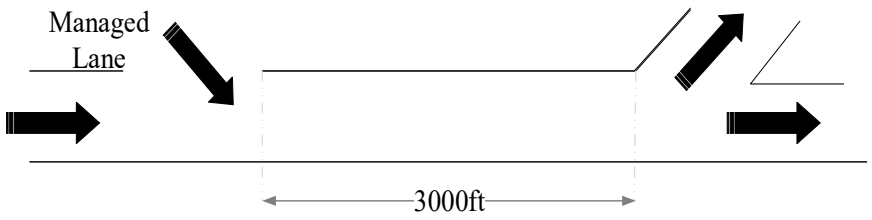

Figure 5-45. Third bottleneck scheme.

The VSL system in this research was studied in two different aspects: 1) VSL effects on congestion, and 2) VSL effects on breakdown characteristics at the bottleneck. First, in order to highlight the effects of VSL on congestion, the area that could be affected by congestion when VSL is not implemented is found based on the real-world extent of the queue. Later, a congestion index is calculated as the mean relative difference of field speed against free-flow speed at all segments of this area using Equation 3-1. In addition, the maximum back of queue, identified based on the most upstream detector reached by congestion, is another measurement used to study the effects of VSL on congestion. The breakdown characteristics considered in this study are: the average speed during breakdown (mph), starting time of breakdown (hh:mm), duration of breakdown (hh:mm), maximum pre-breakdown flow (veh/hr), and queue discharge rate (veh/hr).

Generally, the stochastic simulation models present different output values for repeated simulation runs with different seed numbers. CORSIM was run ten times with different random number seeds to account for the stochasticity in the results. In analyzing the VSL effects, the average of the values from the simulation runs with different seed numbers were used, as recommended by current practices and guidelines. However, when analyzing the VSL effects on breakdown characteristics, this study also considers each run individually and examines the breakdown characteristics from each individual run. This is due to different reasons in real-world simulations (under specific levels of demands): In one run, the breakdown may occur at a specific

time, and in another run, it may occur during another time or it may not even occur at all. Using the average values of system performance would result in smoothed values that dilute the high congestion levels in runs with longer traffic breakdown durations. In addition, when examining the changes between time intervals in the average values of measures such as speed, sharp changes in these measures indicating breakdown would also be eliminated due to the aforementioned diluting effect.

As explained earlier, this study identified the thresholds between different traffic regimes, of which the VSL is to be changed based on exhaustive searches. First, the various ranges for the potential thresholds were identified based on the fundamental diagram and probability of breakdown relationship, as shown in Figure 3-10 (c). Based on the identified range of occupancy for each traffic regime, 30 different combinations of thresholds were generated to perform the exhaustive search mentioned earlier. A comparison of the system's performance based on simulation results indicates that there are two combinations of thresholds that produce the best performance. Since one of these combinations was the same as the thresholds used in the VSL system implemented on the I-4 in Orlando, Florida (*82*), this combination of thresholds was used in this research as the best combination, and is used in the remaining analysis of the paper. Table 5-1 presents the selected thresholds for different traffic regimes.

Table 5-52. Occupancy thresholds and sets of speed limits for traffic conditions

Traffic Condition	Occupancy threshold to switch to more congested condition	Occupancy threshold to switch to less congested condition	Speed limit (mph)
Free-flow condition	<16%	>12 %	50
Light congestion	16% - 28%	12% - 25%	45

condition			
Heavy congestion condition	>28%	<25%	40

As stated in the previous section, the noise in the traffic detector data may lead to fluctuation in the posted speed limit, which has negative effects on the performance of the VSL system. Thus, data smoothing was used. Figure 4-9 shows the posted speed limit based on different strategies of data smoothing. The first three are based on a simple moving average method, and the last one is based on an exponential moving average method. Analyzing the results indicates that in terms of system performance, using the average of the last three minutes of data produces the best results, and it does not lead to fluctuation of the posted speed limit.

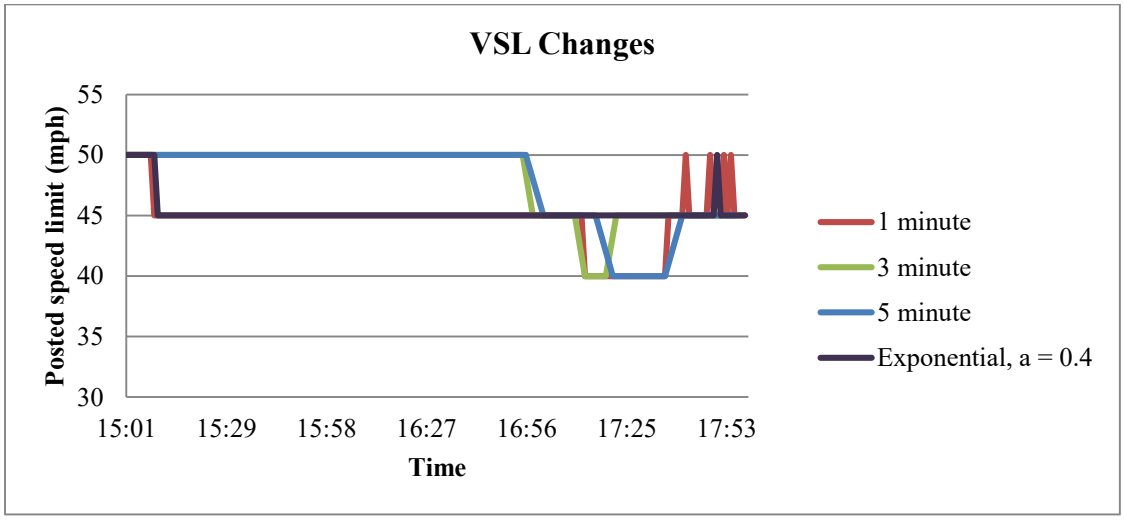

Figure 5-46. Posted speed limits based on different strategies of data smoothing.

As mentioned earlier, one of the benefits of the VSL system is to change the critical occupancy to higher values. Figure 5-8 indicates that the calibrated CORSIM model was able to show this shift in critical occupancy, from 15% to 19.5%. This shift in critical occupancy can have

a positive impact on system performance by shifting the start of the unstable region of the diagram to a higher occupancy.

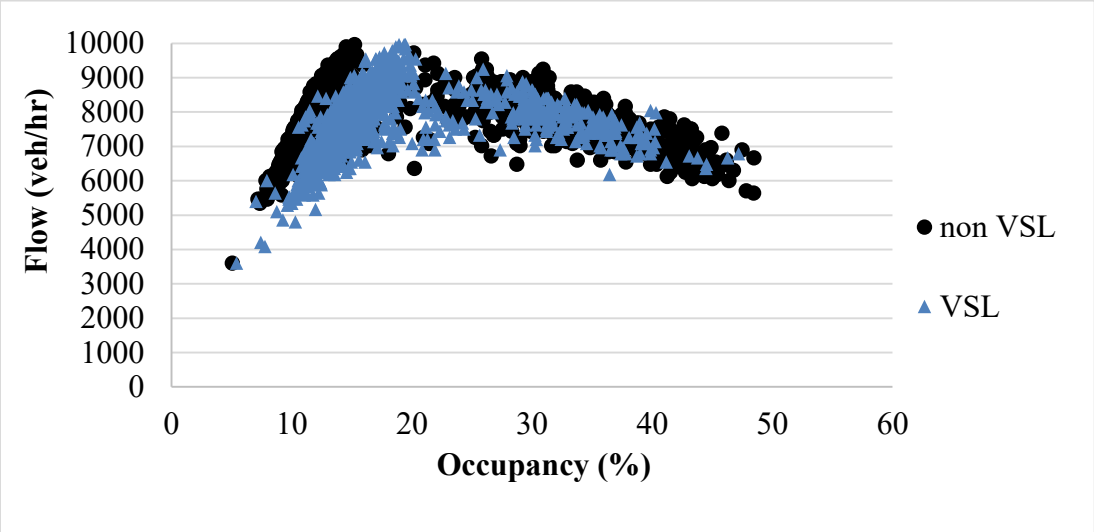

Figure 5-47 Comparison of flow-occupancy relationship between before and after VSL

As explained earlier, in order to highlight the advantages of the proposed shockwave-based VSL, in which the VSL influence area is moved upstream and downstream with the changes in traffic conditions, this study compared the results from this approach with fixed-location VSLs. Four different fixed locations of the VSL signs upstream of the bottleneck were considered: 0.57 miles, 0.88 miles, 1.1 miles, and 1.32 miles. These alternative locations were selected, taking into consideration the geometric constraints of the freeway, such as ramp locations. The shockwave-based VSL locations are allowed to vary from a 0.57-mile segment to 1.32 miles, depending on traffic conditions, as reflected by the probability of breakdown and the location of the back of the queue after breakdown. As previously mentioned, during the first two hours of the simulation analysis, the study's bottleneck is uncongested. The congestion index is calculated based only on data from the first two hours when there is no congestion, during the last hour when there is

congestion, and for the entire study time period. Figure 4-11 shows the congestion index comparison for different scenarios for these different time periods.

As Figure 5-9 indicates that in all scenarios, deactivating the VSL at the head of congestion to encourage vehicles to accelerate produces the same or better results than not having this deactivation. Figure 5-9 (a) shows that among the investigated scenarios, the shockwave-based VSL offers better results than the fixed location-based VSLs. As the VSL influence area becomes larger during uncongested conditions, the travel time and thus the congestion index increase, which is shown in Figure 5-9 (b). During congestion, the shockwave-based VSL produces a better performance compared to the other scenarios, as shown in Figure 5-9 (c). Comparing fixed location-based VSLs during congestion indicates that there is an optimal VSL influence area.

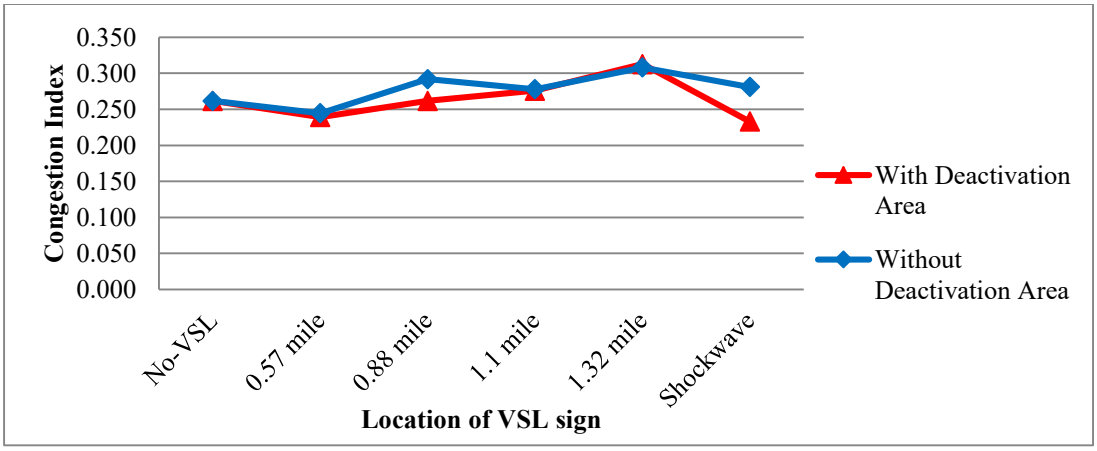

(a) Congestion index during entire study period

Figure 5-48. Comparison of congestion index based on different VSL scenarios

(Continued on next page).

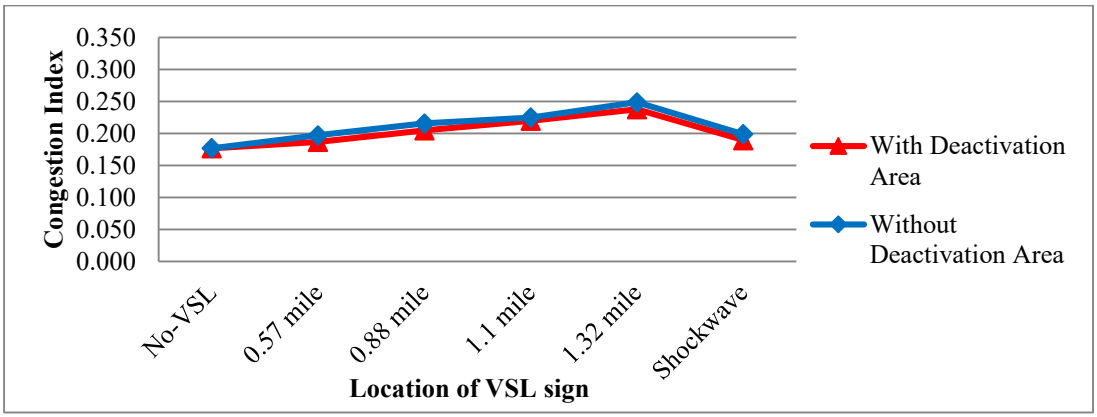

(b) Congestion index during uncongested conditions

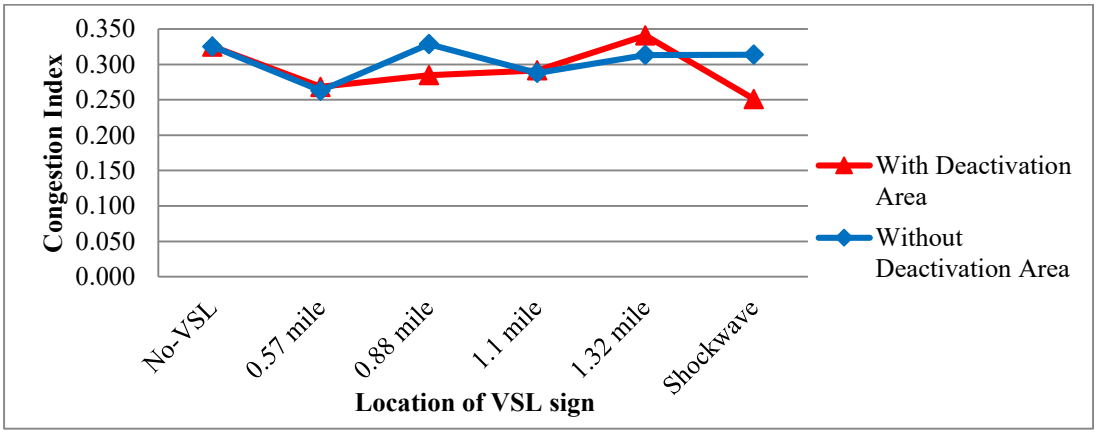

(c) Congestion index during congested conditions

Figure 5-9. Comparison of congestion index based on different VSL scenarios.

In order to have a better understanding of VSL effects on congestion, Table 5-2 presents the congestion index and the maximum back of queue for each VSL alternative. The maximum back of queue was calculated using trajectory data from the simulation model. Table 5-3 displays the improvements in the congestion index and queue length when using each scenario. Table 5-3 shows that the increase of the VSL influence area produces a negative effect on traffic conditions during uncongested conditions. However, in general, the VSL in congested conditions improves congestion, but there is an optimal fixed VSL location, and the shockwave-based VSL performs

better than the best fixed location VSL alternative. The maximum back of queue is reduced by 55% when using the shockwave-based VSL system. In addition, the shockwave-based VSL improves the CI by 22%, and by 10.5% for the congested and whole period, respectively.

Table 5-53. Congestion Index and Maximum Back of Queue Based Different VSL Systems

Scenario	Congestion Index			Maximum Back of Queue (mile)
	Whole Time Period	Uncongested Condition	Congested Condition	
Non-VSL	0.262	0.177	0.325	1.74
0.57 mile	0.239	0.187	0.267	1.14
0.88 mile	0.262	0.205	0.285	1.18
1.1 mile	0.276	0.220	0.292	1.05
1.32 mile	0.313	0.238	0.341	1.35
shockwave-based	0.233	0.190	0.251	0.78

Table 5-54. Effects and Improvements of Each Scenario on Congestion

Scenario	Congestion Index			Maximum Back of Queue
	Whole Time Period	Uncongested Condition	Congested Condition	
0.57 mile	8.55%	-5.64%	17.52%	34.48%
0.88 mile	-0.03%	-15.79%	12.46%	32.18%
1.1 mile	-5.45%	-24.22%	10.37%	39.66%
1.32 mile	-19.55%	-34.41%	-4.76%	22.41%
shockwave-based	10.97%	-7.22%	22.82%	55.17%

Table 5-4 presents a comparison of breakdown characteristics under different VSL alternatives to study the VSL's effect on breakdown conditions at the bottleneck. Table 5-4 indicates that all scenarios are successful in postponing traffic breakdown. The first observation is that all fixed location VSL scenarios have more or less the same effects on breakdown characteristics. The shockwave-based VSL has more positive impacts on breakdown than the fixed location VSLs. While the shockwave-based VSL postpones the breakdown for 18 minutes on average, the fixed location VSLs postpone it for 7 to 12 minutes, depending on the location of the VSL system. The main reason for the better performance of the shockwave-based VSL in postponing breakdown occurrence is that as the occupancy increases and the network becomes more congested based on occupancy measurements, which reflects a higher priority of breakdown, the VSL influence area starts to become extended upstream. The shockwave-based VSL significantly decreases the duration of the breakdown by 43 minutes, which is a 59% decrease in duration. The fixed VSL scenarios reduced the breakdown duration by 22 to 25 minutes, which is about a 35% decrease. Unlike the non-VSL conditions where the pre-breakdown speed is about 50 mph, the pre-breakdown speed with VSL was 40 mph. Traffic speed during the breakdown was increased by 7.5 mph, which means a 36% improvement in traffic speed during the breakdown for the shockwave-based VSL system. The traffic speed during breakdown was increased from 22% to 26% with fixed location VSLs. The impact of VSL on the pre-breakdown capacity and queue discharge was small, according to the simulation analysis.

Table 5-55. Breakdown Conditions at the Simulated Bottleneck under Different Scenarios

Scenario	Start time (hh:mm)	Duration (hh:mm)	Speed Before Breakdown (mph)	Maximum pre-breakdown flow (vph)	Speed during breakdown (mph)	Queue Discharge (vph)
Non-VSL	16:52	1:13	50.91	8057	20.9	7728
0.57 mile	16:59	0:48	40.05	8116	25.45	7733
0.88 mile	17:02	0:50	39.9	8062	25.06	7868
1.1 mile	17:04	0:50	39.81	8007	26.33	7833
1.32 mile	17:03	0:48	40.17	8102	25.48	7770
shockwave-based	17:10	0:30	38.98	8352	28.39	7935

VSL Strategy Based on Connected Vehicle Data

As with the VSL strategy based on infrastructure data, this strategy aims to address the congestion at the third bottleneck. For this purpose, at each time step (1 second), the individual vehicle's data, speed, and location were collected from the simulation runs. The measurements were aggregated in space into 500-foot segments. The accuracy of the collected data depends on the market penetration, which is the portion of drivers equipped with on-board units that enables them to send information through communication technology to the roadside infrastructure. Data collected based on different market penetrations were compared to find the minimum market penetration that provides accurate data. For this purpose, the accuracy of data with different market penetration were compared to that with 100% market penetration using two statistical measurements: the Correlation Coefficient, as shown in Equation 3-8, and the Root Mean Squared Normalized Percent Error (RMSNPE), as shown in Equation 3-10. Figures 5-10 and 5-11 show

the Correlation Coefficient and RMSNPE of speed estimates based on collected data under different market penetrations.

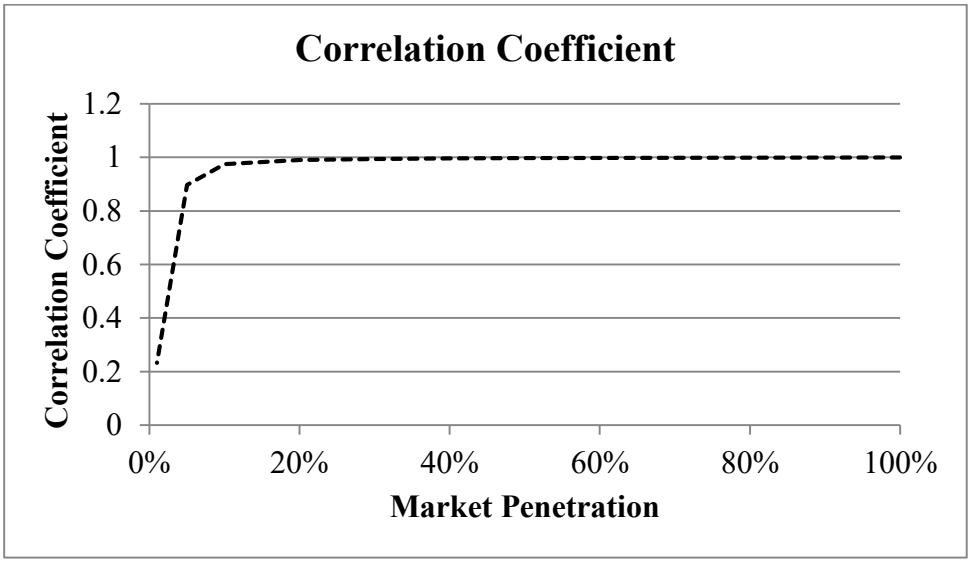

Figure 5-49.Correlation coefficient of speed estimates based on collected data.

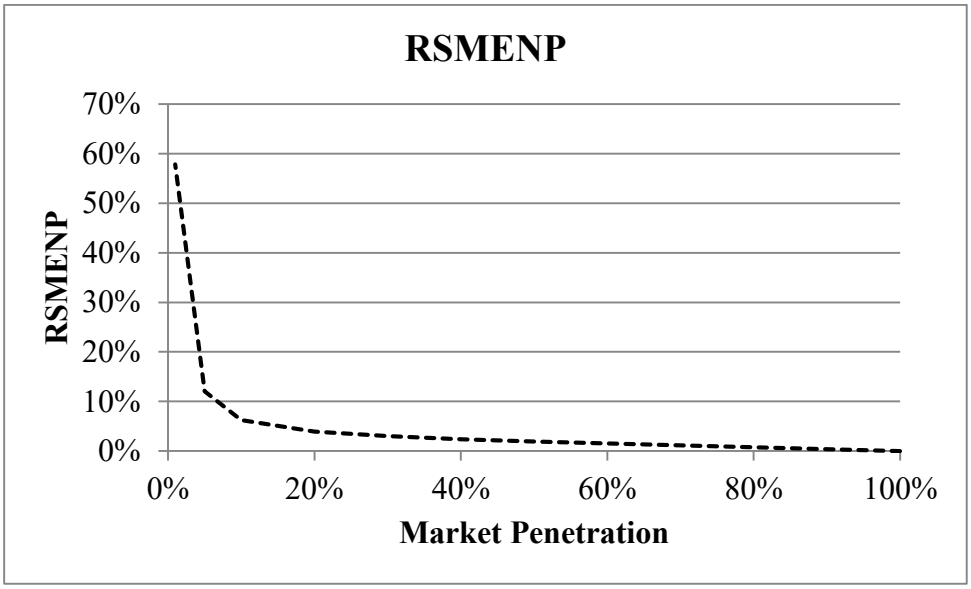

Figure 5-50. RSMENP of speed estimates based on collected data.

Figures 5-10 and 5-11 indicate that a 15-20% market penetration produces results that are well correlated and similar to the 100% market penetration, depending on the aggregation length. As expected, the results indicate that as aggregating length increases, the minimum market penetration rate to produce acceptable results decreases. It can be recommended that as market penetration decreases, the segment length should be increased in order to make the collected data valuable and reliable.

After collecting speed data, in order to find the location of the congested area in the network, a wavelet transform was applied to speed data. Figure 5-12 presents the calculation of wavelet energy of speed data across the network. Figure 5-12 (c) shows the temporal distribution of the energy. The lighter regions of the contour represent larger values of the wavelet transform coefficients, which indicate higher wavelet energy. Figure 5-12 (d) shows the wavelet energy for the speed location-series, which was computed using Equation 3-15, and indicates the head and tail of the congested area.

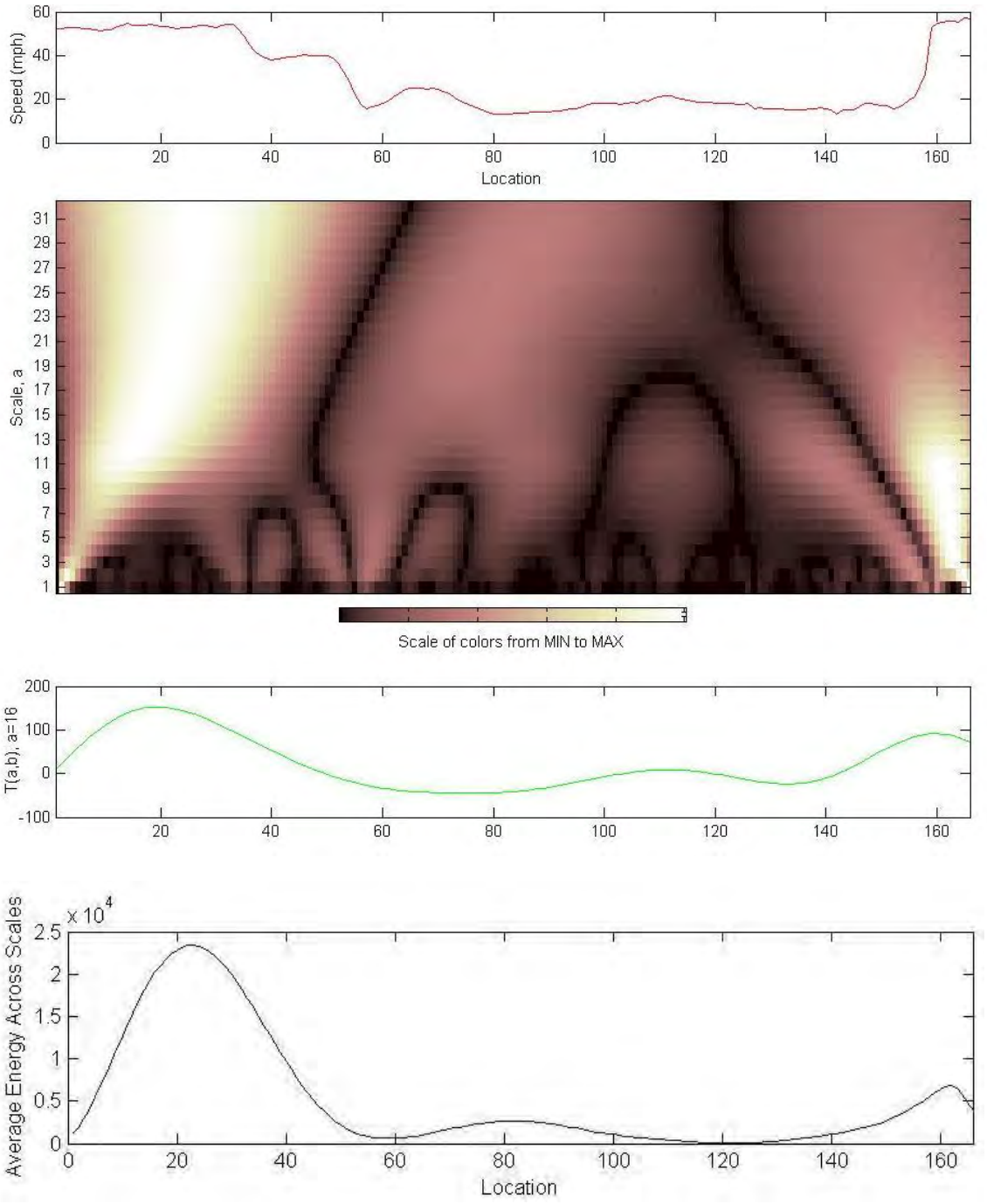

Figure 5-51. Illustration of wavelet transform and energy calculation. (a) Location series plot of speed at 17:25:00 pm; (b) Contour map of the absolute values of wavelet transform coefficients, $|T(\alpha,\beta)|$, from scale $\alpha = 1-32$; (c) WT coefficients, $T(\alpha,\beta)$, at scale $\alpha = 16$; (d) The temporal distribution of average wavelet-based energy across scales.

Tables 5-5 and 5-6 show the results of the VSL strategy based on the Connected Vehicle data and compared it to the VSL strategy based on Infrastructure data. Note that the infrastructure based strategy and Connected Vehicle based strategy used in this comparison are both shockwave-based VSLs.

Table 5-56. Congestion Index and Maximum Back of Queue

Scenario	Congestion Index			Maximum Back of Queue (mile)
	Whole time period	Uncongested	Congested	
Non-VSL	0.313	0.238	0.341	1.32
Infrastructure based	0.233	0.19	0.251	0.71
Connected Vehicle based	0.234	0.19	0.252	0.71

Table 5-57. Breakdown Conditions at Bottleneck

Scenario	Start time (hh:mm)	Duration (hh:mm)	Speed Before Breakdown (mph)	Maximum pre-breakdown flow (vph)	Speed during breakdown (mph)	Queue Discharge (vph)
Non-VSL	16:52:00	1:13	50.91	8057	20.9	7728
Infrastructure based	17:10:00	0:30	38.98	8352	28.39	7935
Connected Vehicle based	17:08:00	0:33	39.78	8272	28.09	7855

As the results indicate, there are small differences between these two VSL strategy outcomes. The main reasons could be attributed to:

1. The locations of the traffic detectors are not far from each other; thus, the location of back of queue can be identified adequately with infrastructure data.
2. Although the Connected Vehicle technology allows more of collecting and detailed information of the current location of congestion, the speed limit cannot be changed as frequently as needed in space and time to take advantage of these detailed data due to safety and compliance concerns.
3. The tested methods do not fully utilize the new types of information gathered from Connected Vehicle.

Compliance Rate

As mentioned earlier, one of the most important factors in having a successful and effective VSL system is the compliance rate. In this research, the VSL can be implemented with different compliance rates and were estimated and compared. As stated earlier, two different ways of informing drivers about speed limits were tested: 1) by VSL sign, and 2) by Connected Vehicle through V2I communication. A difference between these two approaches is how to send the information to drivers in the segment. In the VSL sign approach, only drivers that are about to enter the segment will be notified about the posted speed limit, while drivers in the segment consider the speed limit that they saw while entering the segment as the speed limit even if it changes. However, for the Connected Vehicle, the speed limit is sent to all drivers based on their location. Different compliance rates based on these two approaches were tested to find the lowest

compliance rate that provides an effective VSL system. Figure 5-13 shows the congestion index for different compliance rates for different time windows using the shockwave-based VSL system.

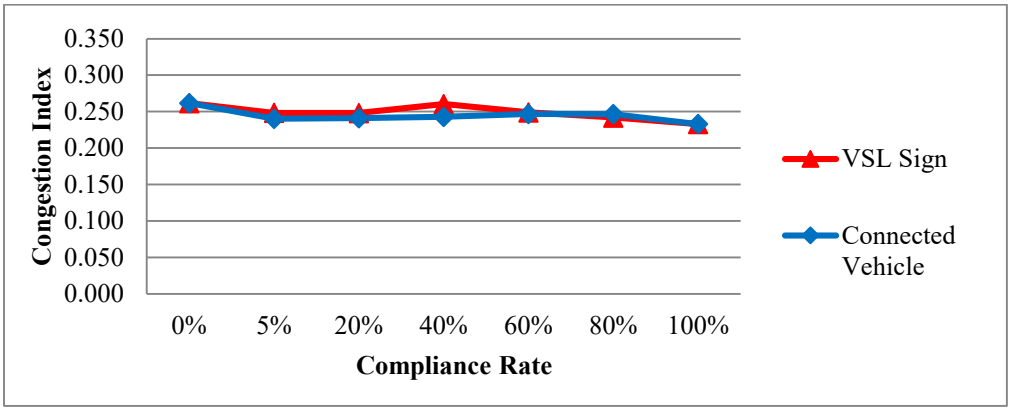

(a) Congestion index during entire study period

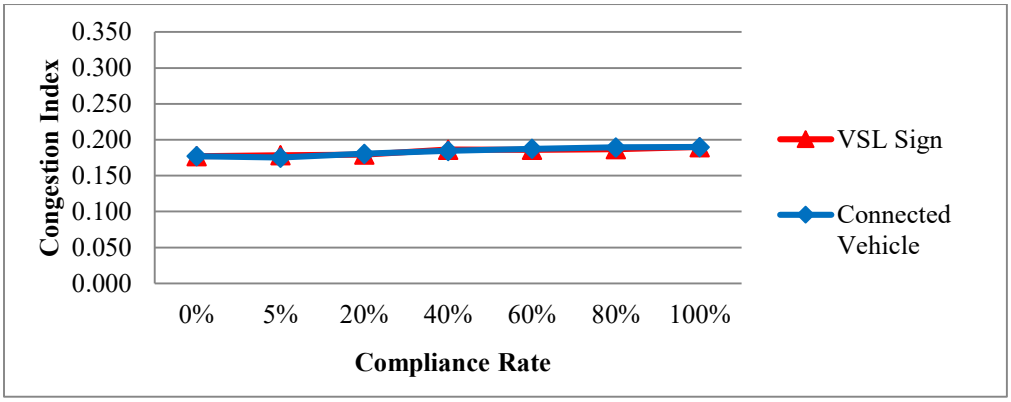

(b) Congestion index during uncongested conditions

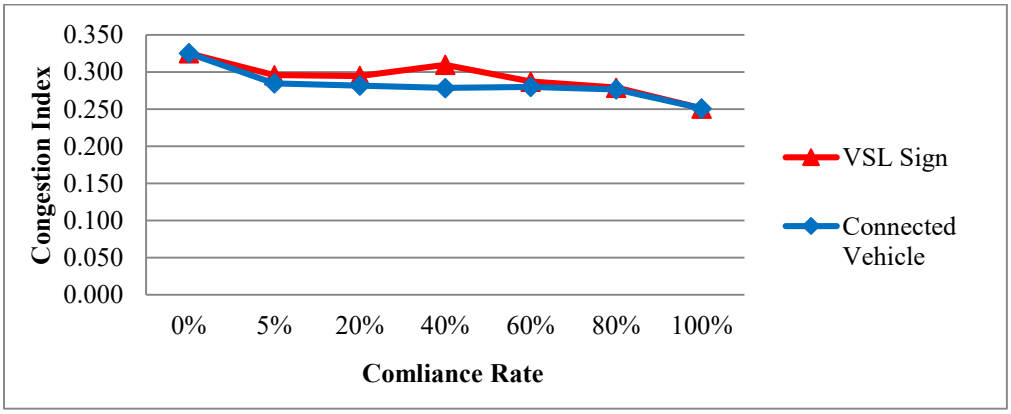

(c) Congestion index during congested conditions

Figure 5-52. Comparison of congestion index based on different compliance rate.

As the results indicate, using the Connected Vehicle to inform drivers is better than using the VSL sign. During the uncongested period, as the compliance rate decreases, traffic speed increases, and as a result, the congestion index decreases slightly. During a congested period, having 40% of drivers comply with the posted speed limit results in higher congestion rate than a lower compliance rate. This result may indicate that having an equal number of compliant and incompliant drivers may result in disturbances with adverse effects on traffic. The results show that informing drivers through Connected Vehicle may stop this situation from happening; this issue needs to be further investigated. As expected, having 100% of compliance produces considerably better results than the lower compliance rates. Tables 5-7 and 5-8 indicate breakdown characteristics based on different compliance rates for both the VSL sign and Connected Vehicle respectively.

Table 5-58. Breakdown conditions at bottleneck with different market penetration using VSL sign

Scenario	Start time (hh:mm)	Duration (hh:mm)	Speed Before Breakdown (mph)	Maximum pre-breakdown flow (vph)	Speed during breakdown (mph)	Queue Discharge (vph)
0%	16:52	1:13	50.91	8057	20.90	7728
5%	16:56	1:02	48.07	8053	21.14	7752
20%	17:01	0:55	46.23	8042	21.64	7712
40%	17:01	0:50	43.41	8067	24.13	7733
60%	17:02	0:43	40.10	8098	25.62	7773
80%	17:02	0:42	40.63	8127	25.01	7765
100%	17:10	0:30	38.98	8352	28.39	7935

Table 5-59.Breakdown conditions at bottleneck with different market penetration using Connected Vehicle

Scenario	Start time (hh:mm)	Duration (hh:mm)	Speed Before Breakdown (mph)	Maximum pre-breakdown flow (vph)	Speed during breakdown (mph)	Queue Discharge (vph)
0%	16:52	1:13	50.91	8057	20.90	7728
5%	16:56	1:02	48.82	8048	21.02	7743
20%	17:01	1:01	46.48	8042	20.94	7712
40%	17:01	0:55	44.32	8091	22.80	7833
60%	17:02	0:42	41.29	8062	24.12	7798
80%	17:03	0:36	40.43	8093	26.11	7845
100%	17:08	0:33	39.78	8272	28.09	7855

Tables 5-7 and 5-8 show that using Connected Vehicle produces slightly better results at the bottleneck, compared to using the VSL signs. Both tables indicate that as the compliance rate decreases, the duration of breakdown increases. The breakdown starts sooner, compared to the 100% compliance rate and the speed during breakdown, which decreases.

SUMMARY

This study developed a shockwave-based VSL system which uses a heuristic switching logic based controller with specified thresholds of prevailing traffic flow condition locations. This VSL strategy aims to improve mobility at recurrent bottlenecks. Before breakdown occurrence, the proposed VSL tries to postpone breakdown by decreasing the inflow and achieving uniform

distribution in speed and flow. After breakdown, the VSL system aims to dampen the congestion by reducing the traffic inflow to the congested area. The shockwave-based VSL system pushes the VSL influence area location upstream as the congested area propagates upstream. In addition, this study investigated the effect of using Connected Vehicle data instead of detector data on VSL system performance. Wavelet transform was used to analyze aggregated individual vehicles' speed data to determine the location of congestion.

The performance of shockwave-based VSL was compared to VSL systems with different fixed VSL message sign locations. The results show that shockwave-based systems outperform other VSL systems, and it can considerably decrease the maximum back of queue and duration of breakdown while increasing the average speed during breakdown. In addition, one of the important issues in implementing VSL systems is whether drivers will obey the speed limit signs. Sensitivity analysis was conducted on VSL system performance with different compliance rates. As expected, the results indicate that as the compliance rate increases, the VSL system is more successful. However, even with low compliance rates, the VSL system can improve traffic mobility at bottlenecks. For VSL to be effective, a level of compliance to speed limits needs to be observed. Increased police enforcement and automatic speed enforcement have proven to be effective strategies to ensure speed limit compliance. It has also been suggested that driver awareness of how the system functions may encourage drivers to comply with speed limits.

CHAPTER 6

RESEARCH SUMMARY

ATDM strategies such as ramp metering and VSL are state-of-the-art methods that are increasingly being considered to improve the efficiency of existing freeway systems. Recent research has indicated that incorporating the probability of breakdown concept into strategies such as ramp metering seems to be promising in postponing the breakdown, reducing the average travel time and reducing the time of congestion.

This project explored and assessed methods to improve the operations at critical bottlenecks utilizing ramp metering and VSL with the consideration of probability of breakdown. The project also developed methods for selecting optimal settings of the parameters of these strategies to maximize traffic operational improvements. These strategies and their impacts were evaluated using the CORSIM mircosimulator calibrated with consideration of breakdown characteristics. In addition, the effects of the utilization of combinations of mobile and infrastructure devices to support these strategies were also explored in this study using simulation. The major findings from the study are listed below.

MICRO-SIMULATION CALIBRATION

The ATMS strategies considered in this study were assessed using a CORSIM microscopic simulation model. Without calibration of the simulation model, there is no assurance that the model's outputs are reliable and that the model will correctly estimate and predict the traffic performance of alternative improvements. Traffic simulation models are widely and increasingly

used in the transportation engineering field. The current methods of calibrating simulation models is generally based on capacity, volume, and system performance values, and do not take the traffic breakdown characteristics into consideration. However, since the proposed ATMS strategies are countermeasures to the impacts of breakdown conditions, inclusion of the breakdown characteristics in the calibration procedure is important in order to obtain a reliable assessment. Several enhancements are proposed in this study, including using the wavelet transform to determine the start and end times of breakdown occurrence, as well as to account for the breakdown characteristics at bottleneck locations in the calibration process. A case study was conducted to test the proposed simulation calibration methodology. Guidelines were produced on how to use simulation models to assess and fine-tune ATDM strategies of the types investigated in this study.

INCORPORATING PROBABILITY OF BREAKDOWN IN RAMP METERING SYSTEM

A series of simulation experiments were designed in this study to assess different modifications to the fuzzy logic ramp metering algorithm, currently utilized on I-95 in Miami, FL. The probability of breakdown concept was incorporated into the ramp meter activation process in an effort to replace time of day operation. In addition, the probability of breakdown was incorporated directly into the fuzzy logic control algorithm to allow the algorithm to better react to potential traffic breakdown conditions. The northbound I-95 ramp metering zone was first modeled in CORSIM and calibrated to replicate existing operations. The modifications to the ramp metering strategies were tested at two ramp sites identified as recurring sources of congestion.

It was concluded that incorporating an activation threshold into the metering operation has the potential to improve or at least replace the current time of day operations. On average, the metering operations with the activation threshold outperformed the current time of day operations by as much as 2.4% in terms of total network travel time. However, the results were inconsistent between individual runs and an increase in travel time occurred in some runs. The use of an activation threshold links the metering operation to real-time traffic performance measures instead of time of day operations. The advantage of this is that in addition to adequately replacing the time of day operation, the metering will become more reactive to non-typical traffic congestion.

A number of different modifications were made to the fuzzy logic ramp metering algorithm to include the probability of breakdown. It was concluded that the effect of these changes on the ramp metering operations typically caused a slightly more restrictive metering strategy. The mainline showed some travel time improvement, but with more restrictive metering rates some delay is shifted toward the ramp traffic. While the modifications showed some potential to improve traffic operations, the overall impact on network performance was minimal. The total travel time showed improvement on the average, but was inconsistent when analyzing individual runs. It is possible that the inconsistencies are a function of the microsimulator, and may not be observed in a field implementation.

Overall, the probability of breakdown modifications may be able to provide some limited operational improvements at specific bottlenecks and/or along the entire network. However, there is no clear pattern regarding when these improvements are observed, and how different traffic demand levels may affect the impact of these modifications. Using an activation threshold to turn on ramp meters is a viable alternative to time of day operation. This would allow less operator involvement and allow the activation process to become demand sensitive.

VARIABLE SPEED LIMIT

VSL strategies dynamically identify and disseminate the appropriate speed limits based on prevailing traffic conditions, sometimes in combination with road surface conditions and weather conditions. Although the traffic safety benefits of implementing VSL are well-established, very few of the studies on previously developed VSL strategies documented improvements on traffic mobility. This study develops a shockwave-based VSL system with a time-variant VSL influence area that uses a heuristic switching logic-based controller with specified thresholds of prevailing traffic flow conditions. This VSL strategy aims to improve operations and mobility at critical bottlenecks. Before breakdown occurrence, the proposed VSL objective is to postpone or eliminate breakdown by decreasing the inflow of traffic at the bottleneck and achieving a uniform distribution in speed and flow. After breakdown, the VSL system aims to dampen the congestion by reducing the inflow of traffic to the congested area. The shockwave-based VSL system pushes the VSL influence area location upstream as the congested area propagates upstream. This study also investigates the use of Connected Vehicle data instead of detector data on VSL system performance. In this system, wavelet transform is used to analyze aggregated individual vehicle speed data to determine the location of congestion.

The performance of shockwave-based VSL with a time-variant influence area is compared to VSL systems with a fixed VSL influence area based on the congestion index (that measures the travel time relative to free flow travel time), maximum back of queue, and breakdown characteristics. The results show that the shockwave-based VSL outperforms other VSL systems, and can considerably decrease the maximum back of queue and duration of breakdown, while increasing the average speed during breakdown. In addition, one of the important issues in

implementing VSLs is whether drivers will obey the speed limit signs. Sensitivity analysis results indicate that as compliance rates increase, the VSL system is more successful. However, even with low compliance rates, the VSL system can improve traffic mobility at bottlenecks. Please note that the utilized algorithm to dynamically select the speed limit is based only on speed data and does not take advantage of other information that will become available from the vehicles though dedicated short range communication or cellular communication. Information such as acceleration deceleration, braking, wiper on/off is expected to be available. New algorithms that utilize this information are expected to further improve system mobility and safety performance.

CHAPTER 7

REFERENCES

1. Schrank, D., T. Lomax, and B. Eisele. *Urban Mobility Report*. Report for the Texas Transportation Institute. College Station, 2011.

2. Papageorgiou, M., J.M. Blosseville, and H. Hadj-Salem. *La fluidification des rocades de l'Ile de France: Un projet d'importance*. Tech. rep. No. 1998-17. Dynamic Systems and Simulation Lab., Technology University of Crete, Chania, Greece, 1988.

3. Elefteriadou, L., R. Roess, and W. McShane. The probabilistic nature of breakdown at freeway-merge junctions. *Transportation Research Record 1484*, 1995, pp. 80–89.

4. Graves T., A. Karr, N. Rouphail, and P. Takuriah. *Real-Time Prediction of Incipient Congestion on Freeways from Detector Data*. NISS Technical Report 79, 1998.

5. Persaud, B., S. Yagar, and R. Brownlee. Exploration of the Breakdown Phenomenon in Freeway Traffic. *Transportation Research Record 1634*, 1998, pp. 64-69.

6. Persaud, B., S. Yagar, D. Tsui, and H. Look. Study of Breakdown-Related Capacity for a Freeway with Ramp Metering. *Transportation Research Record 1748*, 2001, pp. 110-115.

7. Okamura, H., S. Watanabe, and T. Watanabe. An Empirical Study on the Capacity of Bottlenecks on the Basic Suburban Expressway Sections in Japan. *Proceedings of the 4th International Symposium on Highway Capacity*, TRB Circular E-C018, Transportation Research Board, Washington D.C., 2000, pp. 120-129.

8. Brilon, W., Geistefeldt, J., and Regler, M. Reliability of freeway traffic flow: A stochastic concept of capacity. *Proc.,16th Int. Symp. on Transportation and Traffic Theory*, Elsevier, College Park, MD, 2005, pp. 125–144.

9. Brilon, W. *Randomness and Reliability in Freeway Traffic Flow*. TRAIL Research School, Delft, Netherlands, 2005.

10. Kuhne, R., R. Mahnke, and J. Hinkel. Modeling the Effects of Corridor Control Systems on Road Capacity. *5th International Symposium on Highway Capacity and Quality of Service*, Japan Society of Traffic Engineers, Yokohama, Japan, 2006, pp. 289-298.

11. Federal Highway Administration., (2000) "Manual on Uniform Traffic Control Devices" U.S. DOT, Washington, D.C.
12. Buckley, D., and S. Yagar. Capacity Funnels near On-Ramps. *Proceedings of the 6th International Symposium on Transportation and Traffic Theory*, American Elsevier Publishing Company, New York, 1974.

13. Banks, J. The Two-Capacity Phenomenon: Some Theoretical Issues. *Transportation Research Record 1320*, 1991, pp. 234-241.

14. Gazis, D., and R. Herman. The Moving and 'Phantom' Bottlenecks. *Transportation Science*, Vol. 26, No. 3, 1992, pp. 223-229.

15. Daganzo, C., M. Cassidy, and R. Bertini. Possible Explanations of Phase Transitions in Highway Traffic. *Transportation Research A*, 1999, pp. 365-379.

16. Daganzo, C. A Behavioral Theory of Multi-Lane Traffic Flow. Part II: Merges and the Onset of Congestion. *Transportation Research B*, 2002, pp. 159-169.

17. Cassidy, M., and R. Bertini. Some Traffic Features at Freeway Bottlenecks. *Transportation Research B*, 1999, pp. 25-42.

18. Chen, C., A. Skabardonis, and P. Varaiya. Systematic Identification of Freeway Bottlenecks. In *Transportation Research Record*, No. 1867, 2004, pp. 46–52.

19. Dowling, R., A. Skabardonis, and V. Alexiadis. *Traffic Analysis Toolbox,Volume III: Guidelines for Applying Traffic Microsimulation Modeling Software*. Publication FHWA-HRT-04-040. FHWA, U.S. Department of Transportation, 2004.

20. Dowling, R., A. Skabardonis, and J. Halkias. Guidelines for Calibration of Microsimulation Models Framework and Applications. *Transportation Research Record 1876*, 2004, pp. 1–9.

21. Elefteriadou, L. and P. Lertworawanich. Defining, Measuring and Estimating Freeway Capacity. *Transportation Research Board Annual Meeting*. Washington D.C, 2003.

22. Geistefeldt, J. Empirical Relation between Stochastic Capacities and Capacities Obtained from the Speed-Flow Diagram. *Symposium on the Fundamental Diagram: 75 Years*. Woods Hole, MA, 2008.

23. Kondyli, A. *Breakdown Probability Model at Freeway-Ramp Merges Based on Driver Behavior*. Ph.D. Dissertation, University of Florida, Gainesville, Fla, 2009.

24. Ban, X., L. Chu, and H. Benouar. Bottleneck Identification and Calibration for Corridor Management Planning. *Transportation Research Record 1999*, 2007, pp. 40–53.

25. Muñoz, J.C. and C.F. Daganzo. Structure of the transition zone behind freeway queues. *Transportation Science 37 (3)*, 2003, pp. 312–329.

26. Sarvi, M., M. Kuwahara, and A. Ceder. Observing freeway ramp merging phenomena in congested traffic. *Journal of Advanced Transportation 41 (2)*, 2007, pp. 145-170.

27. Zheng, Z., S. Ahn, D. Chen, and J., Laval. Applications of wavelettransform for analysis of freeway traffic: Bottlenecks, transient traffic, and traffic oscillations. *Transportation Research Part B: Methodological*, Vol. 45(2), 2011, pp. 372-384.

28. Elefteriadou, L., Kondyli, A., Brilon, W., Hall, F. H., Persaud, B., and Washburn, S. Proactive ramp management under the threat of freeway flow breakdown. National Cooperative Highway Research Program Project 3-87 Final Rep., National Cooperative Highway Research Program, *Transportation Research Board*, Washington, DC, 2009.

29. Elefteriadou, L., A. Kondyli, W. Brilon, L. Jacobson, F. Hall, and B. Persaud. *Proactive Ramp Management under the Threat of Freeway Flow Breakdown*. Prepared for National Cooperative Highway Research Program, Transportation Research Board of The National Academies, 2009.

30. Kerner, B. Experimental Features of Self-Organization in Traffic Flow. *Physical Review Letters*, Vol. 81, 1998, pp. 3797-3800.

31. Koshi, M., M. Iwasaki, and I. Ohkura. Some Findings and an Overview on Vehicular Flow Characteristics. *Proceedings of the 8th International Symposium on Transportation and Traffic Theory*, Ontario, Canada, 1983.

32. Iwasaki, M. Empirical Analysis of Congested Traffic Flow Characteristics and Free Speed Affected by Geometric Factors on an Intercity Expressway. *Transportation Research Record 1320*, 1991, pp. 242-250.

33. Lu, X. and A. Skabardonis. Freeway Traffic Shockwave Analysis: Exploring the NGSIM Trajectory Data. *Transportation Research Board 86th Annual Meeting*. Washington D.C, 2007.

34. Bloomberg, L., M. Swenson, and B. Haldors. Comparison of Simulation Models and the Highway Capacity Manual. *Transportation Research Board 82nd Annual Meeting*, Washington, D.C, 2003.

35. Chu, L., and H. Liu. A Calibration Procedure for Microscopic Traffic Simulation. *Transportation Research Board 83rd Annual Meeting*, Washington, DC, 2004.

36. Dowling, R., J. Holland, and A. Huang. *Guidelines for Applying Traffic Micro-simulation Modeling Software*, Oakland, 2002.

37. Park, B., and J. Schneeberger. Microscopic simulation model calibration and validation: A case study of VISSIM for a coordinated actuated signal system. *Transportation Research Board Annual Meeting*. Washington D.C, 2003.

38. Hourdakis, J., P. Michalopoulos, and J. Kottommannil.. Practical Procedure for Calibrating Microscopic Traffic Simulation Models. *Transportation Research Record 1852*, 2003, pp. 130–139.

39. Gomes, G., A. May, and R. Horowitz. A Microsimulation model of a congested freeway using VISSIM. *Transportation Research Board 83rd Annual Meeting*. Washington D.C, 2004.

40. Zhang, Y., and L. E. Owen. Systematic Validation of a Microscopic Traffic Simulation Program. Presented at *83rd Annual Meeting of the Transportation Research Board*, Washington, D.C, 2004.

41. Zhang, L., P. Holm, and J. Colyar. *Identifying and Assessing Key Weather-related Parameters and their Impacts on Traffic Operations using Simulation*. Federal Highway Administration Turner Fairbanks Highway Research Center, 2004.

42. Halkias, B., P. Kopelias, K. Papandreou, A. Politou, P. Prevedouros, and A. Skabardonis. Freeway Bottleneck Simulation, Implementation and Evaluation. *Transportation Research Record*, 2007, pp. 84–93.

43. Zhang, M., J. Ma, and H. Dong. *Developing Calibration Tools for Microscopic Traffic Simulation Final Report Part II: Calibration Framework and Calibration of Local/Global Driving Behavior and Departure/Route Choice Model Parameters*. Technical report, California Path Program, Institute of Transportation Studies, University of California, Berkely, 2008.

44. Rakha, H., M. Van Aerde, L. Bloomberg, and X. Huang. Construction and Calibration of a Large-Scale Micro-simulation Model of the Salt Lake Area. *Transportation Research Record 1644*, 1998, pp. 93–102.

45. Henclewood, D., W. Suh, M. Rodgers, M. Hunter, and R. Fujimoto. A Case for Real-time Calibration of Data-driven Microscopic Traffic Simulation Tools. *Proceedings of the Simulation Conference (WSC)*, 2012.

46. Schultz, G., and L. Rilett. Analysis of Distribution and Calibration of Car-Following Sensitivity Parameters in Microscopic Traffic Simulation Models. *Transportation Research Record 1876*, 2004, pp. 41-51.

47. Kim, K., and L. Rilett. A genetic algorithm based approach to traffic micro-simulation calibration using ITS data. *Transportation Research Board 83th Annual Meeting*, Washington D.C, 2004.

48. Park, B., and H. Qi. Development and Evaluation of a Procedure for the Calibration of Simulation Models. *Transportation Research Record 1934*, 2005, pp. 208-217.

49. Lee, J., B. Park, J. Won, and I. Yun. A Simplified Procedure for Calibrating Microscopic Traffic Simulation Models. *Transportation Research Board Annual Meeting*. Washington D.C, 2013.

50. Ma, J., H. Dong, and M. Zhang. Calibration of Micro Simulation with Heuristic Optimization Methods. *Transportation Research Record 1999*, 2007, pp. 208-217.

51. Lee, J., and K. Ozbay. New calibration methodology for microscopic traffic simulation using enhanced simultaneous perturbation stochastic approximation approach. *Transportation Research Record*, 2009, pp.233 -240.

52. Paz, A., V. Molano, and C. Gaviria. Calibration of CORSIM Models Considering all Model Parameters Simultaneously. *15th International IEEE Conference on Intelligent Transportation Systems Anchorage*, Alaska, 2012.

53. Fellendorf, M., and P. Vortisch. Validation of the microscopic traffic flow model VISSIM in different real-world situations. *Transportation Research Board Annual Meeting*. Washington D.C, 2001.

54. Menneni, S., C. Sun, and P. Vortisch. Microsimulation calibration using speed-flow relationships. *Transportation Research Board Annual Meeting*. Washington D.C, 2008.

55. Hollander, Y., and R. Liu. The principles of calibrating traffic microsimulation models. *Transportation*, 35(3), 2008, pp. 347–362.

56. Sisiopiku V. Variable Speed Control: Technologies and Practices. *Proceedings of the 11th Annual Meeting of ITS America*, Miami, FL, 2001.

57. Harbord, B. Application of SISTM to dynamic control on the M25. *IEE Colloquium on Dynamic Control of Strategic Inter-Urban Road Networks*, 1995.

58. Lenz, H., R. Sollacher, and M. Lang. Nonlinear speed-control for a continuum theory of traffic flow. *14th World Congress of IFAC*, Beijing, China, 1999.

59. Kohler, U. Stability of vehicle platoons. *Proceedings of the Sixth International Symposium on Transportation and Traffic Theory*, 1974, pp. 39-55.

60. Robinson, M. Examples of Variable Speed Application. Speed Management Workshop, *Transportation Research Board 79th Annual Meeting*. Washington D.C, 2000.

61. CTC and Associates LLC. *Variable Speed Limit Signs for Winter Weather*. Transportation Synthesis Report, Bureau of Highway Operations, Division of Transportation Infrastructure Development, Wisconsin Department of Transportation, 2003.

62. Steel, P., R. McGregor, A. Guebert, and T. McGuire. Application of Variable Speed Limits along the Trans Canada Highway in Banff National Park. *Annual Conference of the Transportation Associate of Canada*, 2005.

63. Zarean, M., P. Pisano, K. Dirnberger, and M. Robinson. Variable Speed Limit Systems: The-State-Of-The-Practice. *Proceedings of the Rural Advanced Technology & Transportation Systems Conference*, Flagstaff, AZ, 1999.

64. Rämä, P. Effects of Weather-Controlled Variable Speed Limits and warning Signs on Driver Behavior. *Transportation Research Record 1689*, 1999, pp. 53–59.

65. Haas R., M. Carter, E. Perry, J. Trombly, E. Bedsole, and R. Margiotta. *iFlorida Model Deployment*. Final Evaluation Report. Report No. FHWA-HOP-08-050, 2009.

66. PBS&J. *I-4 Variable Speed Limit Effectiveness Study*. Prepared for the Florida Department of Transportation, District 5, 2009.

67. http://www.wsdot.wa.gov/Projects/I5/ActiveTrafficManagement/

68. Lind, G. *Weather and Traffic Controlled Variable Speed Limits in Sweden*. Report, Movea trafikkonsult AB, Stockholm, Sweden, 2006.

69. Young, R. Rural Variable Speed Limit for Southeast Wyoming. *Transportation Research Board 89th Annual Meeting*, Washington D.C, 2010.

70. Lee, C., B. Hellinga, and F. Saccomanno., Assessing safety benefits of variable speed limits. *Transportation Research Record 1897*, 2004, pp. 183-190.

71. Papageorgiou, M., E. Kosmatopoulos, and I. Papamichail. Effects of Variable Speed Limits on Motorway Traffic Flow. *Transportation Research Record 2047*, 2008, pp. 37-48.

72. Hegyi, A. and S.P. Hoogendoorn. Dynamic speed limit control to resolve shock waves on freeways – Field test results of the SPECIALIST algorithm. *13th Int. IEEE ITS*, Madeira Island, Portugal, 2010.

73. Abdel-Aty, M., and A. Dhindsa. Coordinated Use of Variable Speed Limits and Ramp Metering for Improving Traffic Safety on Congested Freeways. *Transportation Research Board 86nd Annual Meeting*, Washington, D.C, 2007.

74. Abdel-Aty, M., J. Dilmore, and A. Dhindsa. Evaluation of Variable Speed Limits for Real-Time Freeway Safety Improvement. *Accident Analysis and Prevention*, 38, 2006, pp. 335-345.

75. Piao J., and M. McDonald. Safety Impacts of Variable Speed Limits – A Simulation Study. *Proceedings of the 11th International IEEE, Conference on Intelligent Transportation Systems*, 2008.

76. Hegyi A., De Schutter B., and Hellendoorn J. MPC-based Optimal Coordination of Variable Speed Limits to Suppress Shock Waves in Freeway. *Proceedings of the American Control Conference*, Denver, Colorado, 2003, pp. 4083–4088.

77. Lin, P., K. Kang, and G. Chang. Exploring the Effectiveness of Variable Speed Limit Controls on Highway Work-Zone Operations. *Intelligent Transportation Systems*, Vol. 8, 2004, pp.1-14.

78. Allaby P., B. Hellinga, and M. Bullock. Variable Speed Limits: Safety and Operational Impacts of a Candidate Control Strategy for Freeway Applications. *IEEE Transactions on Intelligent Transportation System*, Vol.8, No.4, 2007, pp.671-680.

79. Hegyi A., B. De Schutter, and J. Hellendoorn. Model predictive control for optimal coordination of ramp metering and variable speed limits. *Transportation Research Part C*, 13 (3), 2005, pp. 185–209.

80. Ghods, A., A. Kian, and M. Tabibi. Adaptive freeway ramp metering and variable speed limit control: a genetic-fuzzy approach. *Intelligent Transportation Systems Magazine, IEEE*, vol. 1, no. 1, 2009, pp. 27-36.

81. Carlson, R.C., I. Papamichail, M. Papageorgiou, and A. Messmer. Variable Speed Limits as a Mainline Metering Device for Freeways. *Transportation Research Board Annual Meeting*, Washington, D.C, 2010.

82. Elefteriadou, L., C. Letter, and E. Mintsis. *Managed Lane Operations – Adjusted Time of Day Pricing vs. Near-Real Time Dynamic Pricing*, *Volume II: Ramp Signaling and Variable Speed Limits (VSL)*. Prepared for FDOT by the University of Florida Transportation Research Center, Gainesville, FL, 2012.

83. Kondyli, A., I. Soria, A. Duret, and L. Elefteriadou. Sensitivity analysis of CORSIM with respect to the process of freeway flow breakdown at bottleneck locations. *Simulation Modelling Practice and Theory 22(0)*, 2012, pp. 197-206.

84. Talebpour, A., H. Mahmassani, and S. Hamdar. Speed Harmonization: Effectiveness Evaluation Under Congested Conditions. *Transportation Research Board Annual Meeting*, Washington D.C, 2013.

85. Wang, Y., and P. A. Ioannou. New model for variable speed limits. *Transportation Research Record*, vol. 2249, 2011, pp. 38-43.

86. Tignor S., L. Brown, J. Butner, R. Cunard, S. Davis, H. Hawkins, E. Fischer, M. Kehrli, P. Rusch, and W. Wainwright. *Innovative Traffic Control-Technology and Practice in Europe*. International Technology Exchange Program Report to the U.S. Department of Transportation, 1999.

87. Rämä, P., J. Raitio, V. Anttila, and A. Schirokoff. Effects of Weather Controlled Speed Limits on Driver Behaviour on a Two-Lane Road. *VTT Communities and Infrastructure*, Finland, 2001.

88. Brewer, M., G. Pesti, and W. Schneider. *Effectiveness of Selected Devices on Improving Work Zone Speed Limit Compliance*. Texas Transportation Institute, Texas A&M University, College Station, Texas, 2005.

89. Elefteriadou, L., B. Martin, T. Simmerman, and D. Hale. *Using Micro-simulation to Evaluate the Effects of Advanced Vehicle Technologies on Congestion*. Prepared for center for multimodal solutions for congestion mitigation, Gainesville, FL, 2011.

90. Willke, T., P. Tientrakool, and N. Maxemchuk. A survey of inter-vehicle communication protocols and their applications. *IEEE Communications Surveys Tutorials*, vol. 11, no. 2, 2011, pp. 3-20.

91. Park, H., C. Bhamidipati, and B. Smith. Development and Evaluation of an Enhanced IntelliDriveSM Enabled Lane Changing Advisory Algorithm to Address Freeway Merge Conflict. *Transportation Research Board Annual Meeting*, Washington D.C, 2011.

92. Rim, H., C. Oh, K. Kang, and S. Kim. Estimation of lane-level travel times in vehicle-to-vehicle and vehicle-to-infrastructure-based traffic information system. *Transportation Research Record 2243*, 2011, pp. 9–16.

93. Ni, D., J. Li, S. Andrews, and H. Wang. A Methodology to Estimate Capacity Impact due to Connected Vehicle Technology. *Hindawi Publishing Corporation International Journal of Vehicular Technology*, 2012.

94. Najm, W., J. Koopmann, J. Smith, and J. Brewer. *Frequency of Target Crashes for IntelliDrive Safety Systems*. USDOT National Highway Traffic Safety Administration, Washington, D.C, 2010.

95. Dion, F., R. Robinson, and J. Oh. Evaluation of Usability of IntelliDrive Probe Vehicle Data for Transportation Systems Performance Analysis. *Journal of Transportation Engineering*, Vol. 137, No. 3, 2010, pp. 174-183.

96. Shladover, S., and T. Kuhn. Traffic Probe Data Processing for Full-Scale Deployment of Vehicle–Infrastructure Integration, *Transportation Research Record 2086*, 2008, pp. 115–123.

97. Dion, F., J. Oh, and R. Robinson. Virtual Testbed for Assessing Probe Vehicle Data in IntelliDrive Systems. *IEEE Transactions on Intelligent Transportation Systems*, Vol. 12, No. 3, 2011, pp. 635-644.

98. Kianfar, J., and E. Praveen. Placement of Roadside Equipment (RSE) in Connected Vehicle Environment for Travel Time Estimation. *Transportation Research Board Annual Meeting, Washington*, D.C, 2013.

99. Li j., K. Zhou, S. Shladover, and A. Skabardonis. Estimating Queue Length under the Connected Vehicle Technology: Using Probe Vehicle, Loop Detector, and Fused Data. *Transportation Research Board 83th Annual Meeting*, Washington D.C, 2013.

100. Kattan, L., and S. Saidi. Comparative analysis of probe-based ramp metering with detector-based and pretimed ramp metering. *Journal of Advanced Transportation 47(1)*, 2013, pp: 61-78.

101. Goodall, N., J., B. L. Smith, and B. Park. Traffic Signal Control with Connected Vehicles. *Transportation Research Record 2381*, 2013, pp. 65–72.

102. Christofa, E., J. Argote, and A. Skabardonis. Arterial Queue Spillback Detection and Signal Control based on Connected Vehicle Technology. *Transportation Research Board Annual Meeting*, Washington, DC, 2013.

103. Venkatanarayana, R., H. Park, B. Smith, C. Skerrit Jr., and N. Ruhter. Application of IntelliDriveSM to address oversaturated conditions on arterials. *Transportation Research Board 90th Annual Meeting*. Washington D.C, 2011.

104. Comert, G. and M. Cetin. Queue length estimation from probe vehicle location and the impacts of sample size. *European Journal of Operational Research*, 197(1), 2009, pp. 196-202.

105. Zeng, X., K. Balke, and P. Songchitruksa. *Potential Connected Vehicle Applications to Enhance Mobility, Safety, and Environmental Security*. Technical report, The Texas A&M University System, 2012.

106. Liao, C., and G. Davis. Simulation Study of a Bus Signal Priority Strategy Based on GPS/AVL and Wireless Communications. *Transportation Research Record 2034*, 2007, pp. 82-91.

107. Holm, P., D.Tomich, J. Sloboden, and C. Lowrance. *Traffic Analysis Toolbox Volume IV: Guidelines for Applying CORSIM Microsimulation Modeling Software*. Publication FHWA-HOP-07-079, 2007.

108. Meyer, Y. and D. Salinger. *Wavelets and Operators*. Cambridge University Press, 1995.
109. Kaplan, E. L., and Meier, P. Nonparametric estimation from incomplete observations. *J. Amer. Statist. Assn.*, 53, 1958, pp. 457–481.

110. Kondyli, A., L. Elefteriadou, W. Brilon, F. Hall, B. Persaud, and S. Washburn. Development and Evaluation of Methods for Constructing Breakdown Probability Models. *Journal of Transportation Engineering*, 2013, pp. 931–940.

111. Adeli, H., and X. Jiang. *Intelligent Infrastructure: Neural Networks, Wavelets, and Chaos Theory for Intelligent Transportation Systems and Smart Structures*. CRC Press, 2008.

112. Donoho, D.L. Unconditional bases are optimal bases for data compression and for statistical estimation. *Applied and Computational Harmonic Analysis*, Vol. 1, No.1, 1993, pp. 100–115.

113. Anderson, T. W., and Darling, D. A. Asymptotic theory of certain 'goodness-of-fit' criteria based on stochastic processes. *Ann. Math. Stat.*, 23, 1952, 193–212.

114. Shen, L. *Freeway Travel Time Prediction System Using Dynamic Neural Networks*. Ph.D. Dissertation, Florida International University, Miami, FL 2008.